

Anaerobic membrane bioreactors for domestic wastewater treatment: Treatment performance
and fouling characterization

by

Kahao Lim

B.S., California State Polytechnic University, Pomona, 2016

AN ABSTRACT OF A DISSERTATION

submitted in partial fulfillment of the requirements for the degree

DOCTOR OF PHILOSOPHY

Department of Civil Engineering
Carl R. Ice College of Engineering

KANSAS STATE UNIVERSITY
Manhattan, Kansas

2021

Abstract

As the human population continues to grow, increasing stress is placed on the food-energy-water nexus. Wastewater is increasingly being viewed as a sustainable resource to close the loop in this nexus as it contains nutrients, latent chemical energy, and water that can be recovered for beneficial reuse. One technology that has shown promise in harnessing wastewater as a resource is the Anaerobic Membrane Bioreactor (AnMBR). AnMBRs combine anaerobic biological wastewater treatment with membrane filtration technology to achieve superior effluent quality, while generating energy in the form of methane and providing an opportunity to capture nutrients. In this study, a pilot scale gas-sparged AnMBR was operated in Ft. Riley for 472 days under ambient temperature conditions. The AnMBR achieved an average removal efficiency of $88\pm 7\%$ and $88\pm 6\%$ for COD and BOD₅, respectively, at temperatures ranging from 12.7°C to 31.5°C, demonstrating its feasibility for ambient temperature operation. The AnMBR was also paired with downstream nutrient recovery using a coagulation-flocculation-sedimentation process, which removed $94\pm 3\%$ of phosphorus and over 99% of nitrogen, as well as both gaseous and dissolved methane capture, which could generate an estimated 72.8% of the power required for energy neutrality. The successful integration of AnMBRs in a treatment train that addressed the critical challenges of dissolved methane and nutrient capture demonstrates the viability of the technology in achieving holistic wastewater treatment.

While the viability of the pilot scale AnMBR for municipal wastewater resource recovery was successfully demonstrated, membrane fouling was identified to be a major obstacle to the widespread adoption of the technology. In the pilot system, fouling management through gas sparging required 54% of the total energy demand, which could be reduced with improved targeted maintenance strategies that can be developed after a deeper understanding of the

foulants. To better understand fouling behavior in AnMBRs, a suite of analyses was employed to dynamically monitor the initiation and proliferation of fouling to complement the traditional end-of-life membrane autopsies in the pilot-scale AnMBR. Fluorometry and soluble chemical oxygen demand (sCOD) monitoring of the membrane permeate during steady state pilot AnMBR operation complemented end-of-life membrane and sludge cake analyses, such as Fourier Transform Infrared Spectroscopy (FTIR), to identify both organic and inorganic foulants that have been deposited on a membrane surface throughout the pilot operation. The fouling events coincided with spikes in the permeate sCOD, accompanied with an increase in tryptophan and tyrosine like compounds, as measured by the fluorometric excitation-emission (EEM) spectra. Scaling, albeit minor, was mainly accounted by calcium sulfate and calcium phosphate, as opposed to the typically expected calcium carbonate. These findings have implications for optimizing membrane maintenance strategies, informing solids wasting schedules as well as the selection of chemicals for backpulsing.

To further mechanistically understand membrane fouling, a novel lab scale AnMBR with a side tube membrane module was designed to characterize early membrane foulants. A main module was continuously operated to maintain system performance, averaging $83 \pm 7\%$ COD removal during the startup period, while the side tube module was installed and operated in parallel to allow for sampling the membrane fibers without interrupting the main module. The lab scale system underwent extended critical flux testing while being fed with synthetic municipal wastewater only, followed by controlled spikes of tryptophan, tyrosine, and humic acid into the wastewater. The transmembrane pressure hysteresis was much more severe in the spiked test. Endpoint analysis after sub-critical flux operation revealed that cake formation was limited in the side tube samples suggesting that the hysteresis and initial fouling was due to pore

constriction, which is a significantly less studied fouling mechanism compared to cake layer fouling. Cake layer formation in the main module was localized in the top third of the membrane fibers. Heat extraction temperature profiles that were optimized in a separate study were applied for soluble microbial product and extracellular polymeric substance characterization of the membrane extracts and cake foulants after each critical flux test. Humic and fulvic acids appear to be more associated with pore fouling, while proteins appear to be more associated with the cake layer. Free amino acids were not detected in any sample suggesting that the amino acids likely underwent rapid anaerobic transformation. Tryptophan-like and tyrosine-like fluorescence was found in the EEMs of the side tube module extracts and were likely due to amino acid degradation products, such as indoles, due to having peaks in the EEM but the spiked test not increasing in protein concentration. In contrast, the foulant cake's proteinaceous foulants were likely in the form of polypeptides, as confirmed through FTIR and colorimetry. Significant amounts of humic substances in the form of humic and fulvic acids were extracted from the membrane surface and pores and likely also contributed pore fouling, with significantly higher amounts being extracted from the side tube membrane module after the spiked test and the main membrane module at the end of operation. These findings show great promise for guiding future research on early onset of membrane fouling and fouling management strategies to achieve energy positive operation using the AnMBR technology platform.

Anaerobic membrane bioreactors for domestic wastewater treatment: Treatment performance
and fouling characterization

by

Kahao Lim

B.S., California State Polytechnic University, Pomona, 2016

A DISSERTATION

submitted in partial fulfillment of the requirements for the degree

DOCTOR OF PHILOSOPHY

Department of Civil Engineering
Carl R. Ice College of Engineering

KANSAS STATE UNIVERSITY
Manhattan, Kansas

2021

Approved by:

Major Professor
Dr. Prathap Parameswaran

Copyright

© Kahao Lim 2021.

Abstract

As the human population continues to grow, increasing stress is placed on the food-energy-water nexus. Wastewater is increasingly being viewed as a sustainable resource to close the loop in this nexus as it contains nutrients, latent chemical energy, and water that can be recovered for beneficial reuse. One technology that has shown promise in harnessing wastewater as a resource is the Anaerobic Membrane Bioreactor (AnMBR). AnMBRs combine anaerobic biological wastewater treatment with membrane filtration technology to achieve superior effluent quality, while generating energy in the form of methane and providing an opportunity to capture nutrients. In this study, a pilot scale gas-sparged AnMBR was operated in Ft. Riley for 472 days under ambient temperature conditions. The AnMBR achieved an average removal efficiency of $88\pm 7\%$ and $88\pm 6\%$ for COD and BOD₅, respectively, at temperatures ranging from 12.7°C to 31.5°C, demonstrating its feasibility for ambient temperature operation. The AnMBR was also paired with downstream nutrient recovery using a coagulation-flocculation-sedimentation process, which removed $94\pm 3\%$ of phosphorus and over 99% of nitrogen, as well as both gaseous and dissolved methane capture, which could generate an estimated 72.8% of the power required for energy neutrality. The successful integration of AnMBRs in a treatment train that addressed the critical challenges of dissolved methane and nutrient capture demonstrates the viability of the technology in achieving holistic wastewater treatment.

While the viability of the pilot scale AnMBR for municipal wastewater resource recovery was successfully demonstrated, membrane fouling was identified to be a major obstacle to the widespread adoption of the technology. In the pilot system, fouling management through gas sparging required 54% of the total energy demand, which could be reduced with improved targeted maintenance strategies that can be developed after a deeper understanding of the

foulants. To better understand fouling behavior in AnMBRs, a suite of analyses was employed to dynamically monitor the initiation and proliferation of fouling to complement the traditional end-of-life membrane autopsies in the pilot-scale AnMBR. Fluorometry and soluble chemical oxygen demand (sCOD) monitoring of the membrane permeate during steady state pilot AnMBR operation complemented end-of-life membrane and sludge cake analyses, such as Fourier Transform Infrared Spectroscopy (FTIR), to identify both organic and inorganic foulants that have been deposited on a membrane surface throughout the pilot operation. The fouling events coincided with spikes in the permeate sCOD, accompanied with an increase in tryptophan and tyrosine like compounds, as measured by the fluorometric excitation-emission (EEM) spectra. Scaling, albeit minor, was mainly accounted by calcium sulfate and calcium phosphate, as opposed to the typically expected calcium carbonate. These findings have implications for optimizing membrane maintenance strategies, informing solids wasting schedules as well as the selection of chemicals for backpulsing.

To further mechanistically understand membrane fouling, a novel lab scale AnMBR with a side tube membrane module was designed to characterize early membrane foulants. A main module was continuously operated to maintain system performance, averaging $83\pm 7\%$ COD removal during the startup period, while the side tube module was installed and operated in parallel to allow for sampling the membrane fibers without interrupting the main module. The lab scale system underwent extended critical flux testing while being fed with synthetic municipal wastewater only, followed by controlled spikes of tryptophan, tyrosine, and humic acid into the wastewater. The transmembrane pressure hysteresis was much more severe in the spiked test. Endpoint analysis after sub-critical flux operation revealed that cake formation was limited in the side tube samples suggesting that the hysteresis and initial fouling was due to

pore constriction, which is a significantly less studied fouling mechanism compared to cake layer fouling. Cake layer formation in the main module was localized in the top third of the membrane fibers. Heat extraction temperature profiles that were optimized in a separate study were applied for soluble microbial product and extracellular polymeric substance characterization of the membrane extracts and cake foulants after each critical flux test. Humic and fulvic acids appear to be more associated with pore fouling, while proteins appear to be more associated with the cake layer. Free amino acids were not detected in any sample suggesting that the amino acids likely underwent rapid anaerobic transformation. Tryptophan-like and tyrosine-like fluorescence was found in the EEMs of the side tube module extracts and were likely due to amino acid degradation products, such as indoles, due to having peaks in the EEM but the spiked test not increasing in protein concentration. In contrast, the foulant cake's proteinaceous foulants were likely in the form of polypeptides, as confirmed through FTIR and colorimetry. Significant amounts of humic substances in the form of humic and fulvic acids were extracted from the membrane surface and pores and likely also contributed pore fouling, with significantly higher amounts being extracted from the side tube membrane module after the spiked test and the main membrane module at the end of operation. These findings show great promise for guiding future research on early onset of membrane fouling and fouling management strategies to achieve energy positive operation using the AnMBR technology platform.

Table of Contents

List of Figures	xiii
List of Tables	xviii
Acknowledgements	xx
Chapter 1 - Background and Literature Review	1
1.1 Introduction.....	1
1.2 Literature Review	6
1.2.1 Anaerobic Membrane Bioreactors	6
1.2.2 Membrane Fouling.....	13
1.2.3 Fouling Control Methods.....	15
1.2.4 Critical Flux Hypothesis	18
Chapter 2 - Research Hypotheses and Objectives	20
Chapter 3 - Performance of a Pilot Scale Gas Sparged AnMBR for Holistic Wastewater Treatment.....	22
3.1 Materials and Methods.....	23
3.1.1 AnMBR Startup and Process	23
3.1.2 Fouling Control	25
3.1.3 Energy Balance	26
3.1.4 Sample Collection and Preparation.....	27
3.1.5 Laboratory Analyses	28
3.2 Pilot-Scale Gas Sparged AnMBR for Holistic Treatment of Domestic Wastewater	28
3.2.1 Operating Conditions	28
3.2.2 Anaerobic Treatment Performance	30
3.2.3 Effect of Ambient Temperature Operation on Methane Production and Distribution	34
3.2.4 Dissolved Methane Removal	36
3.2.5 Removal and Recovery of Sulfide, Phosphorus, and Ammonia from AnMBR	
Permeate.....	37
3.2.6 Energy Balance	40
3.3 Future Outlook.....	42
3.4 Summary.....	42

Chapter 4 - Membrane Performance and Foulant Characterization in a Pilot Scale AnMBR	44
4.1 Materials and Methods.....	44
4.1.1 Fouling Control	45
4.1.2 Fouling Parameter Analyses	48
4.2 Membrane Performance.....	49
4.2.1 Chemical Cleaning.....	51
4.2.2 Bioreactor Solids and the Potential Role of Soluble COD on Membrane Fouling	54
4.3 Foulant Characteristics and Composition	56
4.3.1 Organic Foulants	56
4.3.2 Inorganic Foulants	60
4.4 Implications and Considerations for AnMBR Design and Operations.....	62
4.5 Summary	63
Chapter 5 - Review of Techniques for Understanding Membrane Fouling.....	65
5.1 Framework for Understanding Membrane Fouling in AnMBRs.....	65
5.1.1 Sampling the Foulant Cake Layer.....	67
5.1.2 Definitions, Components, and Analysis of EPS and SMP.....	68
5.1.3 Fluorescence Spectroscopy	71
5.1.4 Fourier Transform Infrared Spectroscopy	74
5.2 Summary	77
Chapter 6 - Critical Evaluation of Heat Extraction Temperature on SMP and EPS Quantification in Wastewater Processes	79
6.1 Introduction.....	79
6.2 Materials and Methods.....	83
6.2.1 Sampling Information	83
6.2.2 Extraction Procedure and Analyses	84
6.2.3 Colorimetric Analysis Procedures	85
6.2.4 Live/Dead Assay Procedure.....	87
6.3 Results and Discussion	87
6.3.1 BNR Sludge Extraction Data	87
6.3.2 BNR Sludge Fluorometry Data.....	92
6.3.3 Aerobic MBR Sludge Case Study.....	94

6.4 Conclusion	99
6.5 Summary	101
Chapter 7 - Investigation of Early Onset Membrane Fouling under Sub-Critical Flux Operation in a Novel Lab-Scale AnMBR.....	102
7.1 Materials and Methods.....	102
7.1.1 Lab Scale AnMBR Setup.....	102
7.1.2 Reactor Startup and Operation.....	104
7.1.3 Extended Critical Flux Test	106
7.1.4 Sampling Procedures and Analytical Methods	107
7.1.4 Membrane Foulant Sampling.....	108
7.2 Results and Discussion	109
7.2.1 System Performance	109
7.2.2 Extended Critical Flux Tests and Continuous Operation	111
7.2.3 Membrane Foulant Samples	114
7.2.4 Continuous Operation TMP Behavior	119
7.3 Summary.....	121
Chapter 8 - Conclusion and Future Research	122
8.1 Conclusion	122
8.2 Future Research	123
8.2.1 Further Investigations on Pore Foulants	123
8.2.2 Investigating the Partitioning of Foulants in the Bulk Sludge and Membrane Permeate	125
8.2.3 Evaluating Chemical Cleaning Strategies.....	126
8.2.4 Overall Directions for the AnMBR Platform.....	127
References.....	129
Appendix A - Accompanying Chapter 3	147
Appendix B - Accompanying Chapter 4.....	149
Appendix C - Accompanying Chapter 6.....	151
Appendix D - Accompanying Chapter 7	157

List of Figures

- Figure 3.1 A schematic of the pilot-scale gas-sparged AnMBR used in this study. Note that the screened municipal wastewater was fed into the anaerobic bioreactor without primary settling..... 23
- Figure 3.2 Hydraulic Retention Time (HRT), Solids Retention Time (SRT), and Organic Loading Rates (OLR) over the operational period are shown. A biosolids wasting event intended to decrease HRT also significantly lowered SRTs around day 300..... 29
- Figure 3.3 Parameters used to evaluate membrane performance are plotted over the operational period. Biogas sparge flow rates were varied over the project period in optimization experiments to determine conditions that best balance energy consumption and physical membrane scouring to maintain stable transmembrane pressures (TMP) at a constant flux.29
- Figure 3.4 Plots of the system’s treatment effectiveness throughout the entire operational period; (A) Influent and permeate COD on the primary axis with temperature on the secondary axis and (B) Influent and permeate BOD₅ on the primary axis with bioreactor volatile solids (VS) mass data on the secondary axis. As shown in (C), the COD and BOD₅ removal rates were impacted by sudden drops in bioreactor VS, whereas lower temperature operation did not significantly impact performance. The study’s objectives for effluent COD and BOD₅ concentrations were 60 mg/L and 30 mg/L, respectively. VS mass was presented instead of concentration because the bioreactor’s liquid volume was changed throughout this study. 33
- Figure 3.5 (A) A box-and-whisker plot of the AnMBR’s bulk methanogenic yield at three temperature ranges, showing significant differences in mean methane production. (B) A plot of the percentage of methane found in the dissolved fraction at different temperatures. The dissolved methane fraction has a generally decreasing trend as temperatures increase. (C) Membrane contactor dissolved methane and removal efficiencies are shown in a line plot along with influent and effluent concentrations. (D) Membrane contactor removal efficiency as a function of absolute pressure at two different flow rates are shown in a scatter plot.... 36
- Figure 3.6 Average phosphorus concentration removals and efficiencies by process are shown in a pie chart..... 39
- Figure 3.7 Each completed run of the clinoptilolite IX system for ammonia recovery is shown in the bar graph. The second cycle of batch A was not completed due to operating errors..... 40

Figure 3.8 Graph of power consumed and generated from equipment and processes of the system during a period where operating conditions were held relatively constant from days 420-445. Total power consumption for system operation was 0.349 kWh/m³, and the theoretical 0.254 kWh/m³ generated for 72.8% of energy neutrality. Values were calculated assuming pump efficiency of 65% and generator efficiency of 38%. 41

Figure 4.1 A schematic of the pilot-scale gas-sparged AnMBR used in this study adapted to show fouling control methods. 45

Figure 4.2 A plot of transmembrane pressure, flux, net biogas sparge flowrate, chemical cleaning events, and sludge wasting over the study's entire duration. 51

Figure 4.3 Plots of membrane performance. (A) shows the TMP, Flux, and Permeability over the first 80 days. The first 42 days were operated without chemical cleaning and is used as a benchmark for the system's original permeability. (B) plots the percentage of the benchmark permeability from the first 42 days, and chemical cleaning events. 53

Figure 4.4 A period of operation from day 175 to the end of operation on day 472 is shown in (A) to show the effects of wasting solids, which affects concentrations of the bioreactor's total solids as well as the bioreactor's soluble chemical oxygen demand (sCOD), on permeability. (B) and (C) are Excitation-Emission Matrices (EEMs) generated from fluorometer data, which are used to further characterize the soluble organic matter in the membrane permeate. During fouled conditions (B) fluorophore B2, indicative of tyrosine-like compounds, is predominant, but the impacts of a tryptophan-like peak (T1) and a humic-like peak (M) are still apparent. B2 is present during normal operation (C) at lower concentrations. T1 and M, which suggest the presence of tryptophan-like compounds and humic-like compounds respectively are also seen during normal conditions..... 55

Figure 4.5A FTIR spectra of dehydrated foulant from the cake layer. The peak at 3279.55 cm⁻¹, associated with primary amines and amides, and the peaks at 1538.16 cm⁻¹ and 1632.48 cm⁻¹, uniquely associated with amide II and amide III groups, suggest the heavy presence of proteins. Saturated aliphatics were observed at peaks 2920.27 cm⁻¹ and 2851.21 cm⁻¹, and aluminosilicates are suggested by the peak at 1029.33 cm⁻¹. 58

Figure 4.6 Representative micrographs and microscopy results. (A) shows a representative scanning electron microscope image and its accompanying EDX table. (B) is a

transmission electron microscope image of inorganic crystalline calcium sulfate, an unexpected inorganic scalant that was encountered throughout the foulant cake layer. 61

Figure 6.1 Diagram of the extraction procedure for operationally defined SMP and EPS samples. 85

Figure 6.2 Plots of the BNR extraction data. Carbohydrates and proteins were measured using the phenol-sulfuric acid method and bicinchoninic acid method, respectively, and extracted total carbon and total nitrogen measurements were plotted versus extraction temperature. The error (n=3) was less than 10% for all datapoints. 88

Figure 6.3 A plot of the percent increase in lysis compared to extraction at 20°C. 60°C appears to be around the threshold for excessive lysis in the activated (AS) and anaerobic sludge (ANA) but may be past the point of inflection for anoxic sludge (ANX). 90

Figure 6.4 Excitation-Emission Matrices of AS1 (activated sludge) and ANA (anaerobic basin sludge) samples extracted at different temperatures. The tryptophan-like peak (fluorophore T1) was predominant, with an accompanying tyrosine-like peak (fluorophore B2), with increasing relative intensity as extraction temperatures progressively increased. A fulvic-like peak (fluorophore D) was also observed at the two higher extraction temperatures. 93

Figure 6.5 Plots of the extracted carbohydrates and proteins for aerobic membrane bioreactor sludges, AeMBR1 and AeMBR2, as measured using the phenol-sulfuric acid method and bicinchoninic acid method, respectively, as well as extracted total carbon and total nitrogen measurements versus extraction temperature. The error (n=3) was less than 10% for all datapoints. 96

Figure 6.6 EEMs of aerobic membrane bioreactor sludges AeMBR1 and AeMBR2 extracted in the pre-determined temperature range of 45 - 60. Fluorophores T1, B2, and D correspond to tryptophan-like, tyrosine-like, and fulvic-like signatures, respectively. The unlabeled peak (EX 360, EM 450) has been observed in literature to be associated with optical brighteners. 98

Figure 7.1 A schematic of the lab-scale gas-sparged AnMBR used in this study (A) and a picture of the system (B). 103

Figure 7.2 Plots of the system's COD removal performance (A) and solids concentrations juxtaposed with ssCOD (B). 111

Figure 7.3 Extended critical flux testing plots from Stage 1 (A) and Stage 2 (B), both of which used the baseline synthetic wastewater recipe, and Stage 3 (C), which was spiked with tryptophan, tyrosine, and humic acid.....	113
Figure 7.4 Excitation-Emission Matrices (EEMs) of the side tube membrane extracts from the end of Stages 1 and 2, using the baseline synthetic wastewater, Stage 3, using the spiked synthetic wastewater, and the main module at the end of operation.....	116
Figure 7.5 Excitation-Emission Matrices (EEMs) of the main module sample M1 and the foulant cake, both sampled at the end of the system’s operation.....	117
Figure 7.6 Fourier Transform Infrared spectroscopy spectra of the cake layer foulant from the main module after dehydration in a 105°C oven overnight (A) and ignition at 450°C, leaving only the inorganics (B).....	118
Figure 7.7 Plot of the increasing TMP/Time slope versus production cycle, demonstrating the increasing rate of cake formation.....	120
Figure 8.1 A plot of the extractions of Total Carbon (A), Total Nitrogen (B), Carbohydrates (C), and Proteins (D) for permeate SMP, sludge S MP, and sludge EPS. For Total Carbon and Total Nitrogen, all measurements were performed in triplicate and error was less than 10% on each.	126
Figure A1 The COD associated with Volatile Fatty Acids (VFA) measured in the permeate between days 250 and 400. The upset conditions from day 300 to day 355 is associated with elevated VFA concentration	148
Figure B1 Transmission electron microscope crystal diffraction images. The diffraction patterns are diffused due to the high organic content present throughout the wastewater matrix, but diffraction spots can be seen in (A). Measurements to determine d-spacing are shown in (B), which identified the crystalline material as calcium sulfate.....	150
Figure C1 Extraction data for activated sludge sample AS0, taken from the Manhattan, Kansas wastewater treatment plant. The solids concentrations were 2640 mg/L TSS and 2320 mg/L VSS. Despite the differences in sludge concentration, the general trends were consistent with those observed in the AS sample discussed in the main manuscript.	151
Figure C2 Excitation-Emission Matrices of AS1 (activated sludge) SMP extracted at different temperatures. Increasing temperatures beyond 60°C revealed extracted fluorophores	

characteristic of marine humic-like (fluorophore M) substances, but the peak intensities are low and relatively comparable among all extraction temperatures tested. 152

Figure C3 Excitation-Emission Matrices of ANX (anoxic sludge) SMP extracted at different temperatures. The tryptophan-like peak (fluorophore T1) and marine humic-like peak (fluorophore M) appear slightly more intense with increasing temperature, but the peak intensities are low and relatively comparable among all extraction temperatures tested. .. 153

Figure C4 Excitation-Emission Matrices of ANA (anaerobic sludge) SMP extracted at different temperatures. The tryptophan-like peak (fluorophore T1) and marine humic-like peak (fluorophore M) appear slightly more intense with increasing temperature, but the peak intensities are low and relatively comparable among all extraction temperatures tested. .. 154

Figure C5 Excitation-Emission Matrices of ANX (anoxic sludge) EPS extracted at different temperatures. The tryptophan-like peak (fluorophore T1) was predominant, with an accompanying tyrosine-like peak (fluorophore B2), with increasing relative intensity as extraction temperatures progressively increased. A fulvic-like peak (fluorophore D) was also observed at the two higher extraction temperatures. 155

Figure C6 Extraction data for aerobic membrane bioreactor sludge sample AeMBR0 as measured using the phenol-sulfuric acid method and bicinchoninic acid method, respectively, as well as extracted total carbon and total nitrogen measurements versus extraction temperature. The error (n=3) was less than 10% for all datapoints. The trends were similar to those observed in activated sludge extractions..... 156

Figure D1 Excitation-Emission Matrices of humic acid used in the spiked synthetic wastewater recipe..... 157

Figure D2 Excitation-Emission Matrices (EEMs) of the amino acids, tryptophan (A) and tyrosine (B) used in the spiked synthetic wastewater recipe 158

Figure D3 Excitation-Emission Matrices (EEMs) of main module membrane fiber samples M2 and M3, which have almost identical profiles to sample M1 159

List of Tables

Table 1.1 A table showing the different pressure driven membrane processes and their general characteristics. PE = Polyethylene, PP = polypropylene, PES = polyethersulfone, PTFE = polytetrafluoroethylene, PVDF = polyvinylidene difluoride, CA = cellulose acetate, TFC = thin-film composite. Adapted from (Metcalf et al. 2004).....	5
Table 1.2 A summary of various AnMBR performance parameters and their configurations for various studies treating domestic, and industrial wastewaters. WW = wastewater. Membrane materials: CA = cellulose acetate, PE = polyethylene, PES= Polyethersulfone, PP = polypropylene, PVDF = polyvinylidene difluoride. Membrane processes: MF = microfiltration, UF = ultrafiltration.....	7
Table 3.1. Design basis tables for the pilot-scale AnMBR system (A) and the downstream processes (B), including dissolved methane removal using a membrane contactor, and nutrient removal using coagulation-flocculation-sedimentation (CFS) and ion-exchange (IX) processes	24
Table 4.1 The typical maintenance cleaning procedure used in this study. For back-to-back cleans, this procedure is repeated once for each chemical.....	46
Table 4.2 The recovery cleaning procedure used in this study. This procedure was repeated once for each chemical.	47
Table 5.1 A compiled list of fluorophores likely to be found in wastewater and their characteristic excitation and emission wavelengths (Henderson et al. 2009; Hudson and Reynolds 2007)	73
Table 6.1 General sample information and solids characteristics.....	83
Table 6.2 Table of SMP extraction values averaged across temperatures and p-values greater than 0.05 for Tukey’s multiple comparisons across the temperature ranges, suggesting that temperature has no significant statistical effect on SMP extraction.	89
Table 7.1 Design basis table and operating setpoints for the lab-scale AnMBR system.....	104
Table 7.2 Synthetic wastewater recipe used in this study. The spiked components were added to the base recipe only during the spiked testing conditions.....	105

Table 7.3 Table of Total Carbon (TC), Total Nitrogen (TN), carbohydrate, and protein extractions from the side tube membrane fibers after the 3 days of operation of each stage. 115

Table 7.4 Table of Total Carbon (TC), Total Nitrogen (TN), carbohydrate, and protein extractions from the main module membrane fibers (M1, M2, and M3) and the foulant cake, all sampled at the end of the system’s operation. 117

Table A1 The results and coagulant dosing conditions used to determine the approximate rates of chemical addition for the pilot plant’s nutrient recovery system..... 147

Table B1 Table of LSI and pH values over the first 96 days of operation. The LSI values were consistently negative after the startup period, indicating that calcium carbonate scaling was not likely to occur. 149

Acknowledgements

This research was supported by the Department of Defense Environmental Security Technology Certification Program (ESTCP Project number ER-201434; www.serdp-estcp.org/ProgramAreas/Environmental-Restoration/Wastewater-and-Drinking-Water/ER-201434) and the U.S. Environmental Protection Agency under U.S. Army Corps of Engineers Humphreys Engineering Service Center Contract W912HQ-15-C-0001. Segments of this research were also supported by the National Science Foundation (NSF) CBET Environmental Engineering Program (#1440) award #1805631 and the NSF National Research Traineeship (NRT) award #1828571. I would also like to acknowledge Youngseck Hong, Jennifer Lim, Brent Perez, and Adriano Vieira of Suez for helping to provide me with the Zeeblok membrane module used in the lab scale study and Rocco Mazzaferro and Isaac Klassen of Rocco Mazzaferro Inc for helping fabricate the lab scale module and working with me to implement the process control programming.

There are many people who I feel great gratitude for that have helped me immensely, both personally and professionally, along my academic journey. First and foremost, I would like to thank Dr. Prathap Parameswaran for the mentorship, guidance, and support provided throughout my PhD. This has been a long journey and I am proud to be your first PhD graduate! I would also like to acknowledge my first research advisor, Dr. Monica Palomo, who welcomed me into my very first research group and set me on this path by connecting me with Dr. Parameswaran and Kansas State University (KSU). Though I did not know it at the time, Dr. Patrick Evans was also instrumental in my decision to come to Kansas State University, as it was his pilot-scale project that won me over in the end. I thank Dr. Evans for his leadership during

the project and his continued mentorship and support, even joining my committee at the expense of his own retirement.

This research would not have been possible without the help of my colleagues, with whom I shared many laughs, unreasonably late nights and early mornings, and drawn-out conversations with wildly imaginative non-sequitur tangents. Zoe Ao, Keri Brown, Christopher Chiu, Bernadette Drouhard, Mason Ericson, Niloufar Fattahi, Priyasha Fernando, Evan Heronemus, Marleigh Hutchinson, Kristen Jones, Weston Koehn, Amy Kowalczewski, Danielle Larson, Haripriya Naidu, Chad Olney, Tyler Penfield, Emily Randig, Barry Schmidt, Caitlin Swope, Jose Trejo, and Kurtis Wicka, thank you for your friendship. Special thanks to Arvind Kannan, with whom I shared the most growth with during my PhD journey.

The opportunity to continue developing myself as an artist was an integral part of my PhD. For this, I would like to thank Dr. Susan Maxwell and the K-State bassoon studio for helping further my musical journey. Continuing to understand the art of movement through breakdancing with the Feral Catz Crew, shoutout to Lane Tiziu Porter and coach Damian Hilton, and through martial arts with Cole Fowles at the Combative Sports Center has helped me to keep my body as sharp as my mind.

Last but not least, I would like to thank all of my friends and family for being a constant sounding board and support network for my PhD work and beyond. To my close friends Pyotr Towne, Timothy Young, Chung Chan, and all the members of GGLL, thank you for all of the conversations and late-night games; you all have helped me learn to remain composed during times of great hardship and accept responsibility for when we cause our own misfortune. Words are not needed to affirm my appreciation of my greatest supporter on this journey my brother, Dr. Kahui Lim, who constantly reminded me to always be improving my writing and to not let

go of pursuing my artistic endeavors. And finally, I would like to acknowledge my parents, Sutoyo and Darmawati Lim, who I hope I have made proud. The dedication and diligence that went into this work are the result of the ethics and support given to me by my parents, without which this research would not have been possible.

Chapter 1 - Background and Literature Review

1.1 Introduction

As the human population continues to grow, increasing stress is placed on the food-energy-water nexus, as the effects of water scarcity, greenhouse gas emissions, and the threat of food shortages loom (Lu et al. 2015; Lundin et al. 2000; Mo and Zhang 2013). Understanding the dire consequences if left unaddressed, the United Nations (UN), the National Academy of Engineering (NAE), and the American Society of Civil Engineers (ASCE) have each issued challenges for the 21st century to improve infrastructure to provide access to potable water, improve sanitation and public health, master the nitrogen cycle, increase the sustainability of energy production, and combat climate change (Becerik-Gerber et al. 2014; Lu et al. 2015; Malik et al. 2015; NAE 2017). Wastewater treatment lies at the intersection of these goals.

Wastewater has increasingly been viewed as a sustainable resource that is critical in closing the food-energy-water nexus loop and creating a circular economy (Mo and Zhang 2013; Molina-moreno et al. 2017; Nghiem et al. 2017; Nielsen 2017). As climate change continues to exacerbate issues of water scarcity, wastewater reclamation and reuse unlocks a relatively untapped source of fresh water (Friedler 2001; Marlow et al. 2013; Tram et al. 2014). In addition to helping meet water demands, wastewater contains other potentially valuable resources that can be recovered, such as nutrients and chemical energy stored in the carbon (Guest et al. 2009; McCarty et al. 2011; Rittmann et al. 2011; Shizas et al. 2004). Efforts to capture the value latent in wastewater have spurred the development of technologies that embody the resource-from-waste paradigm shift.

Aerobic processes are currently the predominant wastewater treatment platform worldwide, with most installations based on the conventional activated sludge process (Gouveia

et al. 2015; Silvestre et al. 2015). While activated sludge has proven to be a robust process that can consistently meet discharge limits under a variety of environmental conditions, it is fundamentally designed for meeting end-of-pipe discharge limits, rather than resource recovery (Ahansazan et al. 2014; Nghiem et al. 2017). The common biological nutrient removal (BNR) strategies that were developed from the activated sludge process, such as the Bardenpho or A²O processes, can achieve low nutrient concentrations in the effluent, but leave few opportunities for recovery; the nitrification-denitrification process results in inert N₂ gas, and the phosphorus removal occurs when the phosphorus accumulating organisms leave the system as wasted sludge. (Metcalf et al. 2004; Wang and Chu 2016). Furthermore, aeration is an energy intensive process, consuming over 50% of the total energy required in a wastewater treatment plant using activated sludge to biologically oxidize pollutants (Liao et al. 2006; McCarty et al. 2011). These characteristics suggest that aerobic technologies are not the ideal solution to the 21st century engineering challenges facing environmental engineers.

As conventional aerobic technologies, such as activated sludge, are not suited to meet these objectives, significant research interest has been given to developing anaerobic technologies (Gerardo et al. 2013; Lin et al. 2013). Anaerobic biological processes have multiple advantages over their aerobic counterparts because of their metabolic processes. One of my main drivers behind anaerobic treatment is the possibility of energy neutral or energy positive operation (McCarty et al. 2011; Smith et al. 2014). The energy footprint of anaerobic systems is more favorable not only because they can eliminate the energy-intensive aeration process, but also because anaerobic organisms can produce a methane-rich biogas that can be used in co-generation for energy production (Crone et al. 2016; McCarty et al. 2011).

The elimination of aeration also provides an opportunity to recover nutrients in useful forms, where typical biological nutrient removal focuses just on achieving low effluent concentrations (Ashley et al. 2011; El-Shafai et al. 2007). By eliminating aeration, the nutrients tend to remain in more reduced forms which can be better captured in recovered nutrient products for beneficial reuse, including for land application, such as with adsorbed ammonia on clinoptilolite or precipitated minerals such as struvite ($\text{NH}_4\text{MgPO}_4 \cdot 6\text{H}_2\text{O}$), which simultaneously recovers both ammonia and phosphate (De-Bashan and Bashan 2004; Du et al. 2005; Polat et al. 2004; Ueno and Fujii 2001).

Anaerobic processes have several drawbacks that have limited their implementation as the primary liquid stream treatment process. Historically, purely anaerobic treatment systems have been relatively uncommon for municipal wastewater treatment due to their slower kinetics (Metcalf et al. 2004; Rittmann and McCarty 2001). Slow growth rates are advantageous because they produce less sludge compared to activated sludge processes, but also pose a challenge due to longer startup times, biomass loss via washout, and difficulties meeting effluent discharge requirements at lower hydraulic retention times (HRT) (Chong et al. 2012; Galib 2014; Metcalf et al. 2004; Rittmann and McCarty 2001). Additionally, the treatment performance of anaerobic systems' susceptibility to lower temperatures has long been considered a challenge, as the metabolic activity of the anaerobes, particularly the methanogens, slows (Cavicchioli 2007; Ferry 2012). This has implications not just on treatment efficiency, but also on the energy balance. Typically, anaerobic processes require external heating to maintain mesophilic (25-40°C) or thermophilic (45°C and above) temperatures, which are favorable for methanogens (Kocadagistan and Topcu 2007; Metcalf et al. 2004; Xie et al. 2010). Additionally, as temperatures decrease, the fraction of methane that remains in the dissolved phase increases, and

requires further energy input to treat and recover (Crone et al. 2016; Lim et al. 2019). The application of external heating can ameliorate some of these effects, but the additional energy cost may limit the ability to achieve energy neutral operation (McCarty et al. 2011; Smith et al. 2013). An ideal anaerobic wastewater treatment process would be one that can maintain treatment performance under a broad range of temperatures with little to no external heating costs.

Another relatively recent advancement in the realm of wastewater treatment is the membrane bioreactor (MBR). Membrane bioreactors combine biological wastewater treatment, either aerobic or anaerobic, with membrane filtration technology in order to achieve a higher quality of treatment in a compact building footprint (Judd 2008). Where conventional biological wastewater treatment relies on large clarifiers and sedimentation to separate the sludge in the mixed liquor from the treated water, membrane filtration provides a physical screening mechanism that is notable for the virtually complete retention of biomass, resulting in a superior quality effluent with very low suspended solids, often fit for reuse purposes (Cheryan 1998; Hoinkis et al. 2012; Judd 2008). Filtration using membranes involves the physical separation of particulate and colloidal materials, along with a fraction of dissolved constituents from a liquid (Cheryan 1998; Metcalf et al. 2004). The membrane's pore size determines the size of particles rejected; membrane processes are often classified by pore size and selected based on removal criteria, as shown in Table 1.1. Typically, membranes are selected for the largest pore size that fits their operating objectives, as smaller pores are more prone to blockage. For this reason, microfiltration (MF) ultrafiltration (UF) membranes have proven to be the most popular choice for MBR applications.

Table 1.1 A table showing the different pressure driven membrane processes and their general characteristics. PE = Polyethylene, PP = polypropylene, PES = polyethersulfone, PTFE = polytetrafluoroethylene, PVDF = polyvinylidene difluoride, CA = cellulose acetate, TFC = thin-film composite. Adapted from (Metcalf et al. 2004).

Membrane Process	Pore Structure and Pore size	Typical operating range (μm)	Typical constituents removed	Materials
Microfiltration	Macropores > 50 nm	0.08 - 2.0	Suspended solids, turbidity, protozoan cysts and oocysts, some bacteria and viruses	Acrylonitrile, ceramic, PE, PP, PES, PTFE, PVDF, Nylon
Ultrafiltration	Mesopores 2 - 50 nm	0.005 - 0.2	Macromolecules, colloids, most bacteria, some viruses, proteins	Aromatic polyamides, ceramic, CA, PE, PP, PS, PVDF, Teflon
Nanofiltration	Micropores < 2 nm	0.001 - 0.01	Viruses, small molecules, some hardness	Aromatic polyamide, cellulosic, PE, PES, PVDF, TFC
Reverse Osmosis	Dense < 2 nm	0.0001 - 0.001	Very small molecules and ions (including sulfates, nitrate, sodium), color, hardness,	Aromatic polyamide, cellulosic, PE, TFC

While aerobic MBRs have gained significant popularity at various scales, being used to successfully treat a wide variety of waste streams and producing reuse quality effluent, anaerobic membrane bioreactor (AnMBR) technology still has yet to achieve widespread adoption (Hara et al. 2005; Liao et al. 2006). Nevertheless, AnMBRs have generated significant research interest, due to the unique advantages for sustainability conferred by the anaerobic biological treatment paired with the physical treatment provided by membrane filtration, which has been shown to compensate for some of the traditional shortcomings of anaerobic treatment (Evans et al. 2018; Lim et al. 2019; Lin et al. 2013; Smith et al. 2013).

1.2 Literature Review

1.2.1 Anaerobic Membrane Bioreactors

Anaerobic membrane bioreactors (AnMBRs) are a treatment technology that pair anaerobic biological treatment with membrane filtration and gain the benefits of both for a unique combination of biological and physical treatment (Evans et al. 2018; Lin et al. 2013). As an anaerobic technology, AnMBRs possess several potential advantages over aerobic treatment processes in terms of energy balance, nutrient recovery opportunities, and minimizing sludge production. In addition to reducing the energy consumption by avoiding the need for aeration, anaerobic treatment can produce methane-rich biogas that can be combusted for energy recovery, which can push the system to energy neutrality or even energy positive operation (Batstone and Viridis 2014; Hagos et al. 2017; Smith et al. 2014).

The use of membranes compensates for the slow growth rate typical of anaerobic treatment of wastewater. The incorporation of membranes allows for the complete retention of biomass, producing an effluent virtually free of suspended solids, and allowing for the decoupling of HRT and solids retention time (SRT) (Liao et al. 2006; Skouteris et al. 2012). This allows the system to maintain high SRT while operating at low HRT, which helps AnMBRs achieve high rate treatment of chemical oxygen demand (COD) and 5-day biochemical oxygen demand (BOD₅) (Lin et al. 2013; Smith et al. 2014). These characteristics have led to their successful application in a variety of settings, from industrial treatment to domestic wastewater treatment (Chen et al. 2016; Liao et al. 2006; McCarty et al. 2011). The versatility and effectiveness of AnMBRs as a treatment technology has been demonstrated for a wide variety of applications as shown in Table 1.2.

Table 1.2 A summary of various AnMBR performance parameters and their configurations for various studies treating domestic, and industrial wastewaters. WW = wastewater. Membrane materials: CA = cellulose acetate, PE = polyethylene, PES= Polyethersulfone, PP = polypropylene, PVDF = polyvinylidene difluoride. Membrane processes: MF = microfiltration, UF = ultrafiltration

Reactor Configuration	Scale	Exclusion size, Membrane Material and Process	Physical Fouling Control	Influent	Temp. (°C)	HRT	Flux (LMH)	Influent COD (mg/L)	Reference
	Reactor Volume (L)		Chemical Fouling Control			SRT	TMP (bar)	COD Removal (%)	
Sidestream	Bench	0.03 µm, PE, UF	Membrane relaxation	Domestic WW	Ambient: 12°C to 27°C	4 h to 6 h	5 LMH to 10 LMH	100 mg/L to 2600 mg/L	(Wen et al. 1999)
	8.8 L		Chemical cleaning: 5% NaClO			150 d	Up to 0.7 bar	92%	
Sidestream	Bench	0.2 µm, PP, MF; 0.14 µm, Zirconia, MF	Water backflushing	Alcohol distillery WW	55°C	13 h	140 LMH to 400 LMH	400 mg/L	(Kang et al. 2002)
	5 L		Chemical cleaning: HCl, pH 2 and NaOCl			∞	0.6 bar	> 90%	
Sidestream	Pilot	20 kDa to 70 kDa, PES, UF	Backflushing	Food processing WW	37°C	60 h	13.1 LMH to 18.9 LMH	13,000 mg/L	(He et al. 2005)
	400 L		Chemical cleaning: 0.5% NaOH			50 d	2 bar	81% to 94%	
Sidestream	Bench	0.1 µm, PES, UF	Pump recirculation	Sewage sludge	70°C	8 d to 943 d	26 LMH	78,000 mg/L to 94,000 mg/L	(Liew Abdullah et al. 2005)
	20 L		-			16.1 d to 1250 d	2 bar	97% to 99%	
Sidestream	Bench	100 kDa, UF	Pump recirculation	Domestic WW	37°C	15 h	6 LMH to 14 LMH	685 mg/L	(Saddoud et al. 2007)
	50 L		-			-	1 to 2 bar	94%	
Sidestream	Bench	0.2 µm, CA, MF	Manual valve for TMP control	Domestic WW	35°C	16.67 h	450 LMH	480 mg/L	(Kocadagistan and Topcu 2007)
	5 L to 15 L		-			-	0.2 bar to 1.25 bar	> 96%	

Table 1.2 continued. A summary of various AnMBR performance parameters and their configurations for various studies treating domestic, and industrial wastewaters. WW = wastewater. Membrane materials: CA = cellulose acetate, PE = polyethylene, PES= Polyethersulfone, PP = polypropylene, PVDF = polyvinylidene difluoride. Membrane processes: MF = microfiltration, UF = ultrafiltration

Submerged	Bench	70 kDa, PVDF, MF	Biogas sparging at 0.75 LPM Relaxation, Water backflushing	Pulp and paper mill WW	37°C; 55°C	-	7.2 LMH; 2.4 LMH	10,000 mg/L	(Lin et al. 2009)
	10 L		-			230 d	Up to 0.3 bar	97% to 99%	
Submerged in Sidestream Tank	Pilot	38 nm, PES, UF	Permeate backflushing, gas sparging, Membrane relaxation	Domestic WW	35°C; 20°C	17 h to 26 h	7 LMH	630 mg/L	(Martinez-Sosa et al. 2011)
	350 L		-			680 d	0.2 bar	90%	
Submerged	Bench	0.2 µm, PES, MF	Biogas sparging: 4.7 LPM, Permeate backflushing	Synthetic WW (SYNTHES); Domestic WW	15°C	16 h	3.5 LMH	440 mg/L	(Smith et al. 2013)
	5 L		-			300 d	0.45 bar	92%	
Submerged in Sidestream Tank	Pilot	0.05 µm, UF	Pump mixing, Permeate backflushing, Membrane relaxation Biogas sparging	Domestic WW	33°C	6 h	8 LMH to 13 LMH	350 mg/L to 540 mg/L	(Giménez et al. 2011)
	2500 L		-			70 d	0.08 bar	87%	
Sidestream	Pilot	0.04 µm, PVDF, UF	Membrane relaxation, Biogas sparging	Domestic WW	22°C	8.5 h	4 LMH to 17 LMH	224 mg/L	(Dagneu et al. 2011)
	630 L		Chemical cleaning			80 d to 100 d	0.03 bar	79%	
Sidestream, GAC Fluidized	Pilot	0.03 µm, PVDF, UF	GAC Fluidization, Membrane relaxation	Domestic WW	Ambient: 8°C to 30°C	4.6 h to 6.8 h	2 LMH to 11 LMH	207 mg/L to 424 mg/L	(Shin et al. 2014)
	990 L		-			6.2 d to 36 d	0.1 bar to 0.4 bar	94%	

Table 1.2 continued. A summary of various AnMBR performance parameters and their configurations for various studies treating domestic, and industrial wastewaters. WW = wastewater. Membrane materials: CA = cellulose acetate, PE = polyethylene, PES= Polyethersulfone, PP = polypropylene, PVDF = polyvinylidene difluoride. Membrane processes: MF = microfiltration, UF = ultrafiltration

Sidestream	Pilot	0.04 μm , PVDF, UF	Biogas Sparging, Pump recirculation	Domestic WW	23°C	8.5 h	13.7 LMH	383 mg/L	(Dong 2015)
	630 L		Chemical cleaning: 2000 mg/L citric acid 2000 mg/L NaOCl			40 d	0.02 bar to 0.22 bar	92%	
Submerged	Bench	0.2 μm , PES, MF	Biogas sparging: 3 LPM, Permeate backflushing	Domestic WW	3°C to 15°C	16 h to 32.2 h	1.2 LMH to 3 LMH	440 mg/L	(Smith et al. 2015)
	7 L		-			300 d	-	> 95%	
Submerged	Bench	0.4 μm , PVDF, UF	Backflushing	Synthetic WW	37°C	47 d ^{α}	54 LMH	- ^{α}	(Berkessa et al. 2018)
	94 L		-			∞ ^{α}	0 bar to 0.45 bar	- ^{α}	
Sidestream, GAC Fluidized	Pilot	0.03 μm , PVDF, UF	GAC Fluidization, Membrane relaxation	Domestic WW	Ambient: 13.1°C to 32°C	3.9 h	7.9 LMH	210 mg/L	(Evans et al. 2018, 2019)
	1760 L		Chemical cleaning: 750 mg/L NaOCl 2000 mg/L citric acid			11 d	0.01 bar to 0.6 bar	90%	
Sidestream	Pilot	0.03 μm , PVDF, UF	Biogas Sparging Membrane relaxation	Domestic WW	25°C to 30°C	24 h to 60 h	15 LMH to 23.5 LMH	1235 mg/L	(Robles et al. 2020)
	40 m ³		-			70 d to 190 d	0.05 bar to 0.475 bar	90%	
Staged Anaerobic Fluidized MBR	Pilot	0.04 μm , PVDF, UF	Biogas Sparging Membrane relaxation	Domestic WW	Ambient: 18.4°C to 24.7°C	5.3 h to 10 h	6.5 LMH to 12.3 LMH	720 mg/L to 893 mg/L	(Shin et al. 2021)
	4500 L		Chemical cleaning: 500 mg/L NaOCl 2000 mg/L citric acid			21.6 d to 45.1 d	0.08 bar to 0.28 bar	87% to 90%	

α : Berkessa et al. was a fouling specific study operated at high HRT to induce harsh fouling conditions

Historically, AnMBRs have been focused on treating industrial and food processing waste streams because of their characteristically higher temperatures compared to domestic wastewater, which minimizes the amount of energy required for external heating for mesophilic or thermophilic operation, and higher organic loading rates which contributes to higher methane production and energy recovery potential (Christian et al. 2011; Galib et al. 2016; Gao et al. 2011; Skouteris et al. 2012). The high rate treatment of high strength wastewater and its low footprint have made the AnMBR an increasingly popular choice for industrial wastewater treatment (Galib et al. 2016). Adoption of AnMBRs for municipal wastewater treatment has been slower. Compared to high strength industrial wastewaters, the more dilute municipal wastewaters have less energy potential, which makes energy neutrality more difficult to achieve. Additionally, the typically cooler influent temperatures encountered while treating domestic wastewater led to questions regarding the viability of anaerobic treatment at lower temperatures.

For AnMBRs to gain widespread adoption for domestic wastewater treatment, the system must be robust and able to perform under a range of temperatures, ranging from the comfortable mesophilic range down to the psychrophilic range, which has traditionally been seen as a barrier for anaerobic treatment technologies (Ho and Sung 2010; Smith et al. 2015). The treatment performance of anaerobic systems typically decreases with temperature as the metabolism of anaerobes, particularly methanogens, slows down (Cavicchioli 2007; Ferry 2012; Rittmann and McCarty 2001). While AnMBRs at the bench scale have successfully treated domestic wastewaters under mesophilic and even psychrophilic conditions as low as 3°C, the majority of these studies have been under fixed temperature conditions (Gouveia et al. 2015; Liao et al. 2006; Lin et al. 2013; Smith et al. 2013, 2015). To achieve energy neutral operation, external heating needs to be minimized, which would require AnMBRs to operate under ambient

conditions. Ambient conditions potentially pose another challenge to stable treatment performance, as the microbial community has been observed to shift significantly in response to temperature changes (Gao et al. 2011; Lei et al. 2018; Smith et al. 2015). While most pilot scale AnMBRs are operated under ambient conditions, thus far, few have been operated under psychrophilic conditions (Shin and Bae 2018). However, good COD removal (~90%) was achieved under psychrophilic conditions in two ambient temperature studies using a GAC-fluidized AnMBR, indicating that the technology has potential to overcome the low temperature challenge (Evans et al. 2018; Shin et al. 2014).

Lower temperatures can have a significant impact on the energy balance of AnMBRs as well. As the metabolism of methanogens slows in response to the lower temperatures, the rate of methane production also decreases, which negatively impacts the energy balance. In addition to the decrease in overall methane production, more of it is found dissolved in the permeate, rather than in the easily recoverable gaseous form, requiring additional energy input to treat (Crone et al. 2016; Lim et al. 2019). If left untreated, the dissolved methane could escape into the atmosphere and act as a greenhouse gas 25 times more potent than carbon dioxide, making dissolved methane a significant issue for AnMBRs, as it has the potential to overturn its benefits to the environment from both an energy and a greenhouse gas emissions perspective (Crone et al. 2016; Liu et al. 2014).

While nutrient recovery from anaerobic streams has received significant amounts of research attention, its demonstration in AnMBR literature has been lacking. Thus far, studies involving nutrient recovery in AnMBRs has generally been concerned with the concentrations available in the membrane permeate (Pretel et al. 2015; Prieto et al. 2013). The methodology employed by these studies suggest that the permeate can either be used for direct application as

fertilizer or undergo further treatment for capture in other useful forms, which tends to gloss over the challenges encountered when developing actual nutrient recovery techniques for use with AnMBR permeate. For example, while the coagulation-flocculation-sedimentation is a well-documented process for wastewater treatment, there are several challenges to its application to AnMBR permeate, where the presence of phosphate was accompanied by high sulfide concentrations, necessitating the use of more coagulants (Lim et al. 2019; Metcalf et al. 2004). Furthermore, one downside to the direct application of permeate or the coprecipitation of ammonia and phosphate as struvite is that the nutrients can only be applied in fixed ratios. As such, the successful demonstration of recovering useful nutrient products from AnMBR permeate warrants further investigation.

AnMBRs also inherit the central problem that plague membrane-based processes: membrane fouling. Because membranes represent up to 50% of the capital expenditure of new MBR installations, maintaining their performance is critical to ensure that membrane processes are economically feasible (Boyle-Gotla et al. 2014). Membrane performance is usually measured in terms of flux and transmembrane pressure (TMP), or permeability. Flux is defined as the flowrate of permeate through the membrane pores per area of membrane, with typical units of liters per meter squared per hour (LMH) and transmembrane pressure represents as the driving force in ultrafiltration and is a measure of the pressure differential across the membrane, typically measured in kPa (Metcalf et al. 2004). Permeability, the ratio of flux to TMP, often represented in LMH/bar, is often used to reflect both flux and TMP in a single parameter (Judd 2010; Metcalf et al. 2004). The deterioration of membrane performance is often measured by a decrease in permeate flux at constant a TMP, an increase in TMP at a constant flux, or

decreasing permeability. The fouling of membranes remains a key challenge impeding the widespread adoption of AnMBR technology (Skouteris et al. 2012; Xu et al. 2020a).

1.2.2 Membrane Fouling

Membrane fouling refers to a decrease in membrane performance due to the accumulation of material either on the membrane surface or inside the membrane pores, resulting in reduced membrane performance (Boyle-Gotla et al. 2014; Meng et al. 2009a). Foulants are typically categorized as biological, organic, or inorganic, and are influenced by the system's operational parameters, such as SRT, HRT, flux, and fouling control measures, as well as influent characteristics (Meng et al. 2009a). Traditionally, organic foulants have been seen as the primary contributor to fouling, with particular emphasis on humic substances, soluble microbial products (SMP) and extracellular polymeric substances (EPS), but recent studies have suggested the importance of fine inorganics in forming an irreversible foulant matrix (Dagnew et al. 2012; Liu et al. 2019a; Teng et al. 2019). The interactions between the different foulants and system operating conditions lead to different fouling behaviors being observed in different systems.

Fouling behavior is broadly classified into reversible fouling, which can be managed through various physical or chemical maintenance strategies, and irreversible fouling, which is permanent. Reversible fouling can be further classified into mechanically removable fouling, which can be reversed by physical means, and mechanically irremovable, which require chemical treatment (Di Bella et al. 2018; Meng et al. 2009a). While these terms describe the behavior of the foulants in response to management strategies, they do not provide mechanisms for the occurrence of fouling. Several mechanisms have been proposed to describe how fouling occurs on the membranes, with cake layer formation and pore constriction being the two most

popular models (Boyle-Gotla et al. 2014; Jiang et al. 2003; Wang and Tarabara 2008).

Concentration polarization has also been noted to be an inherent fouling mechanism associated with membrane filtration, but has largely been categorized as reversible, particularly by providing high cross flow velocities (Maaz et al. 2019; Skouteris et al. 2012).

Cake layer formation describes the accumulation of solids at the membrane surface to the point where it blocks pores, and has been hypothesized as the predominant fouling mechanism, particularly during operation at higher fluxes (Aslam et al. 2017; Di Bella et al. 2018; Boyle-Gotla et al. 2014). The constituents of the cake layer in AnMBR systems has been primarily biosolids and their associated polysaccharide and proteinaceous materials (Jin et al. 2013; Liu et al. 2019a). Despite being considered the dominant fouling mechanism, cake layer formation is generally considered easier to remove than pore constriction, particularly when mechanical cleaning strategies are employed to shear the foulant cake from the membrane surface, preventing its accumulation (Di Bella et al. 2018; Jiang et al. 2003). The presence of divalent and trivalent metal cations can cause the cake layer to form a compressed gel via chelation with biopolymers, leading to irremovable or irreversible fouling and necessitating the use of chemical cleans for membrane performance recovery, however (Liu et al. 2019a). This interaction highlights the need to understand the contribution of both the organic and inorganic foulants.

Pore constriction is believed to occur due primarily to the adsorption of colloidal or soluble biopolymers, for which we use humic substances as proxies, and the precipitation of inorganics within the pores of the membrane (Charfi et al. 2012; Wang and Tarabara 2008; Zheng et al. 2014). While cake layer filtration develops quickly, it is believed that pore clogging is primarily responsible for the long term, irreversible fouling experienced by membranes, particularly for UF membranes, and will occur inevitably, even during low flux operation (Aslam

et al. 2017; Wang and Tarabara 2008). Because the deposition is occurring inside the membrane pores, mechanical cleaning by imparting shear at the membrane surface is ineffective, so chemical cleaning and backwashing is required to reach and manage the foulants (Liu et al. 2019a; Wang and Tarabara 2008). While often presented as distinct mechanisms, both cake layer accumulation and pore constriction may occur simultaneously in real operation. It has been hypothesized that localized pore constriction may cause conditions that lead to the initial formation of the cake layer, which suggests that the two mechanisms are linked (Ognier et al. 2004; Wang and Tarabara 2008).

1.2.3 Fouling Control Methods

Fouling management strategies usually target biological, organic, or inorganic foulant through a combination of physical and chemical means. Physical management strategies typically work by imparting shear at the membrane surface to scour and attack the cake layer, preventing solids accumulation (Boyle-Gotla et al. 2014; Judd 2010). The most common methods of imparting shear are gas-sparging, during which gas is diffused through a plate diffuser underneath the membranes and mechanically shear the cake layer, and pump recirculation, where the pumps are operated at higher rates to provide sludge mixing in the membrane tank (Judd 2010).

Recently, the use of scouring agents as biological carriers and fouling control agents in sidestream systems has become a popular option to consider for AnMBR operation in a fluidized bed bioreactor (FBBR) configuration (Aslam et al. 2017; Evans et al. 2019). Scouring agents can shear the foulant cake layer accumulating on the membrane surface when recirculated and reduce the amount of pumping energy required to supply high shears, making low-energy physical fouling controls possible (Aslam et al. 2017; Evans et al. 2018). The use of scouring

media as biomass carriers in FBBRs also has the advantage of being an attached growth process, where bacteria will form biofilms on the scouring media, becoming more resilient to temperature fluctuations, and variable and shock influent loadings. The use of granular activated carbon (GAC) in aerobic FBBRs has been extensive, and its applicability has been extended to AnMBR operation as well (Kim et al. 2010; Rogalla and Bourbigot 1990). In one study, a GAC-fluidized AnMBR was able to achieve the same organics removal rates at a 65% lower HRT compared to its gas-sparged suspended growth counterpart while consuming half as much energy (Evans et al. 2019). During long term operation, however, the abrasion of GAC particles can potentially clog the membranes and contribute to membrane fouling through irreversible pore blocking, which would make it impractical to operate such a system at a full scale without additional developments (Evans et al. 2018, 2019).

Most physical cleaning methods are difficult to employ within the pores, necessitating the use of backwashing to address pore clogging (Rabuni et al. 2015). There are many different organic and inorganic species that can be adsorbed in the pores, often necessitating the use of a combination of various cleaning agents in tandem: commonly, HCl, H₂SO₄, and citric acid have been widely used to treat inorganics, NaOH and NaOCl have been used to treat organics and biofoulants, and various additives such as ethylenediamine tetraacetic acid (EDTA) and ammonium bifluoride have been added for chelating effects for the removal of metals (Lee et al. 2001; Porcelli and Judd 2010).

Because there are virtually endless numbers of operational parameters that can be adjusted that would have an impact on membrane fouling, isolating key parameters such as SRT, HRT, flux, and physical and cleaning controls for study has been common. Changes to these parameters for fouling control may have impacts on treatment performance, however. Thus,

there are practical tradeoffs to consider when optimizing fouling management of an AnMBR. In addition to membrane performance, optimization must include treatment performance as well as the economics of operation in order to have a viable system. This highlights the importance of designing and implementing an effective fouling control strategy.

As fouling has been the central problem for AnMBRs, most of the different configurations have been investigations into different fouling control strategies. The two most popular process configurations, the submerged systems and the sidestream systems, are differentiated by how the membrane module is integrated with the bioreactor and how they physically manage fouling. Submerged MBRs set the membranes directly in the main bioreactor and rely on gas-sparging to provide shear at the membrane surface and prevent solids deposition. Sidestream MBRs have the membranes in a tank separate from the bioreactor and rely on pump circulation between the two to impart shear at the membrane surface. While the additional pumping at rates high enough to provide sufficient shear in sidestream MBRs mean that their energy demands are higher, they offer several advantages over submerged MBRs, such as being able to chemically clean the membranes without exposing the biomass to the chemicals, increased hydrodynamic control, and easier access to the membranes for maintenance and replacement when necessary (Judd 2010).

While membrane fouling can incur significant costs in membrane replacement if left unmanaged, controlling fouling can be an expensive and energy intensive process; fouling management has consumed up to 50% of the total energy for AnMBR operation (Aslam et al. 2017; Lim et al. 2019). Furthermore, the heavy use of chemical cleaning to manage fouling can shorten the life of membranes while simultaneously increasing consumable chemical costs (Rabuni et al. 2015). As such, there is a need to characterize the foulants within AnMBR

systems in order to develop more optimal, targeted fouling management strategies. A more detailed review of fouling characterization methods can be found in chapter 5.

1.2.4 Critical Flux Hypothesis

Flux has been a key parameter in membrane fouling studies, particularly since Field et al. (1995) set forth the critical flux hypothesis. The critical flux hypothesis suggests that there theoretically exists a “critical flux,” below which fouling does not occur; this is known as the “strong form” of the critical flux hypothesis (Field et al. 1995). The strong form implies that no solids deposition is occurring on the membrane surface and that solutes are not being adsorbed in the pores. However, since fouling has still been observed even during low flux operations, a “practical form” of the critical flux hypothesis has developed. The practical form states that a critical flux exists that allows for the operation without the need for membrane cleaning for extended periods of time (> 3 weeks) (Cho and Fane 2002; Judd 2010). Because chemical cleans target pore fouling, a lack of chemical cleaning under subcritical flux operation in the practical form of the critical flux hypothesis would suggest that pore constriction would be negligible in the short term and that solids deposition onto the membrane surface is the main mechanism that needs to be managed.

Virtually any operating parameter that affects the biomass can also have an impact on fouling mechanisms. For example, SRT and HRT, are also known to have a significant impact on fouling mechanisms, as they change the behavior of the microorganisms in the system and the SMP and EPS composition of the sludge, which, in turn, can affect their propensity for deposition (Huang et al. 2010; Meng et al. 2009a). Because of this, it is important to note that the critical flux is, itself, a function of operating parameters that affect the properties of the biosolids and their deposition, and that there may be many “critical” parameters that have a

threshold beyond which fouling occurs (Fox and Stuckey 2015). The most prominent example is the critical sparging rate hypothesis, which suggests that at a given flux there theoretically exists critical gas-sparging rate that can provide enough shear at the membrane surface to prevent solids deposition (Fox and Stuckey 2015; Meng et al. 2009a).

Chapter 2 - Research Hypotheses and Objectives

The main objectives of the proposed research are to demonstrate the viability of AnMBRs to achieve holistic treatment of domestic wastewater and to fundamentally characterize AnMBR foulants with an aim to develop proactive strategies to sustain membrane performance. We categorize the following specific objectives:

1. Evaluate gas-sparged AnMBR performance at the pilot- and lab-scales.
 - A. Verify the viability of AnMBRs as a domestic wastewater treatment technology in terms of treatment performance (BOD₅ and COD) as well as for nutrient and energy recovery.
 - B. Design and construct a lab scale AnMBR that allows for the dynamic and live sampling of membrane fibers to mechanistically understand membrane fouling.
 - C. Perform continuous evaluation of membrane fouling through dynamic measurement of conventional parameters (TMP, bioreactor solids, maintenance clean etc.) along with targeted parameters (sCOD).
2. Develop a framework for understanding membrane foulants in the lab scale AnMBR that encompasses direct measurements on the attached foulants, the impact of the bulk bioreactor mixed liquor, and observations in the membrane permeate.
 - A. Use end-of-operation membrane autopsies to characterize the foulant cake layer.
 - i. Develop SMP and EPS extraction and analysis protocols suitable for use on the foulant cake.

- B. Develop viable methods for dynamic monitoring of suspected foulants during AnMBR operation.
 - i. Fluorometry, SMP and EPS extraction and analysis, and sCOD are proposed as promising tools, either alone or in combination.
3. Synthesize conclusions from both end-of-life analysis data and proactive monitoring data to elucidate the nature and behavior of foulants and prescribe predictive protocols for fouling management.

These objectives will be aimed at evaluating the following hypotheses:

1. Fouling mechanisms and propensity are dictated primarily by the conditions of AnMBR operation.
 - a. Operation above the critical flux leads to fouling events primarily controlled by solids deposition. Physical management strategies will be most effective in this mode of operation.
 - b. Operation below the critical flux leads to pore constriction due to adsorption of soluble organic matter and inorganic scaling. Chemical backwashing will be most effective in managing this fouling mechanism.
2. Fouling events are disproportionately affected by colloidal proteinaceous materials of microbial origin.

Chapter 3 - Performance of a Pilot Scale Gas Sparged AnMBR for Holistic Wastewater Treatment

This section has been published in *Environmental Science and Technology*. The citation is as follows:

Lim, K., Evans, P. J., and Parameswaran, P. (2019). “Long-Term Performance of a Pilot-Scale Gas-Sparged Anaerobic Membrane Bioreactor under Ambient Temperatures for Holistic Wastewater Treatment.” *Environmental Science & Technology*, research-article, American Chemical Society, 53(13), 7347–7354.

A pilot scale gas-sparged AnMBR demonstration plant, located in Ft. Riley, Kansas, with dissolved methane and nutrient recovery units, was commissioned under the Department of Defense’s Environmental Security Technology Certification Program (ESTCP). AnMBR treatment performance was evaluated based on its ability to produce an effluent quality that meets the EPA secondary treatment requirements of 30 mg/L 5-day biochemical oxygen demand (BOD₅), under ambient temperature conditions through seasonal variations. The system also was the first AnMBR to integrate dissolved methane recovery with a membrane contactor at a pilot scale to simultaneously reduce greenhouse gas emissions as well as recover the methane for energy generation. A novel nutrient recovery strategy from the AnMBR permeate was implemented for phosphorus and sulfide capture through coagulation-flocculation-sedimentation (CFS), followed by ammonia capture through an ion-exchange (IX) column using clinoptilolite media; neither of the processes have previously been applied to AnMBR permeate in an integrated process train. By treating the organics, capturing both gaseous and dissolved methane for energy generation, and recovering nutrients, this study assesses the potential role of AnMBRs as a technology for the holistic treatment of domestic wastewater.

3.1 Materials and Methods

3.1.1 AnMBR Startup and Process

The AnMBR was inoculated with 1360 L of mesophilic anaerobic digester sludge obtained from the Oakland Wastewater Treatment Plant in Topeka, Kansas with a volatile suspended solids concentration of 12500 mg/L and a total suspended solids concentration of 19000 mg/L. The inoculation was done by filling the bioreactor with nitrogen gas, then displacing the nitrogen with the sludge using a diaphragm pump, ensuring that anaerobic conditions were maintained throughout the inoculation process. The reactor was then fed with screened municipal wastewater from Ft. Riley, Kansas, marking the beginning of the AnMBR operational period.

The process flow diagram can be found in Figure 3.1, along with the design basis in Table 3.1.

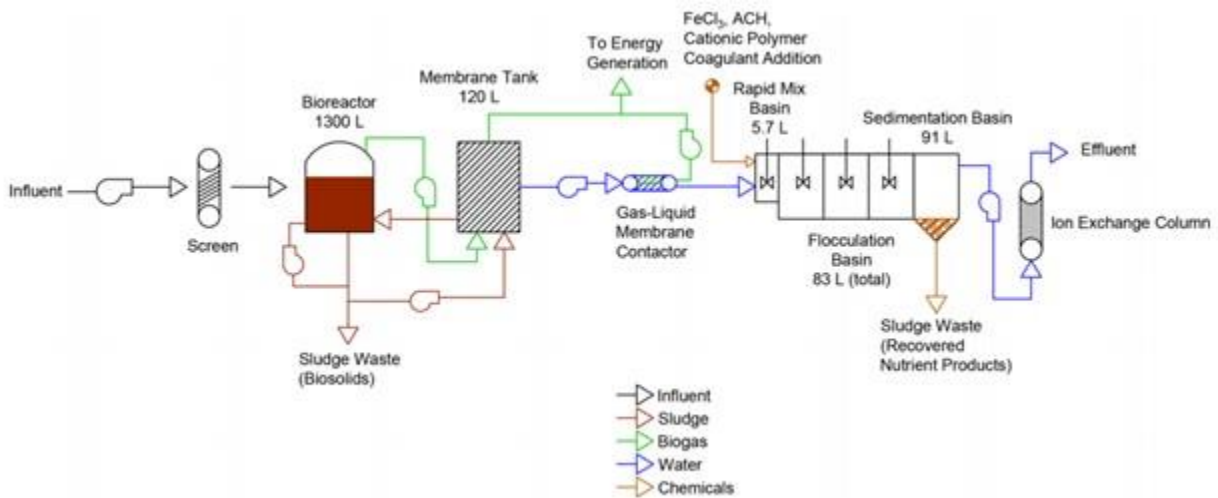


Figure 3.1 A schematic of the pilot-scale gas-sparged AnMBR used in this study. Note that the screened municipal wastewater was fed into the anaerobic bioreactor without primary settling.

Dissolved methane in the AnMBR permeate was removed with a Liqui-Cel Extra-Flow membrane contactor (3M, Separation and Purification Sciences Division, NC, USA). The contactor was a 2.5×8-inch welded housing model G420 that contained 1.5-m² of X40

membranes (serial number 020407L040259 manufactured in 2007). UF permeate was pumped upward through the shell side of the vertically oriented contactor, and a controlled vacuum was pulled from both ends of the contactor. Vacuum was drawn by either a water liquid ring pump (3AV30-1B-NR-XP, Airtech Vacuum, NJ, USA) or a compressed-air operated venturi vacuum pump (EW-78165-30, Cole Parmer, IL, USA; equivalent to HVP-100, Vaccon, MA, USA)). No sweep gas flow was used.

Table 3.1. Design basis tables for the pilot-scale AnMBR system (A) and the downstream processes (B), including dissolved methane removal using a membrane contactor, and nutrient removal using coagulation-flocculation-sedimentation (CFS) and ion-exchange (IX) processes

AnMBR system	value	post-AnMBR processes	value
Influent Screen/Strainer		Methane Contactor for Dissolved Methane Removal	
opening size	1.7 mm	model	2.5 × 8 industrial extra-flow
Primary Bioreactor		membrane type	X40
empty bed bioreactor active volume	1.3 m ³	membrane area	1.5 m ²
flow rate	1.6–5.5 m ³ /d	vacuum pump absolute pressure	25 mmHg
HRT	6 - 20 h	Rapid Mix Basin	
recycle flow rate within primary bioreactor	18 ± 4 m ³ /d	volume	5.7 L
Secondary Membrane Bioreactor		number of mixers	1
empty bed reactor volume	0.12 m ³	mixer speed	400 s ⁻¹
membrane make	Suez	coagulants	ferric chloride (P8281L) aluminum chlorohydrate (P891L) cationic emulsion polymer (P847E) (Chemtreat, VA, USA)
membrane model	ZeeWeed 500d	Flocculation Basin	
membrane type	PVDF on woven polyester	volume, total	83 L (3 chambers)
membrane area	12.9 m ² (three 4.3-m ² modules)	mixer speed in each chamber	10 s ⁻¹
pore size	0.04 μm	Sedimentation Basin	
membrane fiber size (o.d./i.d.)	1.9/0.8 mm	volume	91 L
exposed fiber length	1099 mm	lamella plate surface area	7500 cm ²
membrane surface area per module footprint area	349 m ² /m ³	surface loading rate	1.0–1.5 m/h
number of membranes per module footprint area	64 286 no./m ²	Ion-Exchange Column	
instantaneous flux	7–22 LMH	diameter	15 cm
net flux	5–18 LMH	media manufacturer/make	Clinoptilolite Northern Filter Media, Zeobest
membrane cleaning chemicals	500 mg/L NaOCl 2000 mg/L citric acid	surface loading rate	3.7–13 m/h
reactor HRT	0.7–2.5 h		
recirculation flow rate between bioreactors	14.7 ± 3 L/min		
post-AnMBR processes		value	
Methane Contactor for Dissolved Methane Removal			
type	microporous hollow fiber		
make	3M Liqui-Cel		

Removal of phosphorus and sulfide from the membrane permeate was accomplished using ferric chloride and aluminum chlorohydrate (ACH) as coagulants and cationic cross-linked polymer (P847E, Chemtreat, VA, USA) as a flocculant. The doses for chemical addition were

determined through a series of jar tests, with details shown in Appendix A (Table A1). Average concentrations used in the pilot system were 110 mg-Fe/L, 30 mg-Al/L, and 1 mg-polymer/L.

IX influent and effluent samples were analyzed for ammonia four hours after the initial addition of water. Each run continued until total breakthrough was observed. The saturated clinoptilolite was shipped to the US Army Construction Engineering Research Laboratory (IL, USA) where it was regenerated using either sodium chloride brine or sodium hydroxide and shipped back for another experiment. For replication across the regenerated runs, the clinoptilolite used in the experiment was divided into two batches. After a run with one batch was completed and was shipped out for regeneration, the alternating batch was loaded into the column and the duplicate experiment was performed.

3.1.2 Fouling Control

A double-diaphragm gas blower (KNF model N0150.1.2, KNF Neuberger, NJ, USA) was used to sparge the biogas from the headspace of the bioreactor and impart shear on the membrane surface to physically control the buildup of membrane foulants. Other physical control strategies included extended membrane relaxation, during which permeate production, sludge recirculation, and gas-sparging were stopped, and backpulsing, which was only used in conjunction with chemical cleaning.

Discrete chemical cleaning events were initiated either manually or on a user-defined automated schedule during high TMP events or in response to TMP instability. The chemical backpulse solutions used were 500 mg/L sodium hypochlorite (NaOCl) and 2000 mg/L citric acid, which were employed either alone, or in back-to-back cleaning events. Two types of chemical cleaning events were used in this study: the less intensive maintenance clean procedure

was employed more frequently, while the more rigorous recovery clean procedure was performed only once during the study.

3.1.3 Energy Balance

The system's overall energy balance was a comparison between the energy consumed by various processes of the system and the energy that could be recovered from the gaseous and dissolved methane. Energy consumption associated with pumping of incompressible fluids was estimated as follows:

$$\hat{E}_{pumping} = \frac{Q_{pump} H g \rho}{\eta Q_{permeate}}$$

where $\hat{E}_{pumping}$ is the pumping energy consumed per unit volume of permeate, Q_{pump} is the recirculation or fluidization pump flow rate for which the energy consumption was calculated, H is the head loss associated with pumping, g is the gravitational constant, ρ is the density of water, η is the pump efficiency (assumed to be 65%), and $Q_{permeate}$ is the permeate flow rate averaged over the combined pumping/relaxation cycle (Kim et al. 2010).

Energy consumption associated with adiabatic pumping of compressible fluids (i.e., biogas sparging and vacuum extraction of dissolved methane) was estimated as follows:

$$\hat{E}_{adiabatic} = \frac{k Q_{in} P_{in}}{(k-1) \eta Q_{permeate}} \left[\frac{P_{out}^{\left(\frac{k-1}{k}\right)}}{P_{in}} - 1 \right]$$

where $\hat{E}_{adiabatic}$ is the adiabatic sparging or evacuation energy consumed per unit volume of permeate, k is the heat capacity ratio, Q_{in} is the actual inlet volumetric flow rate, P_{in} is the inlet absolute gas pressure, P_{out} is the outlet absolute gas pressure, η is the pump efficiency (assumed to be 65%), and $Q_{permeate}$ is the permeate flow rate averaged over the combined pumping/relaxation cycle. An average value of 1.3 was used for k based on the values for

methane (1.32), nitrogen (1.4) and carbon dioxide (1.28) (Crone et al. 2016; Green and Perry 2008).

Energy production from generated methane was estimated as follows:

$$\hat{E}_{generation} = \frac{W_{methane} Q_{LHV} \eta}{FW_{methane} Q_{permeate}}$$

Where $\hat{E}_{generation}$ is the electrical energy produced by a generator per unit volume of permeate, $W_{methane}$ is the methane mass flow rate, Q_{LHV} is the lower heating value of methane (0.222 kWh/gram-mole), η is the generator efficiency (assumed to be 38%), $FW_{methane}$ is the formula weight of methane (16 g/mol), and $Q_{permeate}$ is the net permeate flow rate averaged over the combined pumping/relaxation cycle.

3.1.4 Sample Collection and Preparation

Liquid grab samples were collected from the strained influent, bioreactor, membrane permeate, post-coagulation settling basin, and IX column. Prior to collecting a sample for analysis, at least 500 mL was discarded to prevent sampling stagnant water from the pipes. Samples for COD analysis were acidified with sulfuric acid on site to a pH below 2. Samples for BOD₅ and COD tests were sparged with air for at least 5 minutes prior to analysis to remove contributions from H₂S and dissolved methane to the analyses.

Samples for dissolved methane were collected by placing a 54-mL sample vial in a 1-L beaker and overfilling the sample vial under quiescent flow until at least 500 mL was displaced. The cap was then filled with permeate prior to capping the sample vial, ensuring that the vial contained no gas bubbles or headspace, then packaged in a cooler refrigerated to 4°C and shipped overnight to Katahdin Analytical Services (Portland, Maine, USA) for analysis. Membrane permeate samples were analyzed for dissolved methane using a headspace

equilibration method followed by gas-chromatography analysis of the headspace by Katahdin Analytical Services (Kampbell et al. 1989).

3.1.5 Laboratory Analyses

COD, ammonia, and sulfide were analyzed using standard Hach methods (Hach methods 8000, 10205, and 8131 respectively) and a spectrophotometer (Hach DR3900, CO, USA). Turbidity and pH were measured using a turbidimeter (Hach 2100N, CO, USA) and a pH meter (VWR B10P, PA, USA), respectively. Volatile Solids (VS), Total Solids (TS), and BOD₅ were determined in accordance to standard methods 2540E, 2540B, and 5210B, respectively.⁴³ Total phosphorus was determined using a Rapid Flow Analyzer (O.I. Analytical Alpkem RFA300, TX, USA). Sulfate concentrations were found using an ion chromatograph (ICS1000, Thermo Fisher, MA, USA).

3.2 Pilot-Scale Gas Sparged AnMBR for Holistic Treatment of Domestic Wastewater

3.2.1 Operating Conditions

The pilot system operated with an average HRT of 11±3 hours, and organic loading rate (OLR) of 1.3±0.5 kg-COD m⁻³ d⁻¹, which were comparable to previous lab and pilot-scale domestic wastewater studies that had HRTs ranging between 4 to 12 hours (Baek et al. 2010; Dagnew et al. 2011; Liao et al. 2006; Lin et al. 2011). The optimized SRT in this study was 60±27 days (Figure 3.2); previous studies have operated AnMBRs in a wide range of SRTs, from 20 days to 200 days (Liao et al. 2006; Lin et al. 2013; Skouteris et al. 2012).

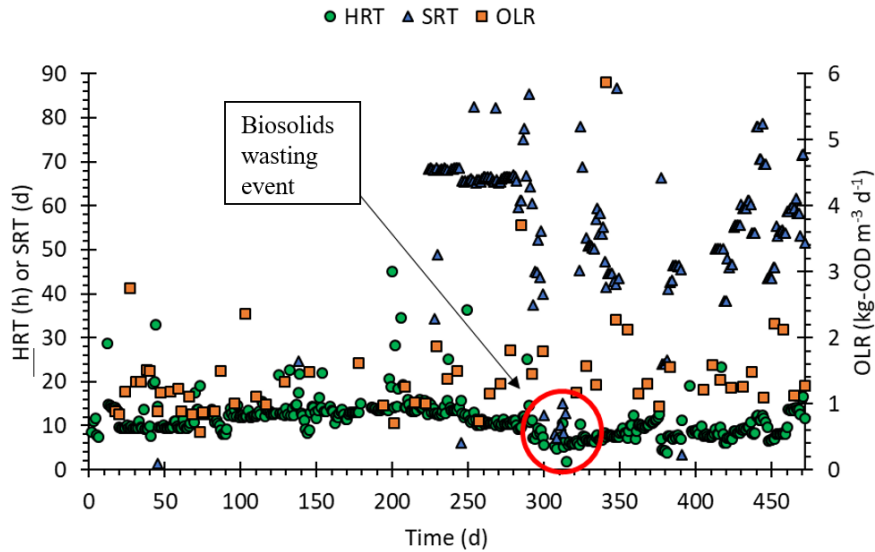


Figure 3.2 Hydraulic Retention Time (HRT), Solids Retention Time (SRT), and Organic Loading Rates (OLR) over the operational period are shown. A biosolids wasting event intended to decrease HRT also significantly lowered SRTs around day 300.

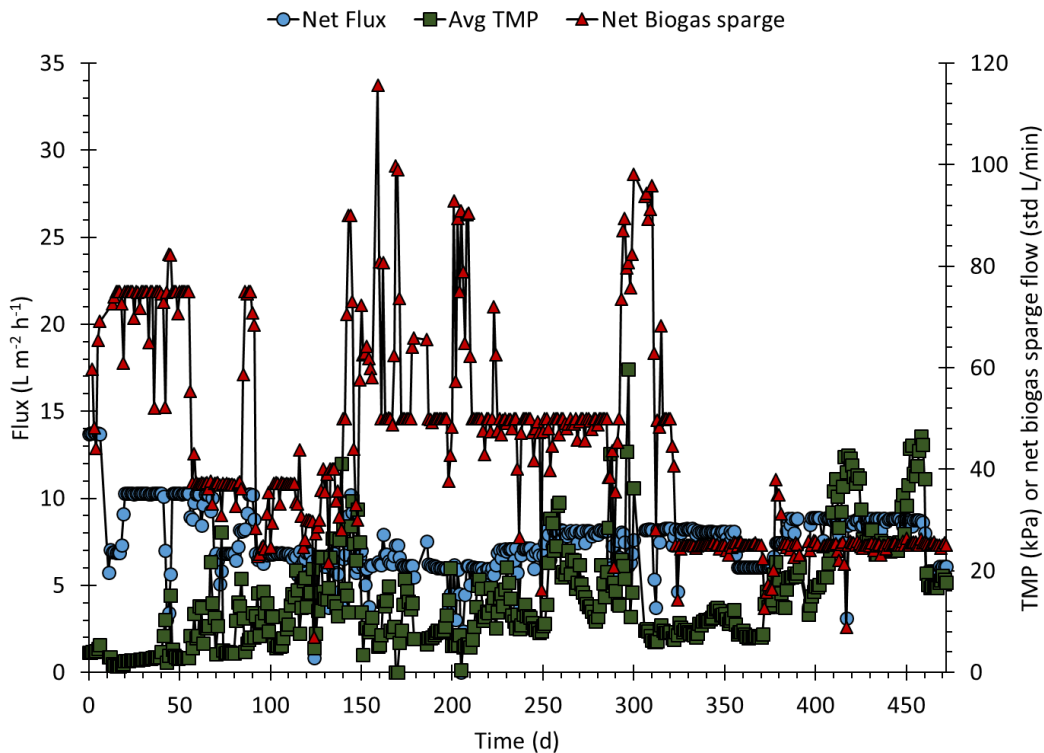


Figure 3.3 Parameters used to evaluate membrane performance are plotted over the operational period. Biogas sparge flow rates were varied over the project period in optimization experiments to determine conditions that best balance energy consumption and physical membrane scouring to maintain stable transmembrane pressures (TMP) at a constant flux.

Membrane performance was monitored throughout the study by measuring transmembrane pressure (TMP) and flux (Figure 3.3). In this study, an average TMP of 13 ± 9 kPa was maintained with an average membrane flux of 7.6 ± 1.6 L m⁻² h⁻¹ (LMH). While many lab scale studies have reported fluxes in the range of between 4 and 12 LMH, a number of studies have reported fluxes above 30 LMH, which approaches the reported critical flux in AnMBRs of between 30 and 50 LMH (Cho and Fane 2002; Liao et al. 2006; Skouteris et al. 2012). Therefore, the flux used in this study is considered reasonable. The focus of this chapter is on organics destruction, energy recovery, and removal of dissolved methane, sulfide, and nutrients, Further discussion on the membrane performance of this system can be found in separate publications and the following chapter (Evans et al. 2018, 2019).

Two critical parameters affecting biological treatment performance that were not adjusted throughout this study were pH and temperature. The average pH of the system was 6.96 ± 0.23 , firmly within the optimal range for methanogenesis (Liu et al. 2014). Wastewater temperature ranged from 12.7°C to 31.5°C (Figure 3.4A). This 18.8°C range is sufficiently broad to allow evaluation of performance variations with respect to temperature. However, it did not allow evaluation of performance at lower temperatures.

3.2.2 Anaerobic Treatment Performance

In addition to the EPA's secondary treatment standard of 30 mg/L BOD₅, a goal of 60 mg/L COD was set, based on the 0.5 BOD₅/COD ratio often seen in the membrane permeate (effluent) in this study; the average BOD₅/COD ratio of the effluent over the entire study was 0.44 ± 0.18 . The treatment goals were first achieved within 40 days of operation, with similar levels of performance maintained throughout the rest of continuous operation except during upset conditions discussed below (Figures 3.4A and 3.4B). This startup time exceeds the

conventional expectations for anaerobic systems, which typically requires months (Grosser 2017; Judd 2010). The reason for the rapid startup time is thought to be associated with use of an active mesophilic anaerobic digester inoculum and warmer temperatures due to starting up in the summer.

The COD and BOD₅ data from the first 16 days of operation were not considered because the organics were primarily associated with the digestate from the inoculum. When considering all the data between days 17 and 472, including the upset conditions explained in the following paragraph, the average BOD₅ concentrations were 250±110 mg/L in the influent and 29±15 mg/L in the effluent, which is similar to the EPA discharge limit, with an average removal efficiency of 88±6%. During that same period, the average influent COD concentration of 610±260 mg/L was reduced to 71±41 mg/L in the effluent, with an average removal efficiency of 88±7%. Sulfate reduction accounted for 44±2 mg/L of the COD consumed. These data demonstrate the AnMBR was capable of achieving good organic removal (~90%), though upsets resulted in transient reductions in performance. However, the average COD in the permeate exceeded the 60-mg/L goal in part because of upset conditions.

Upsets in treatment performance were often preceded by large biosolid wasting events. These wasting events, as indicated by loss of bioreactor VS mass, led to temporary periods of decreased COD and BOD₅ removal (Figure 3.4C) and an accumulation of volatile fatty acids (VFA), indicating an overload (Appendix A, Figure A1). The most significant upset, occurring from days 300 to 355, was associated with an intentional sludge wasting event conducted to address membrane fouling. COD and BOD₅ removals along with relatively low VFA concentrations were re-established around day 355 even though the VS mass remained low demonstrating the ability of the system to recover from system upsets especially as ambient

wastewater temperatures were increasing. Excluding the data during the upset conditions from days 300 to 355, the average effluent concentrations were 58 ± 27 mg/L COD and 25 ± 12 mg/L BOD₅, which meet the treatment goals, and achieving removal efficiencies of $90 \pm 4\%$ and $89 \pm 5\%$, respectively.

The effects of temperature on the COD and BOD₅ removal were less pronounced. Removals above 90% of both COD and BOD₅ were observed at bioreactor temperatures as low as 12.7°C and as high as 31.5°C, suggesting that ambient temperature operation of AnMBRs is feasible. The upset condition around day 300 coincided with a period of intermediate temperatures (Figure 3.4C) suggesting that the VS loss and not the low temperature was the cause of the upset. At lower temperatures, such as around days 150-200, a decreased hydrolysis rate may have contributed to a higher concentration of colloidal COD in the bioreactor (Evans et al. 2018). Colloidal COD can still be physically removed by the UF membranes, as has been observed in previous studies (Chang et al. 2002; Ho and Sung 2010). The system's ability to maintain high levels of treatment efficiency at low temperatures is attributed to the increase in physical rejection of colloidal COD by the UF membranes compensating for the likely decreased biological activity. Further studies of ambient operation of AnMBRs in colder climates is warranted to explore this mechanism and its limits.

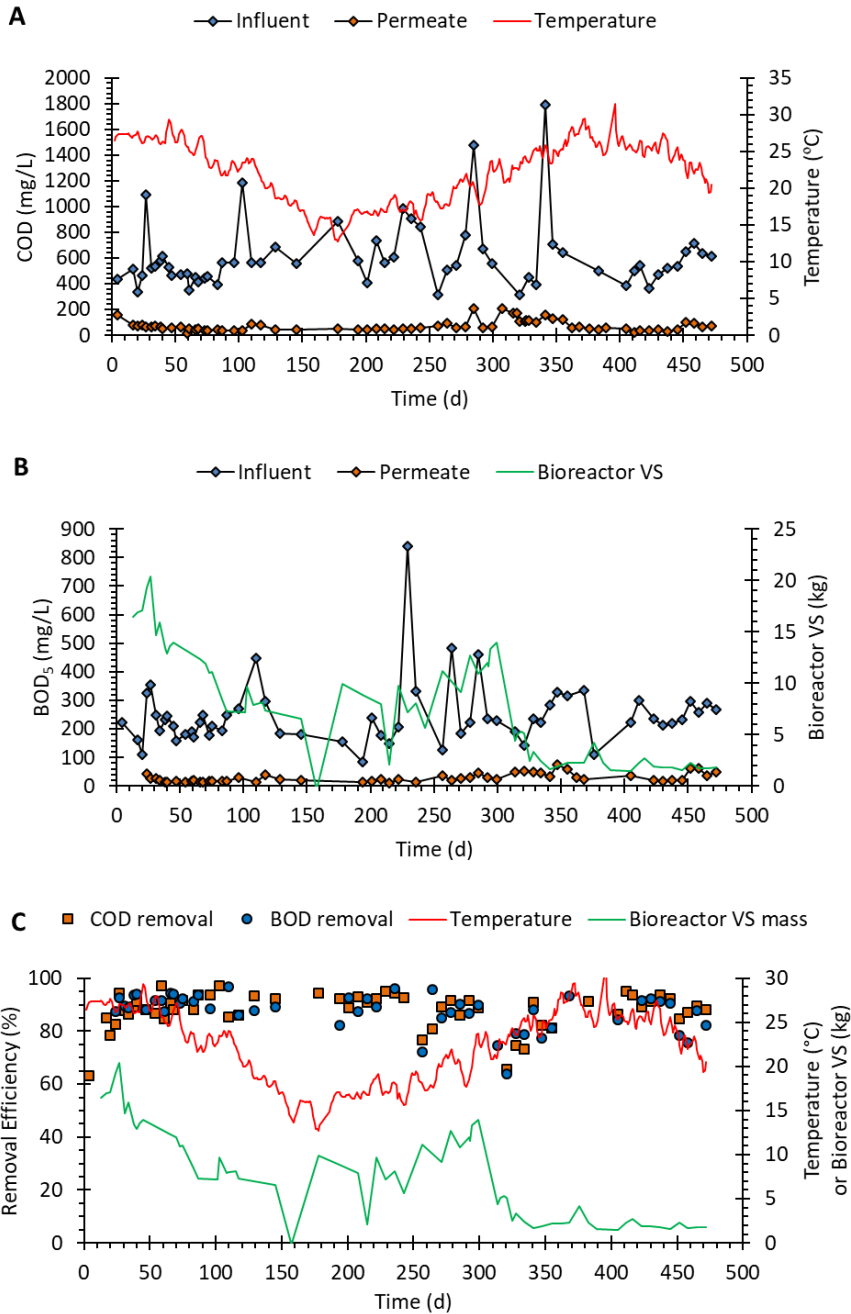


Figure 3.4 Plots of the system’s treatment effectiveness throughout the entire operational period; (A) Influent and permeate COD on the primary axis with temperature on the secondary axis and (B) Influent and permeate BOD₅ on the primary axis with bioreactor volatile solids (VS) mass data on the secondary axis. As shown in (C), the COD and BOD₅ removal rates were impacted by sudden drops in bioreactor VS, whereas lower temperature operation did not significantly impact performance. The study’s objectives for effluent COD and BOD₅ concentrations were 60 mg/L and 30 mg/L, respectively. VS mass was presented instead of concentration because the bioreactor’s liquid volume was changed throughout this study.

3.2.3 Effect of Ambient Temperature Operation on Methane Production and Distribution

Because COD removal occurs through a variety of mechanisms not limited to methanogenesis, such as physical removal by the membranes, this study reports bulk methane yield, defined as L-CH₄ at standard temperature and pressure (STP) produced per g-COD removed, regardless of the mechanism. The bulk methane yields over three temperature ranges show that the average methane production increased with increasing temperatures (Figure 3.5A). This conforms with previous studies, where bulk methanogenic yield increased with temperature through the mesophilic range until an optimal point of 35°C (Ganesh Saratale et al. 2018; Hagos et al. 2017; Tchobanoglous et al. 2003). Methane generation increased from 0.11±0.05 L-CH₄/g-COD at temperatures below 20°C, to 0.15±0.06 L-CH₄/g-COD observed at the 20°C to 25°C range. For the temperatures above 25°C, the bulk methane yield continued to increase, with an average of 0.18±0.05 L-CH₄/g-COD, which is significantly greater than the average at temperatures below 20°C (p=0.00016), indicating that temperature has a strong influence on bulk methane yield. The decreased methane yield observed at lower temperatures is consistent with a mechanism of decreased hydrolysis at lower temperatures.

The observed yields were lower than estimations of theoretical methane yield by anaerobic consortia found in literature, usually reported as around 0.35 L-CH₄/g-COD at STP (Bernet and Buffi 2002; Jennett et al. 2018). The changes in methane yield due to temperature contrasts with the organic treatment performance, which did not vary with temperature. This apparent discrepancy is attributed to decreased hydrolysis at lower temperatures, accumulation of colloidal COD, and rejection of colloidal COD by the UF membranes. The removal of COD by

physical means rather than biological activity would cause the observed bulk methane yields to deviate from theoretical values.

Over the entire project duration, 58% of the methane was in the gaseous fraction, and 42% of the methane was found in the dissolved fraction; the permeate was found to be oversaturated, with an average degree of oversaturation of 1.14 ± 0.21 , as calculated based on temperature corrected Henry's Law constants (Evans et al. 2018; Tchobanoglous et al. 2003). The average methane content of the biogas was $68 \pm 6.5\%$, which is comparable to the methane content in mesophilic AD processes digesting a variety of substrates (El-mashad and Zhang 2010; Vargas et al. 2008). The fraction of total methane found dissolved in the permeate tended to be greater at lower temperatures, with a general decreasing trend as temperatures increased (Figure 3.5B). In the 15°C to 20°C range, on average, 47% of the total methane was dissolved, which falls within the anticipated 40-50% seen in previous studies of psychrophilic AnMBRs (Crone et al. 2016; Smith et al. 2013; Yeo et al. 2015).

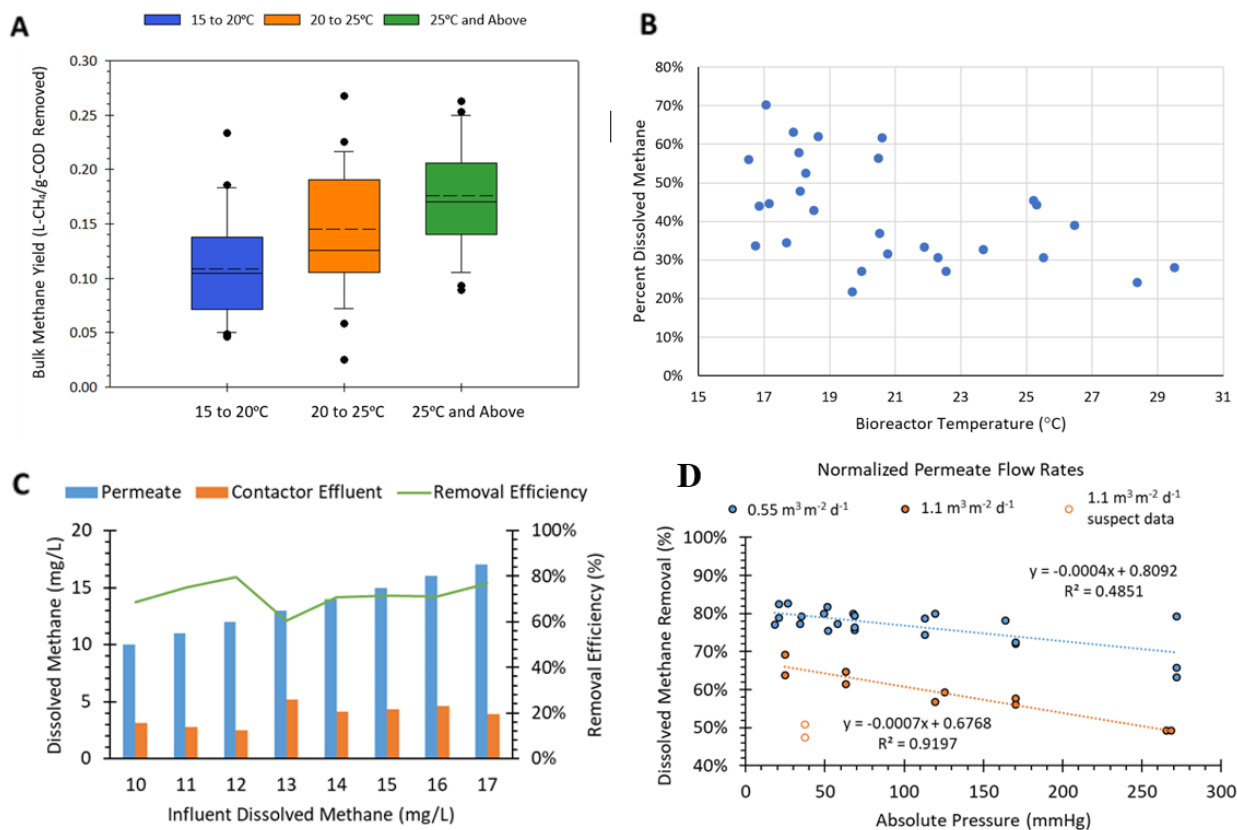


Figure 3.5 (A) A box-and-whisker plot of the AnMBR’s bulk methanogenic yield at three temperature ranges, showing significant differences in mean methane production. (B) A plot of the percentage of methane found in the dissolved fraction at different temperatures. The dissolved methane fraction has a generally decreasing trend as temperatures increase. (C) Membrane contactor dissolved methane and removal efficiencies are shown in a line plot along with influent and effluent concentrations. (D) Membrane contactor removal efficiency as a function of absolute pressure at two different flow rates are shown in a scatter plot.

3.2.4 Dissolved Methane Removal

Recovering the methane using a hollow fiber membrane contactor proved viable, even with the varying concentrations of dissolved methane in the permeate. The membrane permeate contained an average of 14 ± 2 mg/L dissolved methane throughout the study. An average dissolved methane removal efficiency of $70 \pm 5\%$ was achieved with influent dissolved methane concentrations ranging from 10 mg/L to 17 mg/L over a total of 36 tests (Figure 3.5C). The average post-contactor dissolved methane concentration was 3.8 ± 0.94 mg/L, with no clear trend with respect to influent methane loading. The lack of an observable trend may be associated with

the limited range of pre-contactors dissolved methane concentrations. Nevertheless, 70% removal may not be sufficient with respect to minimizing the release of methane into the atmosphere. The amount of dissolved methane, as CO₂ equivalents, remaining in permeate after 70% dissolved methane removal was estimated to be 0.11 kg CO_{2e}/m³. This amount is not insignificant in comparison to other studies (Crone et al. 2016; Jeppsson et al. 2007; Liu et al. 2014; Sweetapple et al. 2013).

Dissolved methane removal efficiencies were affected significantly by the permeate flow rates and applied vacuums. Increased removal efficiencies were observed at lower permeate flow rates and at lower absolute pressures (Figure 3.5D). The average dissolved methane removal efficiency with conditions of 0.55 m³ m⁻² d⁻¹ of normalized flow and 44 mmHg of absolute pressure was 79±2%. Despite being subject to seasonal variations, the results were similar to those observed in an upflow anaerobic sludge blanket (UASB) reactor study (68±7%) and in a temperature-controlled pilot-scale AnMBR study (67%) (Bandara et al. 2011; Crone et al. 2016; Seco et al. 2018). In this study, removal efficiencies up to 66% were observed during tests in the summer, whereas removal efficiencies up to 83% were observed in the fall and winter. This difference may have been due to further optimization of the membrane contactor setup rather than an effect of seasonal variations, however. Regardless, these results suggest that hollow-fiber contactors may not be an appropriate solution for dissolved methane recovery.

3.2.5 Removal and Recovery of Sulfide, Phosphorus, and Ammonia from AnMBR Permeate

High iron dosages (115 mg-Fe/L), relative to those used in conventional wastewater treatment (~30 to 40 mg-Fe/L), were required due to the membrane permeate's high sulfide concentrations (24.0±7.2 mg-S/L) which are typical in anaerobically treated wastewaters

(Kolarik et al. 1996; Tchobanoglous et al. 2003). From days 361 to 479, implementation of the 115 mg-Fe/L dosing, determined through a matrix of jar tests (Appendix A, Table A1), achieved an average effluent sulfide concentration of 0.7 ± 1.7 mg-S/L. Determination of an appropriate coagulant dosing was critical for the nutrient recovery not only to achieve low levels of phosphorus and sulfide, but also to protect the downstream IX column and have a minimal impact on the final water quality. The regeneration process of clinoptilolite in the IX column is hindered by the presence of sulfide or iron in the CFS effluent, encountered as either dissolved species, or unsettled flocs. Ferric chloride alone was insufficient in forming more than pin flocs in the AnMBR permeate. The addition of ACH and cationic polymer as coagulant aids was critical in forming stronger, well-settling flocs. Further optimization is possible and warranted considering the cost and potential environmental impact of using these chemical coagulants for sulfide removal (Evans et al. 2018).

While the targeted method of total phosphorus removal was the CFS unit, the AnMBR demonstrated an ability to reduce phosphorus concentrations from 7.0 ± 2.9 mg-P/L in the screened influent to 4.2 ± 0.6 mg-P/L in the membrane permeate. The removal in the AnMBR does not appear to be associated with phosphorus-accumulating organisms (Evans et al. 2018). It is possible that the observed phosphorus removal was attributable to chemical precipitation in the AnMBR and precipitate retention by the UF membranes. The CFS unit removed the majority of the phosphorus in the treatment train with an average concentration of 0.72 ± 0.36 mg-P/L in the sedimentation basin effluent (Figure 3.6). The clinoptilolite IX column also removed some phosphorus, producing a final effluent phosphorus concentration of 0.43 ± 0.29 mg-P/L in the clinoptilolite effluent for an overall removal of $94 \pm 3\%$. The phosphorus removal by the IX column was likely associated with carryover iron from the CFS process.

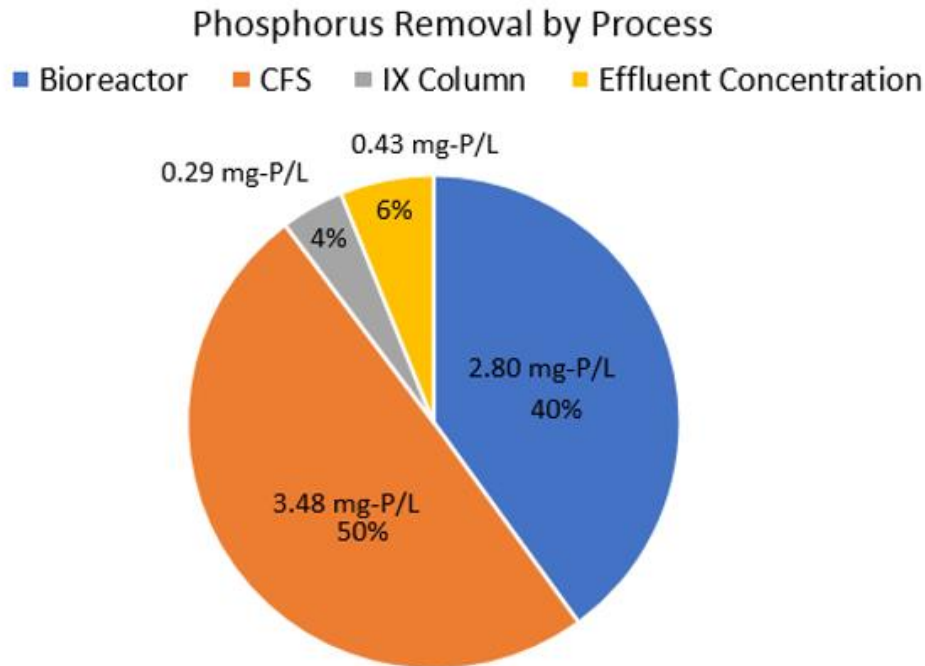


Figure 3.6 Average phosphorus concentration removals and efficiencies by process are shown in a pie chart.

The IX column was able to successfully remove greater than 99.5% of the ammonia in each run, achieving an average effluent concentration of 0.05 ± 0.05 mg-N/L from influent concentrations of 37 ± 4 mg-N/L, with regeneration cycles having little impact on ammonia capture efficiency (Figure 3.7). The average breakthrough time for the various clinoptilolite runs was around 50 to 100 bed volumes, and longer than comparable bench-scale experiments for ammonia capture from anaerobic centrate, but still small enough to require a continuously regenerated system. Iron carry over from the CFS system reduced ammonia loading capacity on the clinoptilolite which appears to have limited the observed bed volumes prior to breakthrough. (Evans et al. 2018; Guo et al. 2008) Thus, clinoptilolite has potential for post-AnMBR ammonia removal provided further optimization of the CFS system is conducted. Placement of the IX process prior to the CFS process warrants investigation as well.

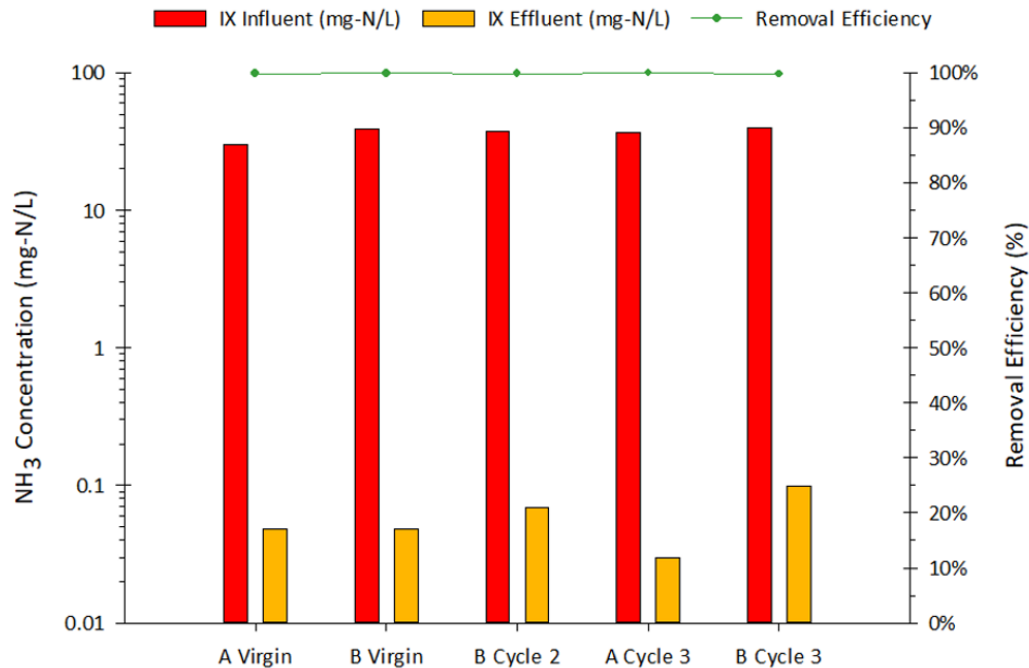


Figure 3.7 Each completed run of the clinoptilolite IX system for ammonia recovery is shown in the bar graph. The second cycle of batch A was not completed due to operating errors.

3.2.6 Energy Balance

The averaged energy consumption and power generation normalized per volume of wastewater treated are shown for days 420-445, a period where operating conditions were held relatively constant (Figure 3.8). The system consumed a total of 0.349 kWh/m³ with the largest energy demand being used for continuous gas-sparging with the biogas blower, which accounted for 0.19 kWh/m³. This is within the expected range of external-configuration membrane tanks, where just the processes associated with membrane maintenance and biogas sparging have typically required between 0.03 kWh/m³ to 5.7 kWh/m³ (Le-clech et al. 2006; Lin et al. 2013). Mixing, which utilized both the recirculation and WAS/mix pumps consumed 0.12 kWh/m³. The recirculation pump alone consumed 66% of the total mixing energy cost to pump mixed liquor between the bioreactor tank and the membrane tank in addition to mixing of the bioreactor

contents. The pilot-scale bioreactor design was not optimized for efficient mixing and improvements in mixing energy consumption are possible by using alternative methods such as vertical linear motion mixers, which have successfully reduced the mixing energy consumption in anaerobic digesters (Massart et al. 2008; Meroney and Sheker 2014).

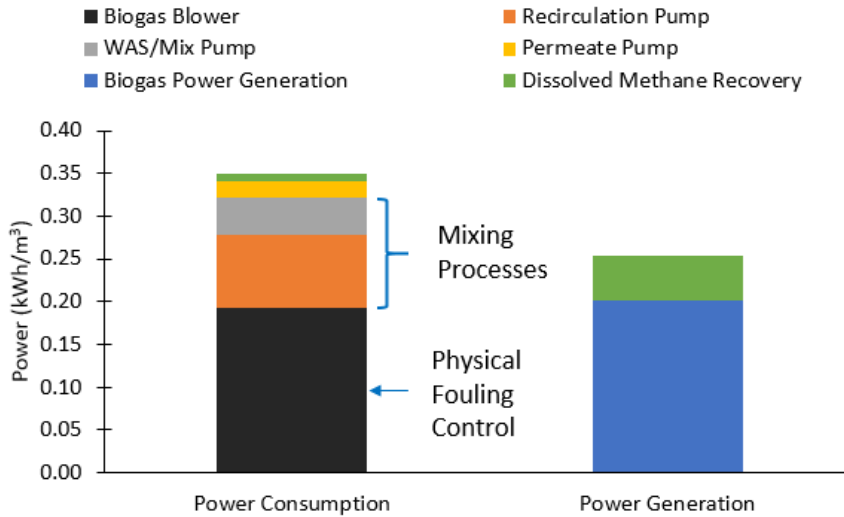


Figure 3.8 Graph of power consumed and generated from equipment and processes of the system during a period where operating conditions were held relatively constant from days 420-445. Total power consumption for system operation was 0.349 kWh/m³, and the theoretical 0.254 kWh/m³ generated for 72.8% of energy neutrality. Values were calculated assuming pump efficiency of 65% and generator efficiency of 38%.

Through biogas capture and an assumed dissolved methane recovery efficiency of 79%, an estimated 0.254 kWh/m³ would be able to be generated, contributing 72.8% towards energy neutrality. The 0.008 kWh/m³ input required to recover dissolved methane using a membrane contactor produced 0.052 kWh/m³ of energy, indicating an energy incentive to employ this strategy in this system. The energy associated with dissolved methane recovery was the energy required to operate a vacuum pump to generate 44 mmHg absolute pressure with a permeate flow rate of 0.56 L/min, which was the average operating condition in this study. The implementation of more efficient biogas sparging technologies, such as recently developed techniques that involve sparging in pulses at high flow rates, could reduce energy demand on the

most energy intensive process in gas-sparged AnMBR operation and help achieve energy neutrality.

A COD balance was conducted by totalizing the amounts of wastewater COD, permeate COD, gaseous and dissolved methane, sulfate reduction, and wasted sludge volatile solids and calculating their COD equivalents. The sludge recovered from the bottom of the bioreactor was also included in the COD balance. The mass balance was not complete with 35% of the COD unaccounted (i.e. other). Possible explanation for the missing COD includes underestimation of the wasted solids, instrumentation inaccuracy (e.g. flowmeters and gaseous methane analyzer) and analytical inaccuracy.

3.3 Future Outlook

AnMBRs continue to be a promising technology that fit into holistic wastewater treatment. This pilot-scale demonstration met its treatment objectives for a long period of operation and behaved similar to previous lab scale studies, suggesting its scalability. Furthermore, it managed to do so under ambient and seasonally varying wastewater temperatures, which potentially expands its viability for implementation in temperate climatic regions. This study demonstrated just one possible configuration of a holistic AnMBR treatment train. Future studies are required to demonstrate alternative nutrient removal strategies, dissolved methane removal technologies, and their impact on the economics of operation and scale up.

3.4 Summary

This study has demonstrated the viability of AnMBRs as a technology capable of holistic wastewater treatment [Chapter 2, Objective 1A]. Operating under ambient temperatures for 472 days, the AnMBR achieved an average effluent quality of 58 ± 27 mg/L COD and 25 ± 12 mg/L BOD₅ at temperatures ranging from 12.7°C to 31.5°C. The average total methane yield was

0.14±0.06 L-CH₄/g-COD fed, with 42% of the total methane dissolved in the permeate.

Dissolved methane removal using a hollow fiber membrane contactor achieved an average removal efficiency of 70±5%, producing effluent dissolved methane concentrations of 3.8±0.94 mg/L. The methane recovered from gaseous and dissolved fractions could generate an estimated 72.8% of the power required for energy neutrality. Nutrient recovery was accomplished using coagulation, flocculation, and sedimentation for removal of sulfide and phosphorus, followed by a clinoptilolite ion-exchange column for removal of ammonia, producing effluent concentrations of 0.7±1.7 mg-S/L, 0.43±0.29 mg-P/L and 0.05±0.05 mg-N/L. The successful integration of AnMBRs in a treatment train that addresses the critical challenges of dissolved methane and nutrients demonstrates the viability of the technology in achieving holistic wastewater treatment.

Chapter 4 - Membrane Performance and Foulant Characterization in a Pilot Scale AnMBR

This section has been published in *Environmental Science: Water Research and Technology*. The citation is as follows:

Lim, K., Evans, P. J., Utter, J., Malki, M., and Parameswaran, P. (2020). “Dynamic monitoring and proactive fouling management in a pilot scale gas-sparged anaerobic membrane bioreactor.” *Environmental Science: Water Research and Technology*, Royal Society of Chemistry, 6(10), 2914–2925.

The design basis of the pilot-scale AnMBR system, its description, operating conditions, and treatment performance have been previously described in chapter 3. The focus of this chapter is on the performance of the membranes, the effectiveness strategies used for fouling control, and foulant characterization.

4.1 Materials and Methods

The AnMBR was operated continuously for 472 days, treating domestic wastewater from Ft. Riley, Kansas. A schematic of the pilot-scale AnMBR and its fouling control appurtenances is shown in Figure 4.1. Municipal wastewater from Ft. Riley was passed through a 1.7 mm screen (Eaton model DCF400) prior to being fed to the AnMBR, which operated at an average HRT of 11 ± 3 hours. Sludge was recirculated between the bioreactor and the membrane tank using two progressive cavity pumps (Moyno model 33304) in order to promote mixing, with one of the pumps also being used to waste the sludge from the bioreactor.

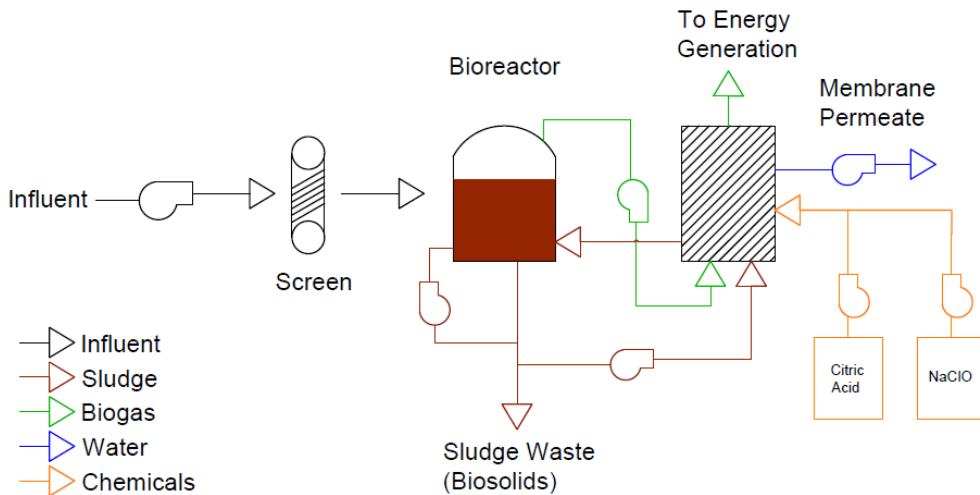


Figure 4.1 A schematic of the pilot-scale gas-sparged AnMBR used in this study adapted to show fouling control methods.

4.1.1 Fouling Control

The fouling control strategy used in this study were primarily physical. Sparging was accomplished using a double-diaphragm gas blower (KNF model N0150.1.2, NJ, USA) to pump the biogas from the headspace of the bioreactor. The net sparge flow rate, measured in standard liters per minute (SLPM) was varied over the course of pilot operation through a series of experiments. Other physical control strategies included extended membrane relaxation, during which permeate production, sludge recirculation, and gas-sparging were stopped, and backpulsing.

Discrete chemical cleaning events were initiated either manually or on a user-defined automated schedule during high TMP events or in response to TMP instability. The chemical backpulse solutions used were 500 mg/L sodium hypochlorite (NaOCl) or 2000 mg/L citric acid, which could be employed either alone, or back-to-back. Maintenance cleans were initiated on a more regular basis, usually in response to high TMP events, and could involve using the chemicals either alone or back-to-back. The more intense recovery cleaning procedure was only

used once throughout the operational period and involved extended chemical soaking periods using each chemical. Representative cleaning procedures for maintenance cleans and the recovery clean are shown in Table 4.1 and Table 4.2, respectively.

Table 4.1 The typical maintenance cleaning procedure used in this study. For back-to-back cleans, this procedure is repeated once for each chemical

		Maintenance Clean Procedure	Time (s)	Action
		Membrane relaxation	300	Permeation is paused, biogas sparging continues
		Chemical backpulse	120	Biogas sparging and pump recirculation are paused, permeate pump is reversed and chemical is backpulsed at 20 LMH
		Membrane relaxation	300	Permeate pump is paused
5 Cycles		Chemical backpulse cycle	30	Permeate pump backpulses chemical at 20 LMH
		Membrane relaxation cycle	270	Permeate pump is paused
		Clean water Backpulse	120	Permeate pump backpulses water at 20 LMH
		Membrane relaxation	60	Permeate pump is paused
		Biogas Sparge	300	Biogas sparging is resumed

Table 4.2 The recovery cleaning procedure used in this study. This procedure was repeated once for each chemical.

	Recovery Clean Procedure	Time	Action
	Membrane relaxation	5 min	Permeation is paused, biogas sparging at 50 SLPM, pump recirculation continues
	Drain membrane tank	N/A	Biogas sparging and pump recirculation are paused, drain the membrane tank's contents to the waste line
	Fill membrane tank with permeate	N/A	Backpulse membrane tank until filled with 110 L of permeate
	Biogas Sparge	5 min	Permeate backpulse is paused, biogas sparging is resumed
	Drain membrane tank	N/A	Biogas sparging is paused, drain the membrane tank to the waste line
Repeat until 90% of the membrane tank is filled	Chemical backpulse cycle	2 min	Permeate pump backpulses chemical at 33 LMH
	Membrane relaxation cycle	2 min	Permeate pump is paused
	Chemical soak: NaOCl	4 min	Permeate pump remains paused for 4 minutes after the final cycle
	Drain 30% of the membrane tank	N/A	Drain the 30% of the membrane tank's total volume to the waste line
Repeat until 90% of the membrane tank is filled	Chemical backpulse cycle	2 min	Permeate pump backpulses chemical at 33 LMH
	Membrane relaxation cycle	2 min	Permeate pump is paused
	Chemical soak	4 min	Permeate pump remains paused for 4 minutes after the final cycle
	Drain 30% of the membrane tank	N/A	Drain the 30% of the membrane tank's total volume to the waste line

Recovery Clean Procedure (cont.)	Time	Action
Fill membrane tank with permeate	N/A	Backpulse permeate at 33 LMH until membrane tank is full, diluting the dosed cleaning chemical
Chemical soak	6 h	Allow membrane to soak in residual chemical
Drain membrane tank	N/A	Drain the membrane tank's contents to the waste line

The maintenance clean procedure began with 5 to 10 minutes of sparging the membranes while the permeate pump was turned off. After the specified time, sparging and sludge recirculation were paused, and a chemical cleaning solution was backpulsed through the membranes at 20 LMH for 2 minutes, after which the membranes were relaxed for 4.5 minutes. The membranes then underwent 5 to 10 cycles of 30 second chemical backpulses at 20 LMH followed by 4.5 minutes of relaxation. After the chemical backpulsing, the membranes were backpulsed with clean permeate at 20 LMH for 2 minutes. The membranes were then sparged for 5 to 10 minutes prior to returning to normal operation.

4.1.2 Fouling Parameter Analyses

TMP was measured by taking the difference between a pair of pressure transmitters (Endress and Hauser Cerabar PMC51, Reinach, Switzerland) taking pressures from the membrane tank's bulk sludge and from the permeate line. Flux was a derived parameter calculated from the permeate flow rate, taken using an electromagnetic flow meter (Endress and Hauser 5P1B15, Reinach, Switzerland), and dividing it by the total membrane surface area (12.9 m²). Permeability is calculated as the ratio of flux to TMP and is presented in units of LMH/bar (Judd 2010; Metcalf et al. 2004). A baseline permeability was established by taking the

averaging the permeability during the period of operation during which the virgin membranes were operated under stable conditions without the use of chemical cleaning. The percentage of baseline permeability data was then calculated by dividing the permeability of the sample point by the established baseline permeability.

Membrane permeate samples collected for soluble chemical oxygen demand (sCOD) and fluorometry measurements. 500 mL of permeate was collected on site and immediately acidified to a pH of below 2 with sulfuric acid. Samples were sparged with air for 10 minutes to eliminate the contribution of hydrogen sulfide and filtered through 1.2 μm filter paper (Whatman 1822-047, Maidstone, United Kingdom). COD measurements were performed on these samples using Hach method 8000 and a Hach spectrophotometer (Hach DR3900, CO, USA). The samples were aliquoted in quartz cuvettes (Starna 3-Q-10, Ilford, UK) and analyzed using a Horiba Aqualog fluorometer (Horiba, Kyoto, Japan) to generate excitation-emission matrices (EEMs).

Membrane fibers were collected at the end of operation for autopsy analyses. American Water Chemicals, Inc (AWC, FL, USA) performed a membrane autopsy, which included Loss on Ignition (LOI) testing to determine the organic content of the foulants, scanning electron microscopy (SEM) with energy dispersive x-ray spectroscopy (EDX) to determine the elemental composition of the foulants, and Fourier Transform Infrared Spectroscopy (FTIR) to analyze functional groups. In addition to the analyses done by AWC, analyses using transmission electron microscopy (TEM) and electron diffraction were performed at Kansas State University's Microscopy Facility using a Philips CM-100 microscope with a tungsten filament.

4.2 Membrane Performance

Over the 472-day operation period, the AnMBR operated at an overall average net flux of $7.6 \pm 1.6 \text{ L m}^{-2} \text{ h}^{-1}$ (LMH) and an average TMP of $13 \pm 9 \text{ kPa}$ (Figure 4.2). The first 40 days of

operation were used to establish a baseline for the system's membrane performance without the use of chemical cleaning; the average permeability during this period was 336 ± 81 LMH/bar, with an average flux of 10.1 ± 2.2 LMH, net biogas sparge flowrate of 75 SLPM, and average TMP of 2.7 ± 1.0 kPA (Figure 4.3A). The ability to operate for long periods, defined in literature as over three weeks, without any maintenance cleaning is consistent with subcritical flux operation, during which solids deposition is minimal (Cho and Fane 2002). The maintenance clean executed on day 42 was able to recover 80% of the baseline permeability, suggesting that no appreciable irreversible fouling had occurred, and that the system was being operated under subcritical conditions.

The permeability decreased by 92% from the start of operation to an average permeability to 28 ± 6 LMH/bar in the last 40 days of operation (Figure 4.3B). The first irreversible reduction in permeability coincided with a user-controlled net biogas sparge flowrate reduction to 37 SLPM, initiated on day 56, while maintaining a flux setpoint of 10 LMH (Figure 4.3A). Subsequent attempts to recover the baseline permeability by increasing biogas sparge flowrate were not able to be sustained, suggesting that physically irremovable fouling had occurred, and that the system was operating below the critical sparging rate, which is the theoretical sparging rate above which no solids deposition would occur. The presence of irremovable fouling has been hypothesized to increase the propensity for local fouling and consequently lower the critical flux of the overall system, which lowers the overall membrane permeability (Cho and Fane 2002; Fox and Stuckey 2015). When operating above the critical flux, the hypothesis is that fouling attachment is more likely to proliferate and form a cake layer in localized areas that have experienced irremovable fouling, so lowering the operating flux should theoretically ameliorate these effects. Indeed, lowering the flux setpoint from 10 LMH to

6.8 LMH on day 74, while still operating at the reduced sparging rate of 37 SLPM, was able to restore stable membrane performance without chemical cleaning or any other parameter adjustments, further supporting the critical sparging rate hypothesis. Thus, managing the initial deposition of foulants appears to be critical for maintaining membrane performance.

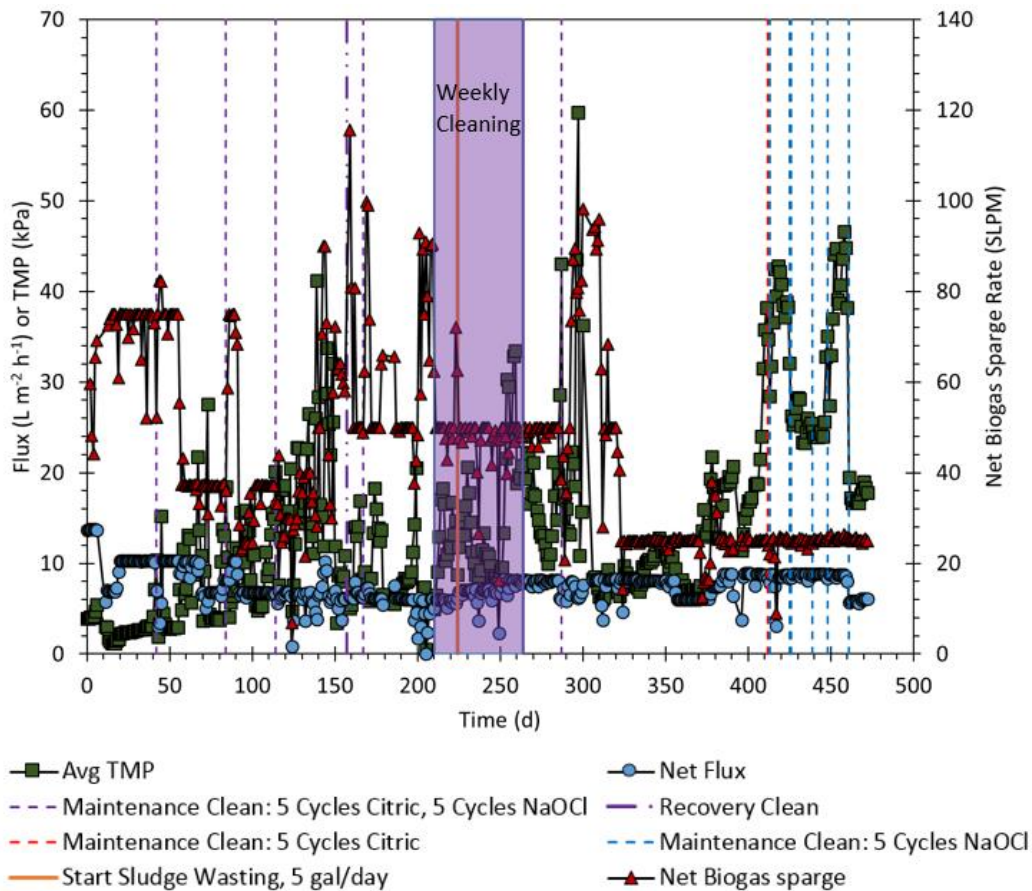


Figure 4.2 A plot of transmembrane pressure, flux, net biogas sparge flowrate, chemical cleaning events, and sludge wasting over the study’s entire duration.

4.2.1 Chemical Cleaning

The first major reduction in permeability occurred between days 40 to 42, and prompted a maintenance clean that was able to recover nearly all of the lost permeability (Figure 4.3A). Although the cleaning procedure occurs within 40 minutes from initiation to resuming normal operation, the maximum recovery of permeability appears to be slightly delayed, occurring 7

days following the cleaning event (Figure 4.3A). This delayed recovery was observed following each chemical cleaning event that was initiated after an extended period (more than 3 weeks for subcritical conditions) without any maintenance cleans (days 42, 84, and 114, as shown in Figure 4.3B), with the maximum recovered permeabilities being observed 6 ± 2 days after the initiated clean, on average (Cho and Fane 2002). This effect is less pronounced during periods of regular maintenance cleaning. One possibility is that the final backpulsing may not have been sufficient for removing the partially dissolved foulants from the pores or the membrane surface, and that the physical mechanism of biogas sparging likely completes this process in the days after the cleaning. Regular maintenance cleans may interrupt the solids deposition onto the cake layer to the point where the physical removal mechanisms do not have as large of an impact on recovering permeability.

The effectiveness of the maintenance cleans also decreased progressively with time; cleaning events recovered 80%, 34%, 7%, and 2% of the baseline permeability on days 42, 84, 114, and the final clean on day 461, respectively, indicating that the foulant becomes less susceptible to chemical cleans as AnMBR operation continues (Figure 4.3B). The reasons for this progression of chemically resistant irreversible fouling require further investigation and may have implications on fouling control strategies. Elucidating the main foulants at each stage of the membrane's operational life may lead to more targeted control strategies aimed at specific fouling agents.

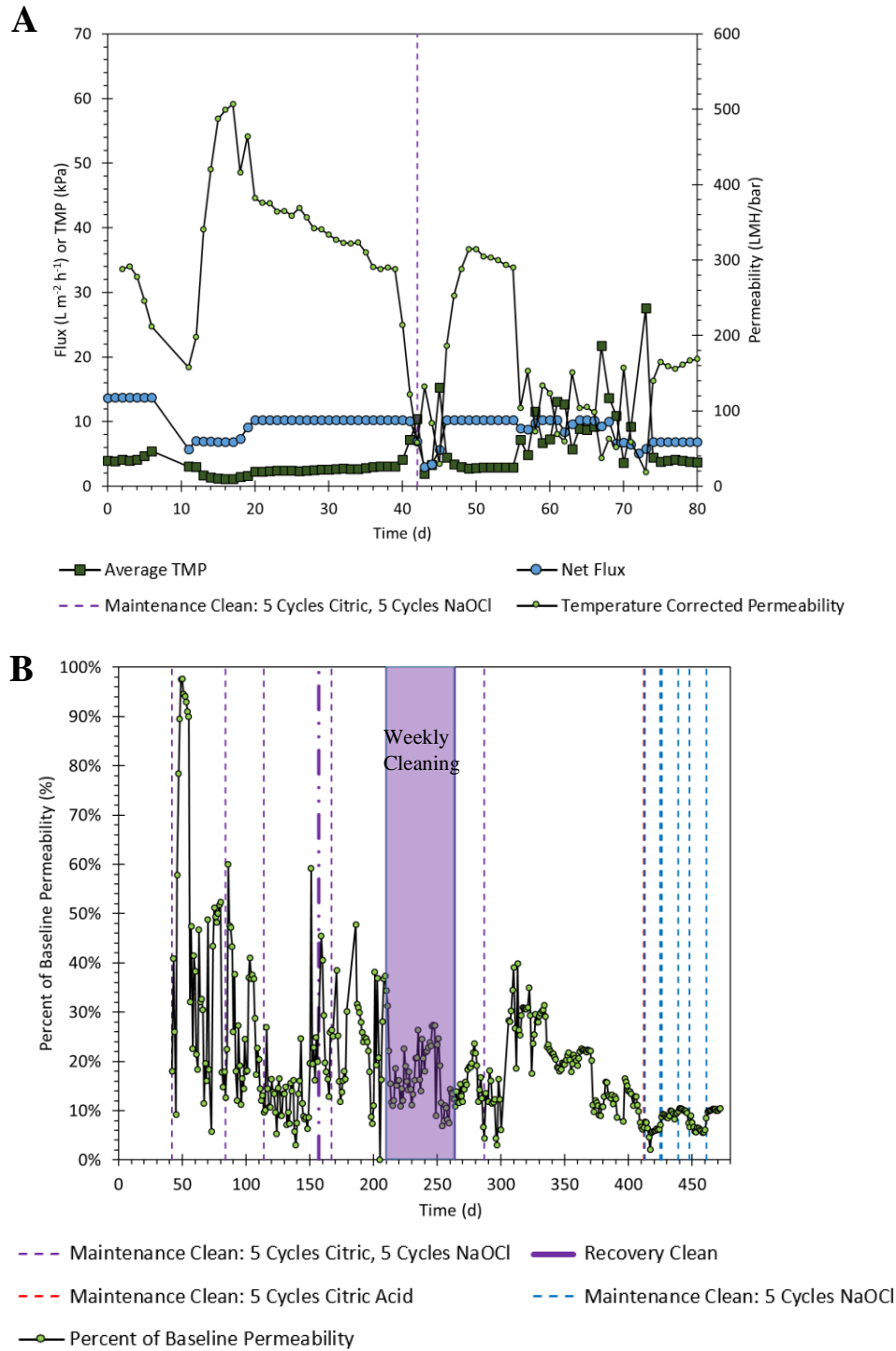


Figure 4.3 Plots of membrane performance. (A) shows the TMP, Flux, and Permeability over the first 80 days. The first 42 days were operated without chemical cleaning and is used as a benchmark for the system’s original permeability. (B) plots the percentage of the benchmark permeability from the first 42 days, and chemical cleaning events.

4.2.2 Bioreactor Solids and the Potential Role of Soluble COD on Membrane

Fouling

Chemical cleaning, even when used regularly, was not always able to considerably recover permeability, as observed from days 210 to 270, where permeability was unstable and relatively low despite regular maintenance cleaning (Figure 4.4A). Some fouling events appear to be correlated with bioreactor solids concentration or sCOD. The largest recovery of permeability occurred from days 299 to 316, where the solids wasting caused a 64% decrease in bioreactor TS and an 80% decrease in sCOD concentrations, recovering 34% of the baseline permeability, significantly more effective than chemical cleaning during this period of operation. The system was operated from day 323 to day 411 with solids wasting as the only control strategy actively being employed, without any maintenance cleans. TMP stability seemed to be improved at lower sCOD concentrations as well, indicating more consistent membrane performance. The large wasting event did lead to a temporary period of decreased treatment performance for 55 days following the loss of biomass (Lim et al. 2019), It is likely that this performance loss could have been avoided had the sludge wasting been conducted periodically, rather than all at once. Nonetheless, treatment performance was able to be recovered without any additional action aside from regular operation.

A previous AnMBR study found the impact of solids concentrations less than 20 g/L were due mostly to colloids and the solids would have negligible impact when operating at subcritical fluxes(Dagneu et al. 2012). The average bioreactor TS during the system's operation was 9200 ± 6000 mg/L, well below 20 g/L. Because of this, it is likely that the improved membrane performance was due to the reduction of sCOD concentration rather than TS concentration.

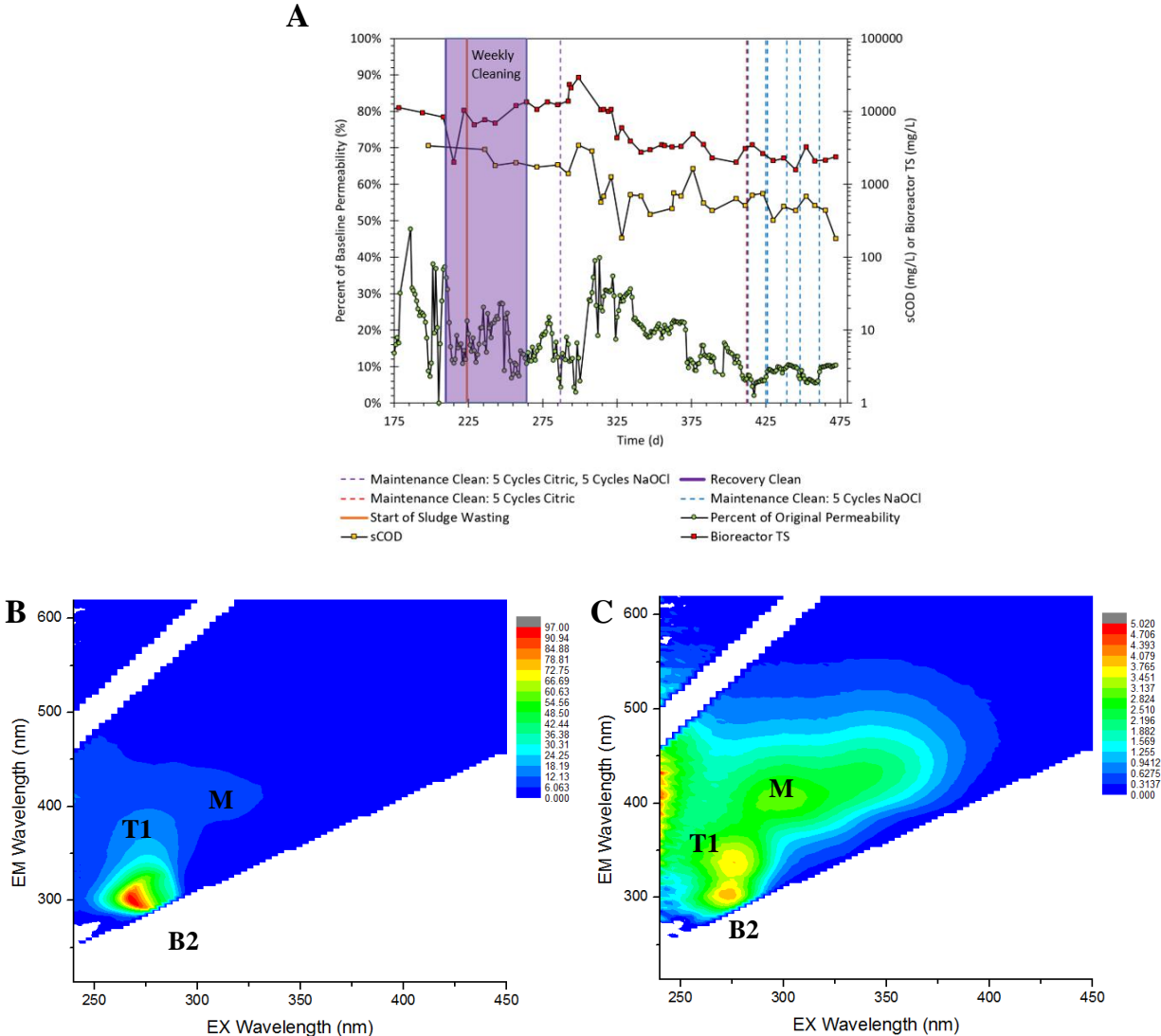


Figure 4.4 A period of operation from day 175 to the end of operation on day 472 is shown in (A) to show the effects of wasting solids, which affects concentrations of the bioreactor’s total solids as well as the bioreactor’s soluble chemical oxygen demand (sCOD), on permeability. (B) and (C) are Excitation-Emission Matrices (EEMs) generated from fluorometer data, which are used to further characterize the soluble organic matter in the membrane permeate. During fouled conditions (B) fluorophore B2, indicative of tyrosine-like compounds, is predominant, but the impacts of a tryptophan-like peak (T1) and a humic-like peak (M) are still apparent. B2 is present during normal operation (C) at lower concentrations. T1 and M, which suggest the presence of tryptophan-like compounds and humic-like compounds respectively are also seen during normal conditions.

A preliminary characterization of the colloidal fraction was conducted using a fluorometer to analyze the dissolved organic compounds in the permeate during days 452 and

472, which correspond to a period of decreased membrane performance and a period of stable membrane performance, respectively (Figures 4.4B and 4.4C). The fouling event occurring during day 452 appears to be caused by higher concentrations of proteinaceous materials, particularly tyrosine-like compounds, as indicated by the higher concentrations of the B2 fluorophore compared to what was observed on day 472 (Henderson et al. 2009; Hudson and Reynolds 2007). Tryptophan-like and humic-like compounds, as indicated by fluorophores T1 and M, respectively, are present in both EEMS, but their impacts are relatively masked due the higher concentrations of tyrosine-like compounds (Henderson et al. 2009; Hudson and Reynolds 2007). Further research is required to confirm if colloidal proteinaceous materials have a disproportionate impact AnMBR fouling, and if they can be candidates for continuous monitoring in the membrane permeate.

4.3 Foulant Characteristics and Composition

4.3.1 Organic Foulants

The foulant layer contained black and brown clay and silt-sized particles, with an organic matter content of 59% as determined by the LOI test. Organic filaments consistent with those of filamentous bacteria were observed only in samples taken from the bottom of the membrane module, indicating that the spatial distribution of foulants is non-uniform and may have implications for maintenance procedures. Annelids and algae were also found throughout the cake layer, and although their impact on fouling is unknown, it indicates that the cake layer is a complex matrix governed by more than just biofilm properties.

FTIR analysis of the foulant cake (Figure 4.5A) confirmed that the fouling was largely organic. The strong peak at 1029.33 cm^{-1} has been suggested as indicative of the presence of polysaccharide and polysaccharide-like organic substances due to symmetric and asymmetric

C=O stretching, as observed in previous lab scale AnMBR studies (Kimura et al. 2015; Sahinkaya et al. 2018; Yurtsever et al. 2016). However, a similar peak can be observed in the FTIR spectra from the ignition residue (Figure 4.5B), which suggests that the peak may be inorganic in nature; the peak is consistent with spectra obtained from crystalline silica and the actual peak may be signatures of aluminosilicate materials (Evans et al. 2018). The peaks at 1538.16 cm^{-1} and 1632.48 cm^{-1} are consistent with amide II and amide III groups, respectively, which have been noted for being unique to secondary protein structure and indicative of proteins in the foulant cake (Maruyama et al. 2001; Sahinkaya et al. 2018). The peak at 3279.55 cm^{-1} is also associated with proteins, and suggests primary amine or amide (Coates et al. 2000). The two peaks at 2920.27 cm^{-1} and 2851.21 cm^{-1} indicate the presence of saturated aliphatic compounds, which have also been observed to be present in urease protein samples (Coates et al. 2000; Evans et al. 2018). Altogether, the FTIR analysis of the foulant cake corroborates the EEM analysis and suggests that proteins are the primary foulant on the AnMBR membrane fibers, which is consistent with previous AnMBR studies (Ding et al. 2015; Gao et al. 2010).

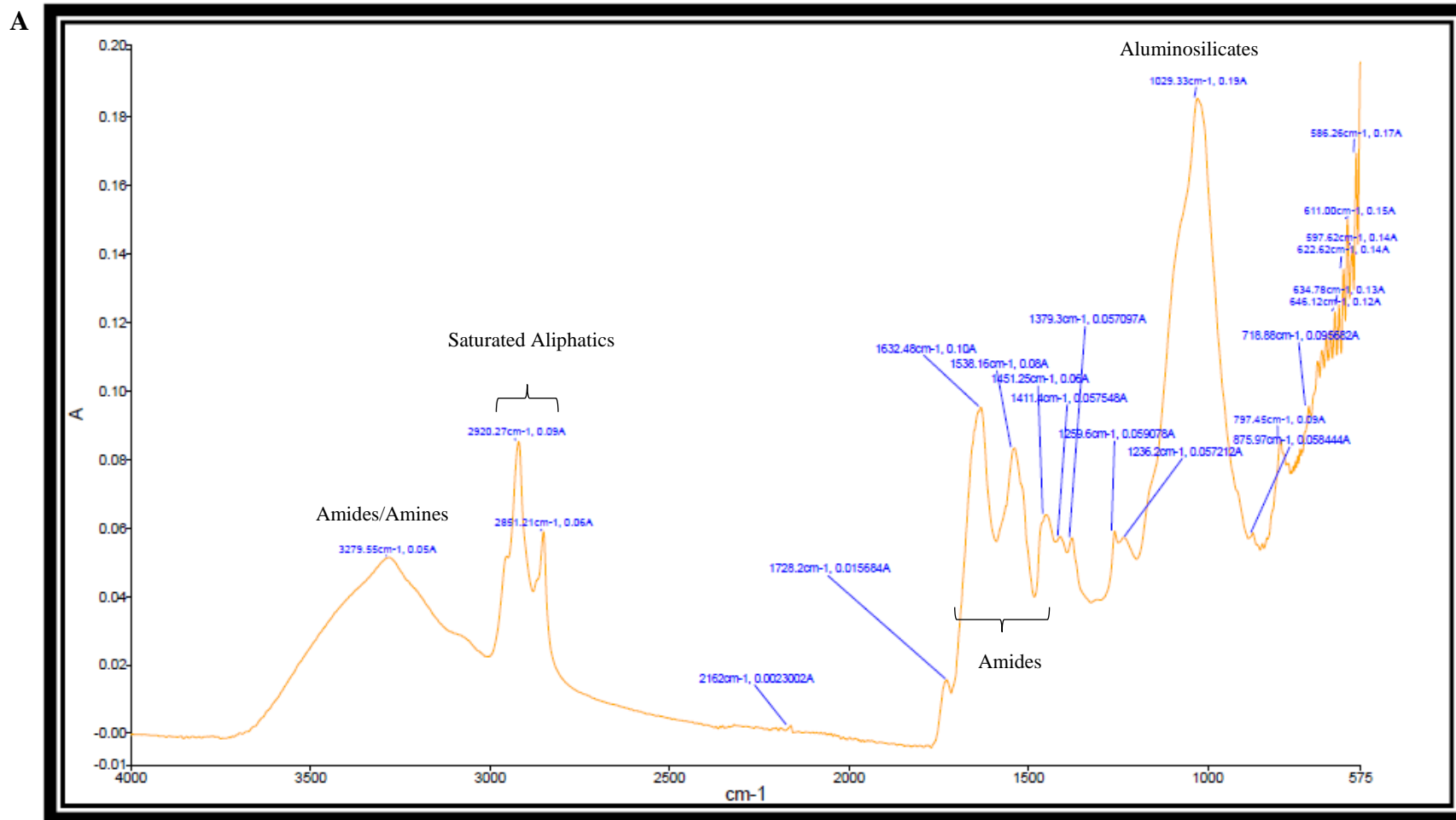


Figure 4.5A FTIR spectra of dehydrated foulant from the cake layer. The peak at 3279.55 cm^{-1} , associated with primary amines and amides, and the peaks at 1538.16 cm^{-1} and 1632.48 cm^{-1} , uniquely associated with amide II and amide III groups, suggest the heavy presence of proteins. Saturated aliphatics were observed at peaks 2920.27 cm^{-1} and 2851.21 cm^{-1} , and aluminosilicates are suggested by the peak at 1029.33 cm^{-1} .

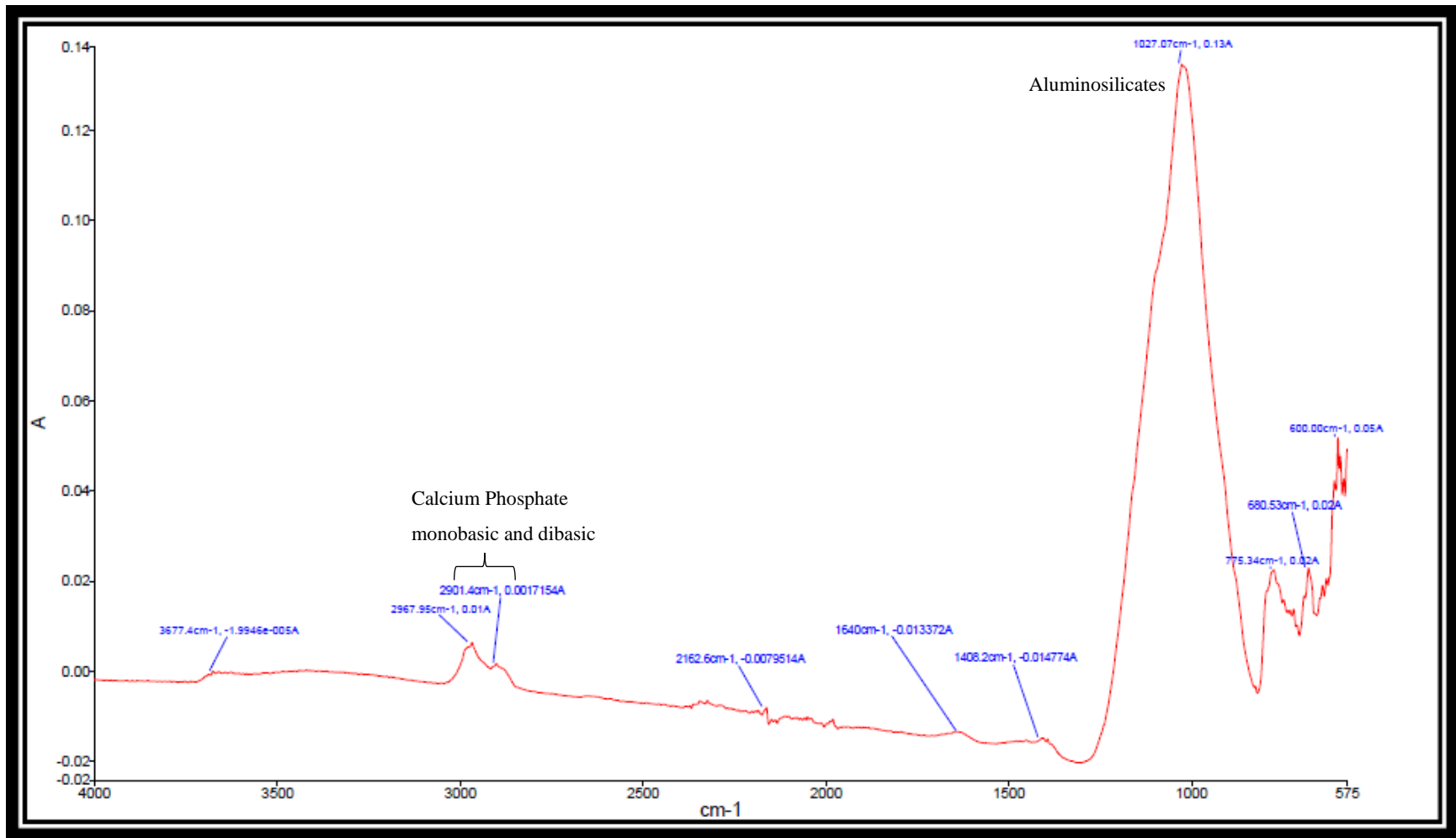
B

Figure 4.5B FTIR spectra of foulant after ignition at 450°C for 8 hours to combust the organic materials present, leaving only inorganics. The peaks at 2967.95 cm^{-1} and 2901.4 cm^{-1} are indicative of calcium phosphate dibasic and monobasic. The large peak at 1027.07 cm^{-1} is indicative of aluminosilicates

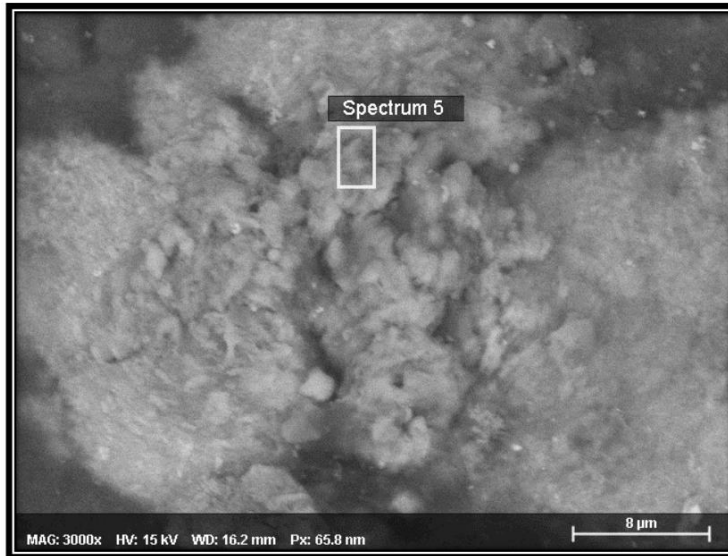
4.3.2 Inorganic Foulants

Inorganic scaling was observed using SEM, EDX, and TEM. The main elements, excluding carbon, and oxygen, found were fluorine, which is associated with the membrane material, silicon, calcium, iron, phosphorus, sulfur, sodium, aluminum, magnesium, titanium, potassium, whose average atomic percentages are listed in Figure 4.6A. The most commonly encountered precipitates were calcium sulfate, calcium and iron phosphates, iron hydroxide, and titanium oxide. Notably, calcium carbonate formation was not observed using FTIR or microscopic methods. This is consistent with an average Langelier Saturation Index (LSI) of -0.20 ± 0.3 during the first 96 days of operation (Appendix B, Table B1). However, because the LSI is specific to calcium carbonate, it does not preclude the possibility of scaling due to other calcium precipitates such as calcium sulfate and calcium phosphate.

Sulfur precipitation was observed primarily as calcium sulfate. Calcium sulfate's presence was readily found throughout the vertical profile of the membrane, and its presence was confirmed independently through SEM-EDX and TEM with X-ray diffraction (Figure 4.6A; 4.6B; Appendix B, Figure B1). No heavy metal-sulfide precipitates were observed, which is in contrast with previous lab-scale studies which suggested that the increase in sulfur concentration in the foulant cake was due to metal-sulfide precipitates, particularly FeS (Sahinkaya et al. 2018; Yurtsever et al. 2016).

While metal-sulfide precipitates were not found, phosphate minerals were found throughout the entire vertical profile of the membrane. Calcium phosphate was ubiquitous along the entire membrane module's profile, consistent with observations and modeling done on previous AnMBR studies that suggest phosphate was the strongest competitor for calcium ions and may be the dominant scalant in AnMBRs (Jun et al. 2017; Zhang et al. 2007).

A



Spectrum 5		Carbon, Nitrogen and Oxygen Ignored	
Element	Atom [%]	Element	Atom [%]
Fluorine	10.89	Fluorine	39.30
Silicon	0.36	Silicon	1.76
Phosphorus	0.21	Phosphorus	1.01
Sulfur	5.24	Sulfur	25.33
Calcium	5.49	Calcium	27.29
Iron	0.32	Iron	1.69
Sodium	0.39	Sodium	1.92
Aluminium	0.24	Aluminium	1.18
Potassium	0.11	Potassium	0.52
Nitrogen	6.67		
Carbon	40.46		
Oxygen	29.61		
	100.00		100.00

B

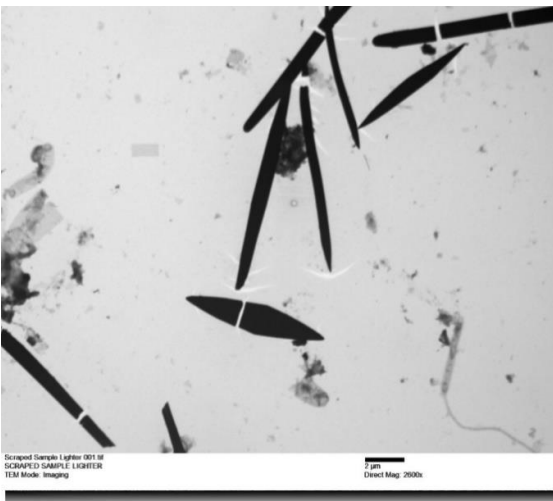


Figure 4.6 Representative micrographs and microscopy results. (A) shows a representative scanning electron microscope image and its accompanying EDX table. (B) is a transmission electron microscope image of inorganic crystalline calcium sulfate, an unexpected inorganic scalant that was encountered throughout the foulant cake layer.

Aluminum phosphate was also observed, but only in samples from the top of the membrane module. The ubiquity of phosphate precipitates along with the lack of phosphorus accumulating organisms in the microbial community analysis shown in the final report on the system suggests that the observed phosphorus removal in the AnMBR is abiotic in nature (Evans et al. 2018; Lim et al. 2019).

4.4 Implications and Considerations for AnMBR Design and Operations

The findings of this study suggest several possible improvements for optimizing membrane fouling strategies in AnMBRs in future as a result of a more fundamental characterization of the foulants. One of the main findings of this study was that the chemical cleaning was not consistently effective, suggesting that the design and operation strategies could be improved upon. In this study, the system tended to be operated at subcritical fluxes, which implies that the gas sparging rates and fluid dynamics were not as favorable for solids deposition. When the blower rate was decreased beyond the critical rate and the operating flux likely exceeded the critical flux, neither chemical cleaning nor increasing the sparging rate were able to restore the lost permeability. This indicates the need for proper, targeted responses to the different types of fouling events.

One of the design assumptions that was challenged was the composition of the foulants, which dictated the choice of chemical cleaning agents. The 2000 mg/L citric acid was selected for inorganic fouling control under the assumption that calcium carbonate would be the main scalant, but both the LSI (Appendix B, Table B1) and the end-of-life membrane analyses suggested that calcium carbonate was undersaturated and not precipitating. Instead, as verified by SEM-EDX and TEM, calcium sulfate and calcium phosphate were ubiquitous. While citric acid is an effective antiscalant for calcium sulfate control when administered at concentrations above 2500 mg/L, it has been observed to encourage calcium sulfate crystal growth at concentrations below 2500 mg/L, suggesting that the 2000 mg/L citric acid chemical cleans employed in this study may have actually had a negative impact on membrane performance (Hoang et al. 2009; Titiz-Sargut et al. 2007). Citric acid has also been shown to have mixed results in removing calcium phosphate scales as well, with several alternatives, such as mellitic

acid or hydroxyethylene diphosphoric acid, being far more effective (Amjad 1989; Greenberg et al. 2005; Qin et al. 2009). It is possible that the chemically irreversible fouling in this study were due to cleaning agent selection, and that more targeted cleaning strategies may have been more suitable for recovering permeability, highlighting the importance of AnMBR foulant characterization.

The large improvements to membrane permeability as a response to solids wasting increases the priority of managing proteinaceous foulants. The presence of proteinaceous foulants in this system was independently corroborated through FTIR and fluorometry, and sCOD may be a simple method for regularly monitoring their approximate concentration. Previous studies have shown that the proteinaceous foulants were primarily from EPS (Gao et al. 2010). Should this be the case, then the sludge wasting could improve membrane permeability through two mechanisms: the permeability could improve as a response either to the decrease in sCOD or protein concentration, or the change in SRT can select for microbes that produce EPS with different properties and impacts to fouling (Al-halbouni et al. 2008; Huang et al. 2010). Further studies are required to verify that the protein foulants are primarily associated with EPS, and what the primary mechanism is for improved membrane performance as a result of solids wasting.

4.5 Summary

This study focused on the fouling aspects of pilot scale AnMBR operation [chapter 2, objective 1B]. It utilized a suite of analyses from both the operational period and end-of-life autopsy to begin developing a framework for the fundamental characterization of AnMBR foulants [chapter 2, objective 2]. The identification of calcium phosphates and sulfates as the predominant scalants in this study may be used to improve future chemical cleaning

strategies: the citric acid cleans in this study may have been at too low a concentration for it to have been effective [chapter 2, objective 3]. This study also offered further support of the critical flux and critical sparging rate hypotheses and suggests that reversible fouling is largely due to solids deposition when operating above the critical flux [chapter 2, hypothesis 1]. Additionally, the tandem use of FTIR, fluorometry, and sCOD measurements suggests that proteinaceous foulants are key in irreversible fouling and pore constriction, and that further research is warranted [chapter 2, hypothesis 2].

Chapter 5 - Review of Techniques for Understanding Membrane Fouling

5.1 Framework for Understanding Membrane Fouling in AnMBRs

Foulant characterization has been a significant challenge in AnMBR systems. One reason is that removing the membranes while maintaining process performance (which requires anaerobic conditions) is extremely challenging. This influence leads to significant data gaps concerning the progression of AnMBR fouling. A significant drawback is that many studies only consider virgin membranes or membranes at the end of operation (Berkessa et al. 2018; Cho and Fane 2002). The issue with analyzing the membranes at the end of operation also extends to the cake layer, which often can only be analyzed at the termination of the experiment. This fails to capture the development of the fouling layer and makes it difficult to determine how fouling behavior changes in response to various conditions such as shock loadings or maintenance cleans.

Because it is difficult to obtain membrane and foulant cake layer samples during operation, measurements from the bulk sludge and membrane permeate have been employed to measure fouling behavior indirectly (An et al. 2009; Ding et al. 2015; Gao et al. 2010). Direct observation of fouling on the membranes and on the cake layer as an alternative to finding correlations in the bulk sludge and membrane permeate to membrane fouling can be a powerful way to develop monitoring parameters for precise and early prediction of fouling events. Ultimately, understanding fouling behavior is only possible by integrating the characteristics of bulk sludge, the foulants, and the permeate.

While bulk sludge, permeate, and the foulants may exhibit different characteristics, changes in each provide valuable information in evaluating the development of fouling.

Enrichment of certain microbes from the bulk sludge to the foulant cake layer may provide insights into the conditions favorable for the bacterial colonizers in biofouling events (Gao et al. 2010). Changes in the community structure of microbes in the foulant layer may also have observable impacts on the dissolved organic matter (DOM) and inorganic species composition found in the membrane permeate. Tying together insights from the microbial communities of the bulk sludge and the foulant layer, the physical structure of the foulant layer, and the permeate characteristics may lead to more fundamental understanding of fouling behavior in AnMBRs. This highlights the need for the use of techniques that can be used either alone or in combination to examine a wide range of substrates in both solid and aqueous phases.

This review assesses various tools and techniques that can be used to characterize the fouling phenomena in AnMBR systems. Many of the techniques have not been used in the context of AnMBRs, but a case for their application can be made due to their successful application in other fields. Recontextualizing techniques used in fields such as geology, where inorganic and organo-metallic characterization has been conducted, for example, can help to understand the complex interactions between the various constituents of the membrane fouling layer.

This review proposes a few techniques that show promise for use in tracking various constituents of interest in the bulk sludge, foulant cake layer, and permeate. Particular attention is given to SMP and EPS, which have been identified as significant factors in AnMBR fouling (Cho and Fane 2002; Dereli et al. 2015). While this study acknowledges that microbial community analysis is key towards deciphering fouling mechanisms, the protocols are already well described in wastewater literature and would not benefit from being reviewed and recontextualized for use in AnMBR systems (Gao et al. 2011; Smith et al. 2013). For similar

reasons, microscopy techniques are not discussed, as standard imaging and elemental analysis techniques are adequate. However, as the sampling methods for the cake layer are not standard, a brief discussion is warranted. Ultimately, the goal is to develop a framework for advancing the understanding of fouling for use as monitoring methods and inform fouling control strategies.

5.1.1 Sampling the Foulant Cake Layer

While sampling methods for the permeate and bulk sludge have well established standard methods similar to sampling effluent and mixed liquor, respectively, at wastewater facilities, no analog exists for sampling the anaerobic cake layer. As such, it is worth discussing the sampling procedure to maintain the integrity of the foulant cake. No standard method or procedure exists for removing the foulant cake from the membrane surface. The most often encountered methods for sampling the cake layer was to use a combination of lightly scraping, often with a plastic scraper, and rinsing with deionized water (An et al. 2009; Evans et al. 2018; Gao et al. 2010).

Scraping is acceptable for chemical and DOM analyses, but may be destructive to the physical structure of the fouling cake matrix. Preparation techniques for electron microscopy may be different depending on the analyses being performed for each study. Within AnMBR literature, the most common procedure is to section the membrane with an intact foulant layer to isolate the area of interest, coating with gold or a platinum alloy, and then imaging the sample (Berkessa et al. 2018). This may not adequately preserve the physical structure of the foulant cake. One method that has been used to preserve physical structure has been to place the sectioned membrane fiber with the foulant cake layer intact into a 7.2 pH buffered glutaraldehyde fixative, then dehydrating the cake layer using an ethanol series prior to coating (An et al. 2009; Kang et al. 2002). Using the fixative followed by dehydration is a standard procedure that is appropriate for preserving the structure of microorganisms and inorganics in

many samples and would result in more intact ultrastructure than directly coating and imaging. However, the dehydration step may not be appropriate for characterizing the foulant layer, as EPS is comprised of a highly hydrated gel matrix; dehydration may serve to collapse the structure and result in misleading conclusions about the physical structure of the cake layer. While no literature in the field of membrane science was found that used fixative without dehydration to preserve the hydrated gel matrix, further research is warranted, as it may provide a more accurate representation of the foulant layer structure and organization.

5.1.2 Definitions, Components, and Analysis of EPS and SMP

The terms SMP and EPS have been used loosely, and sometimes even used interchangeably, making it critical to establish explicit definitions for this study. While the definitions of EPS and SMP can vary, one commonality is that they each refer to fractions of cellular products that contain carbon and electrons, but are not active cells themselves (Laspidou and Rittmann 2002). EPS has commonly been defined as the large, insoluble, polymeric molecules that surround the bacteria within a floc or biofilm community (Laspidou and Rittmann 2002). It is important to establish that EPS composition is a function of the community, with contributions from the various microorganisms within the floc or biofilm. EPS is composed of a hydrated gel matrix of carbohydrates, proteins, lipids and nucleic acids (Gao et al. 2010). While polysaccharides are usually the dominant component, proteins and nucleic acids have also been observed to predominate depending on the treatment process the sample matrix was taken from (Nielsen et al. 1997). In contrast with the insoluble EPS, SMP has been defined as soluble cellular components that may be released during cell lysis or otherwise excreted for cellular functions (Laspidou and Rittmann 2002; Namkung and Rittmann 1986). SMP can be further divided into utilization associated products (UAP), which form from a microorganism's

metabolic processes, and biomass associated products (BAP), formed by the decay of a microorganism (Rittmann and McCarty 2001). Regardless of origin, SMP is associated with soluble proteins, polysaccharides, and humic-like substances (Gao et al. 2010). The loose definitions of EPS and SMP lead to each have their own operational definitions that dictate their extraction procedures and analyses.

The most common extraction method, both in general as well as specifically within AnMBR literature is the heat extraction method (An et al. 2009; Dereli et al. 2015; Gao et al. 2010). This procedure involves centrifuging the sample to settle any suspended material; the pellet would contain only EPS, while the supernatant would contain a portion of the EPS and all the SMP. A portion of the supernatant was then filtered through a 0.45 μm filter and analyzed for DOM, which would quantify SMP. The remaining supernatant could be analyzed for DOM without filtration, and the results would reflect a portion of the EPS as well as the SMP in the sample. The EPS DOM in the supernatant could be determined by subtracting contributions of SMP as was previously measured. Heat is then applied to the pellet to solubilize the EPS bound to the inorganics, and then the DOM content is measured. Quantification of DOM has focused on proteins and carbohydrates, using bovine serum albumin and glucose as comparative standards. The heat applied during heat extraction varied by study, but a range of between 80°C and 100°C for between 10 minutes to 1 hour have been used (Abzac et al. 2010; Dereli et al. 2015; Gao et al. 2010). Centrifugation speeds also vary from study to study, but 20,000g for 20 minutes at 4°C has been notable for being a less degradative technique for the extraction in the context of granular sludges (Abzac et al. 2010). While heat extraction is the most common method for EPS and SMP extraction, it may lead to contamination through the lysing of the microbial biomass (Redmile-Gordon et al. 2014).

There are several alternatives to heat extraction for EPS and SMP measurements. One alternative that has been increasingly popular is the use of cation exchange resins (CER), which has several advantages including the preservation of the original chemical structures of the EPS, high extraction efficiency of proteins, and being less susceptible to contamination by cell lysis (Abzac et al. 2010; Redmile-Gordon et al. 2014). The process of sequential CER extraction is more involved both in terms of materials and labor and the standard method does not differentiate between EPS and SMP (Park and Novak 2007; Redmile-Gordon et al. 2014). Chemical extraction procedures have also been employed in wastewater treatment SMP and EPS analysis, using chemicals such as ethanol, EDTA, and formaldehyde, but reactions with the DOM itself may obfuscate the results (Abzac et al. 2010). Furthermore, due to the differing biases from each extraction technique, results between different techniques being applied to different sample matrices may make comparisons difficult (Redmile-Gordon et al. 2014). As such, the simplest method may be to employ the heat extraction method unless an exhaustive fractionation of the EPS and SMP DOM is desired.

Several methods exist to quantify the sugars and proteins within SMP and EPS after extraction, each of which comes with their own set of known and unknown biases, so determining an accurate, practical, reproducible, high-throughput method for foulant cake analysis is a major objective. The Bicinchoninic Acid Assay (BCA) is a standard colorimetric method that relies on the conversion of Cu^{2+} to Cu^+ for the quantification of proteins, improving upon the still commonly used Lowry Assay, and has been used successfully in the context of AnMBRs (Chuen et al. 2015; Walker 2009). Carbohydrates have several common methods for quantification, with the phenol-sulfuric acid method and the anthrone method being the most popular (Dai et al. 2016; Gao et al. 2010; Liu et al. 2019a). All of the above methods are

amenable for use with a microplate reader, which improves their accuracy, repeatability, and throughput. While SMP and EPS extraction has been done in several AnMBR studies, their use of different extraction methods paired with different analytical techniques makes drawing conclusions between them difficult, as each combination likely introduces its own set of biases, which can be especially present in matrices as complex as membrane foulants (Chuen et al. 2015; Liu et al. 2019a; Sahinkaya et al. 2018). Hence, it may be worth developing a protocol for the extraction of SMP and EPS for membrane foulant studies and determining the general biases of previous studies for more accurate comparisons; one such method for heat extraction is presented in Chapter 6.

5.1.3 Fluorescence Spectroscopy

Fluorescence spectroscopy has been an increasingly popular tool for characterizing DOM, with wide applications in biological sciences and water and wastewater treatment (Henderson et al. 2009; Stedmon et al. 2005). The technique relies on exciting molecules in a sample using a beam of light, typically in the ultraviolet range, and measuring the light emitted in response using a fluorometer. Plotting excitation and emission wavelengths observed can provide a profile for the dissolved organic material composition in the sample (Henderson et al. 2009; Hudson and Reynolds 2007). Fluorometry has been applied to analyze river systems, waste streams, and polluted environments, and is notably promising as a commercially adoptable monitoring solution in drinking and wastewater plants, as the analysis is rapid and requires relatively little sample preparation in samples (Henderson et al. 2009; Hudson and Reynolds 2007). The potential applications of fluorometry in AnMBR fouling studies are numerous: determining and comparing the DOM components that are present in the influent, bulk sludge,

and foulant cake layer and correlating certain components to fouling events would be important from both a fouling management perspective as well as for monitoring.

The interpretation of excitation emission matrix (EEM) data can be done through visual peak identification or through multivariate data analysis techniques such as parallel factor analysis (PARAFAC), which has the advantage of being able to quantify each individual DOM components' fluorescence signals (Stedmon and Bro 2008). Visual peak identification provides qualitative data to determine the fluorescent peaks resulting from a matrix of humic-like, fulvic-like, protein-like, and polysaccharide-like components; Table 1 is a compiled list of fluorophores likely to be encountered in AnMBR fouling studies based upon water reuse monitoring studies (Her et al. 2003; Hudson and Reynolds 2007). PARAFAC analysis adds a quantitative component by generalizing principal component analysis to higher dimension arrays and enables the tracking of DOM production and removal (Stedmon et al. 2005; Stedmon and Bro 2008).

Sample preparation for fluorometry can increase in complexity depending on the sample matrix, degree of fractionation desired for analysis. Because fluorometry is applied to dissolved species, the removal of solids is critical for the analysis of samples such as sludge or the foulant cake layer. Dissolved organic extraction of dewatered anaerobic digestion sludge with minimal targeted extraction, allowing for the analysis of the overall profile, has been accomplished by adding deionized water until a solid to water ratio of 1:20 (w/v) is achieved, shaking the mixture for 24 hours at room temperature, and then filtering the sample through a 0.45 μm filter (Li et al. 2014). It is also possible to analyze the DOM from extracted fractions of SMP and EPS; a combination of centrifugation, resin extraction, and thermal digestion has been used on anaerobic digestion sludge, and AnMBR sludge and membrane foulant cake layers (Ding et al. 2015; Luo

et al. 2013). These extractions enable the tracking of changes of each DOM component, which can be useful in determining what conditions and fractions are correlated to AnMBR fouling.

Table 5.1 A compiled list of fluorophores likely to be found in wastewater and their characteristic excitation and emission wavelengths (Henderson et al. 2009; Hudson and Reynolds 2007)

Fluorophore	Component/Source	λ (nm)	
		Excitation	Emission
A	Humic-like	237-260	400-500
C1	Humic-like	320-340	410-430
C2	Humic-like	370-390	460-480
B1	Tyrosine-like	225-237	30-321
B2	Tyrosine-like	275	310
T1	Tryptophan-like	275	340
T2	Tryptophan-like	225-237	340-381
D	Fulvic-like	255-280	400-455
M	Algal manipulation of nutrients or "marine humic-like"	290-310	370-410
	DOM from Optical Brighteners (such as washing powder)	375, 350, 330	410-450

Previous AnMBR fluorometer studies have used EEMs to analyze differences between influent, permeate, and extracted EPS and SMP from both the foulant cake layer and bulk sludge (An et al. 2009; Ding et al. 2015). Both An et al. and Ding et al. identified humic substances and proteinaceous materials as being the dominant fractions of the AnMBR foulant layer. An et al. observed a decrease in fluorophores B and C, tyrosine-like and humic-like peaks respectively, from the influent to the effluent, indicating that they were partially removed by the AnMBR. The group also found that peaks B and C were in the cake layer, indicating that the membrane rejection may concentrate these proteinaceous materials and visible humic substances, which may have been redeposited as key foulants (An et al. 2009). However, An et al. did not perform

EEM analysis on the bulk sludge, so no relative comparison can be made from their study. In a separate study, Ding et al. focused on the comparison between bulk sludge and the foulant cake and found a similar presence of tyrosine-like and humic-like peaks, but also observed fulvic-like and tryptophan-like peaks in both samples. The cause of the differences in observations between An et al. and Ding et al. are unclear, as influent data was not presented in Ding et al. Regardless, Ding et al. observed a significant increase in tryptophan-like and tyrosine-like peak intensities in the foulant cake layer compared to the bulk sludge, indicating that proteins may have a disproportionate impact on AnMBR fouling (Ding et al. 2015). Preliminary fluorometer data from the pilot scale AnMBR study conducted at Ft. Riley also found an increase in proteinaceous peaks, suggesting that more extensive use of fluorometry would be a promising research direction. No AnMBR study was found that had used fluorometry to dynamically track the progression of fouling events or attempted to correlate EEM peak intensities with sCOD or TMP, which could be potentially developed into new monitoring strategies [chapter 2, objective 3].

5.1.4 Fourier Transform Infrared Spectroscopy

FTIR has been a powerful tool for the rapid analysis of organic and inorganic substances in a variety of fields including geology (J. Madejová 2003), food processing (Anjos et al. 2015), and water and wastewater treatment (Berkessa et al. 2018; Tang et al. 2007). Its wide applicability across different fields for different substrates suggest that FTIR may be a powerful tool for characterizing the complex matrix of inorganic and organic foulants, and potentially their interactions in the cake layer, as well as on the membrane itself (Berkessa et al. 2018). Fourier transform infrared (FTIR) spectroscopy involves passing infrared (IR) radiation through a sample and measuring the amount of radiation that has been absorbed by the sample, with each component producing characteristic molecular vibrations (Bates 1976; Smith 2011). Different molecules will absorb

certain spectral components to varying degrees depending on its structure, which affects peak position, height, and width, and quantification of substances can be done by comparing the sample spectrum to the spectra of samples of known concentrations and using Beer's Law (Smith 2011). FTIR has many advantages that have made it popular in various industries due to being inexpensive, user friendly, rapid, and applicable to both aqueous and non-aqueous samples (Jensen et al. 2003; Smith 2011).

Various techniques have been applied to account for various optical properties, but transmission and attenuated total reflectance, and diffuse reflectance infrared Fourier transform (DRIFT). Transmission FTIR is the most commonly used technique, which measures the IR radiation that is transmitted through the sample. Attenuated total reflectance (ATR) is a rapid technique, of particular interest for characterizing proteins and their structure, that is based on measuring changes that occur in an internally reflected IR beam that contacts a sample through a crystal, typically zinc selenide, germanium or diamond (Beasley et al. 2014; Tang et al. 2007). DRIFT measures the reflectance stemming from the penetration of the IR beam into the sample and its interaction with the sample particles, which is the namesake diffuse reflectance (Beasley et al. 2014). ATR and DRIFT require additional accessories, but their applications in various fields suggest their viability as diagnostic tools for AnMBR fouling.

FTIR has been used in geology for the identification and characterization of clay-like materials, which have been observed in AnMBR studies at the pilot scale (Evans et al. 2018; J. Madejová 2003). The different absorption bands owing to OH and Si-O groups can be used to differentiate clay minerals and their orientations using transmission IR spectroscopy. Characteristic patterns in the O-H stretching region can be used to differentiate between coordination of hydroxyl groups, which can be used to infer whether the clays are arranged in

1:1 or 2:1 layers and whether they were di- or tri-octahedral (J. Madejová 2003; Merlic and Strouse 1997). This information can be used to develop more targeted chemical cleaning strategies that more effectively address the inorganic foulants. Of interest in membrane fouling is the interaction between the organic and inorganic foulants at the membrane interface, which FTIR can also help elucidate; alkyl and aryl modifications of inorganic clays have been able to be distinguished using DRIFT. The modified organo-clays have been known to adsorb organics, and this type of interaction between organics and inorganics may be a key factor in cake layer development and irreversible fouling (J. Madejová 2003; Meng et al. 2009b).

The most common method applied to membranes is a transmission FTIR scan of the membranes themselves, comparing virgin membranes, modified coated membranes, and fouled membranes (Berkessa et al. 2018; Ding et al. 2015; Tang et al. 2007). Tang et al. used FTIR was to evaluate the uniformity of the applied coatings on RO membranes by comparing the spectra from coated and uncoated membranes and found that they were distinct due to an increase of O-H groups consistent with the fact that the coatings used were oxygen rich (Tang et al. 2007). While the treatment of deliberately coating RO membranes is different, the principle of evaluating membranes before and after a treatment can be applied to AnMBR fouling. Evaluating the uniformity of membrane coating material in UF membranes and comparing virgin membranes to fouled membranes may reveal defects that are conducive to fouling. The application of FTIR in AnMBR literature has been relatively limited, but largely follows the same ideas as with reverse osmosis membrane analysis. Berkessa et al. used FTIR to examine a fouled AnMBR fiber and were able to confirm that the cake layer was comprised principally of macromolecules such as proteins, carbohydrates, and phospholipids. The macromolecules were found not only deposited on the membrane surface, but also in the membrane pores, where they

possibly contribute to irreversible pore constriction. Ding et al. utilized ATR-FTIR on virgin and fouled membranes and found that the surface spectrum of the fouled membrane contained acidic moieties and a distinct peak corresponding to amides (Ding et al. 2015). While membrane surface scanning provides useful data, it can only be done at the end of operation, making this technique less suitable for routine monitoring.

One strategy with potential for development is tandem characterization of the foulants on the membrane surface paired with the data from the membrane permeate or bulk sludge. The application of FTIR to wastewater streams has shown that bulk sludge and effluent SMP and EPS differ significantly, and it is expected that they would also differ from the cake layer in AnMBR systems (Ramesh et al. 2006). Furthermore, characterizing the cake layer deposited on the surface and comparing it with FTIR spectra from the permeate and bulk sludge, it may be possible to decipher patterns in fouling and would be a feasible monitoring tool.

5.2 Summary

There are many potential techniques for analyzing AnMBR fouling, only a small fraction of which have been applied in AnMBR studies [Chapter 2, Objective 2B]. The foulant cake layer, being a complex matrix of inorganics and organics, necessitates the use of multiple techniques in tandem in order to characterize its components. By using a suite of techniques to characterize the solid phase and aqueous components of the fouling layer, it may be possible to determine the physical and microbial structures involved in the fouling phenomena, both at its onset and proliferation. However, as sampling from the cake layer is difficult during regular operation, developing correlations between the bulk sludge, the cake layer, and the permeate appears to be a promising strategy. Achieving this using versatile techniques that can yield data that can be compared across all three sample matrices, such as fluorometry and FTIR, can yield

additional insights into the development and impacts of fouling throughout the AnMBR process. The ultimate goal is to develop a framework that connects the microbial community structure, the physical structure of the cake layer, and the impacts to the membrane permeate. Increasing this understanding is critical to developing more efficient fouling management strategies, which would aid in the viability of AnMBRs as a commercial technology for wastewater treatment.

Chapter 6 - Critical Evaluation of Heat Extraction Temperature on SMP and EPS Quantification in Wastewater Processes

Despite the variety of SMP and EPS extraction methods available, there is little in the way of standardized methodology. The heat extraction method was the most used technique in the wastewater context but comparing the results from various studies yielded vastly different results; one possible question was the choice of extraction temperature. This necessitated a critical evaluation of the effect of extraction temperature before proceeding. This study investigated the effect of the heat extraction temperature on aerobic, anoxic, and anaerobic BNR sludge samples, then used the findings to investigate aerobic MBR sludge.

6.1 Introduction

Soluble microbial products (SMP) and extracellular polymeric substances (EPS) have been widely studied within the context of various biological wastewater treatment configurations as they can exert major influence on the chemical and physical characteristics of the suspended solids or mixed liquor, including flocculation, settleability, and surface charge, in addition to impacting effluent quality (Hu et al. 2019; Kunacheva and Stuckey 2014; Morgan et al. 1990; Sheng et al. 2010). Understanding the behavior of SMP and EPS continues to gain importance especially with the widespread adoption of membrane bioreactor (MBR) technology for wastewater treatment due to their impacts on treatment performance as well as their relationship with the critical issue of membrane fouling (Huang et al. 2010; Ishiguro et al. 1994; Reid et al. 2006; Xu et al. 2020b). However, there is major difficulty in comparing data between studies due to the lack of a standard protocol and inconsistent definitions of SMP and EPS. (Kunacheva and Stuckey 2014; Laspidou and Rittmann 2002; Sheng et al. 2010).

EPS has commonly been defined as the largely insoluble proteins, carbohydrates, lipids, nucleic acids, and other macromolecules secreted by bacteria, and are found surrounding the surface of bacteria within a floc or biofilm community as a hydrated gel matrix (Gao et al. 2010; Judd 2010; Laspidou and Rittmann 2002). In contrast with the relatively insoluble EPS, SMP has been defined as soluble cellular components that may be released during cell lysis or otherwise excreted for cellular functions as well as the products resulting from substrate breakdown (Laspidou and Rittmann 2002; Namkung and Rittmann 1986). SMPs are associated with soluble proteins, polysaccharides, and humic-like substances, and it is generally accepted that soluble EPS and SMP refer to the same components (Gao et al. 2010; Jang et al. 2006; Laspidou and Rittmann 2002). In addition to loose definitions for EPS and SMP measurements, there are a variety of extraction techniques, including cation exchange, chemical extractions, and thermal extractions, each with their own operational definitions.

Due to its broad applicability and ease of execution, heat extraction, either standalone or as part of a procedure, is a common EPS and SMP extraction method that has been used with anaerobic, anoxic, and aerobic wastewater sample matrices (Dereli et al. 2015; Hu et al. 2019; Li and Yang 2007; Morgan et al. 1990). While heating is a common extraction step among many procedures including NaOH, sonication, and thermal extraction methods, exposure to excessively high temperatures leads to the lysing of the microbial biomass, demonstrating a need to determine an acceptable extraction temperature (Dai et al. 2016; Lv et al. 2019; Redmile-Gordon et al. 2014). Additionally, the heat extraction temperature varied by study, typically between 40°C and 100°C for 10 minutes to 1 hour, which makes comparisons between studies difficult due to differences both in extraction efficiency and extent of lysis; in one pure culture study by Lv et al., 2019, heat extractions were performed at 45°C, which extracted less than 5

mg/g of carbohydrates, and 60°C, which extracted 55 mg/g, which highlights the difficulty even between comparisons of the same sample (Abzac et al. 2010; Dereli et al. 2015; Gao et al. 2010; Lv et al. 2019). This study aims to broadly investigate the effect of temperature on SMP and EPS extraction and cell lysis applied to sludge samples encountered in wastewater biological treatment processes.

After extraction, the dissolved organic matter (DOM) can be analyzed for a range of constituents, but the carbohydrate and protein profiles and their overall properties are often the focus (Kunacheva and Stuckey 2014). Colorimetric analysis remains the predominant method of quantifying carbohydrates and proteins (Felz et al. 2019). However, despite the improvements made through modifications or adaptations for use with a microplate to improve their accuracy and repeatability, colorimetric measurements have been shown to be inadequate. This is primarily due to the dependence of these quantification methods on the standard compound selected and interfering substances, particularly humic-like and phenolic compounds that are characteristically present in SMP and EPS samples, which leads to the need for advanced tools for analysis (Felz et al. 2019).

One potential tool to address this deficiency is fluorescence spectroscopy, which has increasingly been used to characterize DOM in the wastewater field (Kimura et al. 2015; Lim et al. 2020; Ramesh et al. 2006; Sheng et al. 2010). Fluorometry provides a field-deployable, sensitive, non-destructive and rapid analytical method that can show a profile of the various DOM constituents, including protein-like materials, humics, and fulvics, presented using excitation-emission matrices (EEMs) and provides insight into the physicochemical properties of the SMP and EPS that colorimetric methods may fail to capture (Henderson et al. 2009; Sheng et al. 2010). However, fluorometry falls short for use as a complete tool to quantify SMP and EPS

constituents, mainly due to visual interpretation of peaks and principal component analysis only providing qualitative or semi-quantitative data, unless more extensive analyses such as parallel factor analysis are employed (Stedmon and Bro 2008). Pairing EEMs with quantitative analyses, such as colorimetry, total carbon (TC) or total nitrogen (TN) measurements can be a simple check that each analysis has not been excessively compromised by the interfering effects of the constituents present in the sample matrix and provides a deeper investigation into the SMP and EPS profiles.

Because of the difficulties in comparing SMP and EPS data between studies due to the inadequacies of current analytical methodologies as well as the inconsistent operational definitions based on extraction procedures, this study seeks to address these drawbacks through the following objectives: (1) determine the effects of extraction temperature on SMP and EPS profiles, (2) determine the effects of extraction temperature on cell lysis, (3) compare the commonly obtained extraction data obtained through colorimetry, Total Carbon (TC), and Total Nitrogen (TN) analyses, versus fluorometry, and (4) compare and contrast the response profiles across common wastewater sludges. This study will particularly examine the effects of temperature on SMP and EPS extraction from sludges from various zones of a BNR process (activated sludge, anoxic sludge, and anaerobic sludge) to achieve an acceptable extraction efficiency while minimizing cell lysis and preserving the structure of the constituents for protein and carbohydrate quantification. The broad findings from the BNR sludge experiments will then be used to estimate a range of possible acceptable extraction temperatures for SMP and EPS extractions from MBR sludge.

6.2 Materials and Methods

6.2.1 Sampling Information

The experiment was designed to evaluate the effect of extraction temperature on activated sludge (AS), anoxic (ANX) sludge, anaerobic (ANA) sludge, collectively referred to as the BNR sludges, and aerobic MBR (AeMBR) sludge. Key information about the sampling can be found in Table 6.1.

Table 6.1 General sample information and solids characteristics.

Sample	Sample ID	TSS (mg/L)	VSS (mg/L)	Sample Date	Location
Activated Sludge Aeration Basin	AS0	2100±90	1700±70	11/16/2020	Manhattan, Kansas WWTP Middle of Aeration Basin
	AS	2300±140	1900±120	2/4/2021	
Activated Sludge Anoxic Sludge	ANX	2100±160	1600±70	2/5/2021	Manhattan, Kansas WWTP Middle of Anoxic Basin
Activated Sludge Anaerobic Sludge	ANA	1900±140	1600±70	2/5/2021	Manhattan, Kansas WWTP Middle of Anaerobic Basin
Aerobic Membrane Bioreactor Sludge	AeMBR0	8300±300	6700±180	11/19/2020	De Soto, Kansas BioMicrobics Test Site Membrane tank
	AeMBR1	2700±80	2500±90	3/5/2021	
	AeMBR2	2700±60	2300±60	3/12/2021	

The Manhattan water resource recovery facility’s BNR system is typical for a treatment system designed for a midwestern city’s municipal waste, but notably is operated to accommodate for a transient student and military population. BioMicrobics’ AeMBR in De Soto, Kansas also treats municipal wastewater, but the residential flow primarily originates from a retirement community. There are two notable differences between AeMBR0 compared with AeMBR1 and AeMBR2. Firstly, AeMBR0’s comparatively higher solids concentrations are due to being collected before a major sludge wasting event. Secondly, AeMBR1 and AeMBR2 were experiencing foaming during the sampling dates; the reactors smelled of detergent, and the bubble morphology likely indicated that it was caused by surfactants. The unplanned conditions in the two latter samples

provided a valuable coincidence to test the robustness of the procedures used in this study. Total Suspended Solids (TSS) and Volatile Suspended Solids (VSS) analyses were performed on the sludge samples according to standard methods for wastewater 2540D and 2540E, respectively (Eaton et al. 2005).

6.2.2 Extraction Procedure and Analyses

The procedural outline of this study can be found in Figure 6.1. All centrifugation steps were performed using an Eppendorf 5920 R (Eppendorf, Hamburg, Germany) at 4000g and 4°C for 15 minutes; the centrifuge speed was determined by a series of experiments to find the minimal speed that could settle all the tested sludges into stable pellets. Notably, AS and AeMBR samples settled more compactly than ANX and ANA samples. Heat extraction was performed at room temperature, 40°C, 60°C, and 80°C to determine the effect of temperature on SMP and EPS extraction.

The SMP and EPS extraction data consists of Total Carbon and Total Nitrogen (TC-TN) analysis, and 96-well microplate colorimetric analysis methods for carbohydrates and proteins. Sample processing and analyses began within two hours of sample collection and immediately continued to completion without interruption. TC-TN analyses were performed using a Shimadzu TOC-L and TNM-L (Shimadzu, Kyoto, Japan) analyzer. Carbohydrate and protein analyses were performed in triplicate on a BioTek microplate reader (BioTek Epoch 2, VT, USA) with Greiner Bio-One µClear Bottom 96-well plates (Greiner Bio-One, Kremsmünster, Austria). All concentrations reported in this study have been normalized to the 45 mL of sludge sample collected. In addition to the extraction data, fluorometry was performed on a Horiba Aqualog fluorometer (Horiba, Kyoto, Japan) with the samples aliquoted in quartz cuvettes

(Starna 3-Q-10, Ilford, UK). Statistical analysis was completed using the PROC GLM procedure on SAS Studio 3.8 (Enterprise Edition).

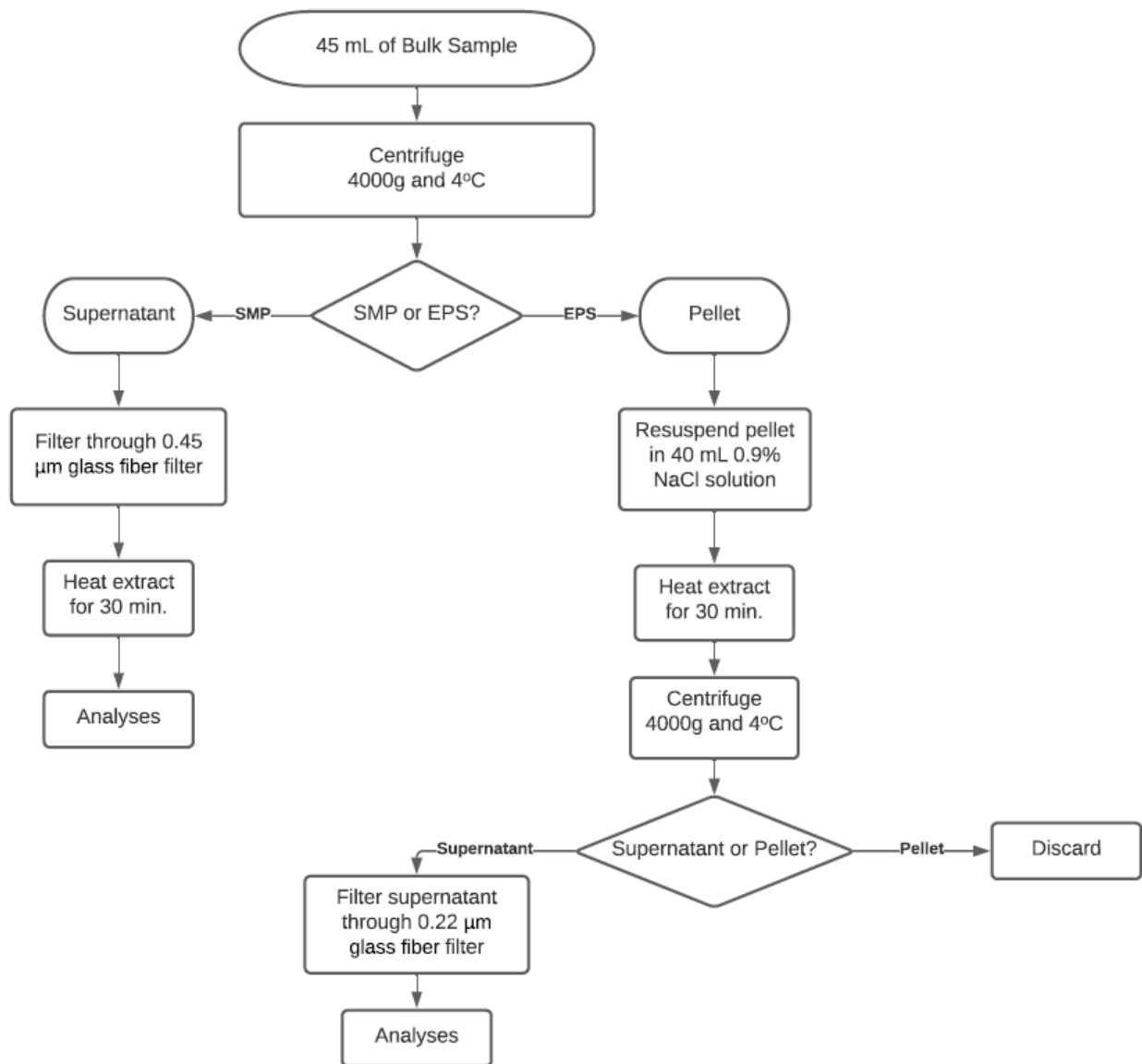


Figure 6.1 Diagram of the extraction procedure for operationally defined SMP and EPS samples.

6.2.3 Colorimetric Analysis Procedures

This study utilized the phenol sulfuric microplate method previously developed for carbohydrate analysis (Masuko et al. 2005). It was performed by adding 50 μL of sample followed by forcefully and quickly adding 150 μL of concentrated H₂SO₄ into each well and

shaking until the solution develops a homogeneous yellow-brown color that indicates the presence of sugars. After the color develops, 30 μL of 5% w/v phenol was added into each well, and the solution was incubated for 10 minutes at 20°C in the microplate reader before reading the absorbances at 490 nm. Glucose was chosen as the carbohydrate calibration standard, as it was the most commonly used standard encountered in wastewater literature (Berkessa et al. 2018; Jin et al. 2013; Kunacheva and Stuckey 2014; Leyva et al. 2008). While the anthrone method is a common alternative to the phenol sulfuric method, the latter has a more rapid and simpler procedure, which contributes to its popularity (Dai et al. 2016; Gao et al. 2010; Leyva et al. 2008; Liu et al. 2019b; Masuko et al. 2005).

Protein analysis was performed using the BCA assay with methods from Sigma Aldrich (BCA1, MO, USA), which included their BCA solution (B9643, MO, USA), containing bicinchoninic acid (BCA), sodium carbonate, sodium tartrate, and sodium bicarbonate in 0.1 N NaOH. 25 μL of each sample was added to the well plate, followed by forcefully and quickly adding 200 μL of BCA reagent and then sealed and incubated at 37°C for 30 minutes. The plates were then cooled to 20°C before having absorbances read at 562 nm. BSA was used as the protein calibration standard, as it was the most commonly used standard encountered in wastewater literature (Abzac et al. 2010; Felz et al. 2019; Hu et al. 2019; Xiong et al. 2015). While the Lowry method is a common alternative, also relying on the conversion of Cu^{2+} to Cu^+ for protein quantification, its reliance on the Folin-Ciocalteu reagent causes interference from reducing agents, which the BCA method and its modified procedures replace with bicinchoninic acid, to help minimize analytical artifacts (Le et al. 2016).

6.2.4 Live/Dead Assay Procedure

Lysis was investigated using the BacLight Bacterial Viability Kit (L7012, Thermo Fisher, MA, USA) live/dead staining assay. After heat extracting each sample, each pellet was resuspended, then diluted with 0.9% NaCl to achieve an OD₆₇₀ of ~0.6. A 1:1 staining solution of 3.34 mM SYTO 9 and 20 mM propidium iodide (PI) was used for this experiment. 100 µL of each sample was then mixed with 100 µL of the working solution and incubated in the dark for 15 minutes prior to its analysis using a fluorescent microplate reader (BioTek Synergy H1, VT, USA).

6.3 Results and Discussion

6.3.1 BNR Sludge Extraction Data

The results of one representative set of each BNR sludge sample's microplate and TC-TN analyses are shown in Figure 6.2. While direct comparisons between the absolute concentration values obtained between different days can vary (Figure 6.2; Appendix C, Figure C1), the influence of temperature produced consistent trends in the measured parameters for each sample matrix. Additionally, in all samples, the TC and TN data generally corroborated the trends in the carbohydrate and protein data, respectively.

Temperature did not have a statistically significant impact on the SMP values in any of the BNR sludges tested (Figure 6.2; Table 6.2). For all samples tested, there was no statistically significant impact of temperature on SMP measurements for carbohydrates or proteins, and the TC and TN results were similarly unresponsive. These results could be expected based on a priori knowledge that SMP constituents are, theoretically, already solubilized and do not require further extraction.

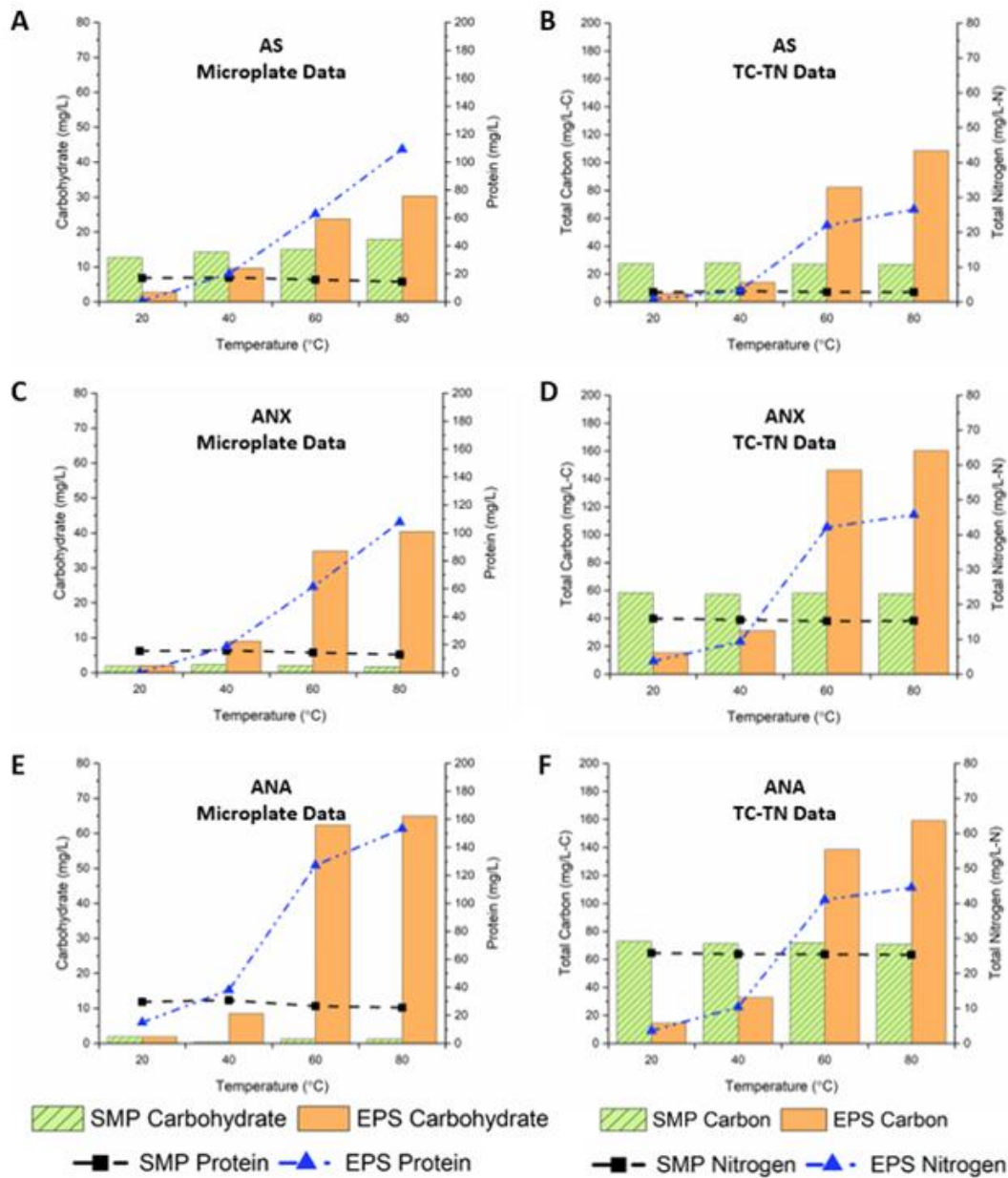


Figure 6.2 Plots of the BNR extraction data. Carbohydrates and proteins were measured using the phenol-sulfuric acid method and bicinchoninic acid method, respectively, and extracted total carbon and total nitrogen measurements were plotted versus extraction temperature. The error (n=3) was less than 10% for all datapoints.

Table 6.2 Table of SMP extraction values averaged across temperatures and p-values greater than 0.05 for Tukey’s multiple comparisons across the temperature ranges, suggesting that temperature has no significant statistical effect on SMP extraction.

SMP Sample	Protein mg/L (p-value)	Carbohydrate mg/L (p-value)	TN mg/L-N (p-value)	TC mg/L-C (p-value)
ANA	28.2±2.5 mg/L (p=0.06)	1.2±0.6 mg/L (p=0.35)	25.6±0.4 mg/L-N (p=0.29)	71.9±1.3 mg/L-C (p=0.26)
ANX	14.7±1.3 mg/L (p=0.06)	2.0±0.3 mg/L (p=0.27)	15.5±0.3 mg/L-N (p=0.15)	58.2±1.1 mg/L-C (p=0.26)
AS	16.2±1.3 mg/L (p=0.10)	15.0±2.2 mg/L (p=0.25)	4.8±0.1 mg/L-N (p=0.54)	29.8±0.9 mg/L-C (p=0.06)

The EPS extractions, in contrast to the SMP observations, responded greatly to the increasing temperatures applied (Figure 6.2). AS, ANX, and ANA samples all showed increases in concentrations for extracted carbohydrates and proteins as well as TC and TN with temperature, with the steepest increase occurring between 40°C and 60°C, which indicates that the bulk of the extraction occurs somewhere between these temperatures.

The extraction data for activated sludge are shown in Figure 6.2A and Figure 6.2B. The four parameters generally followed the same trend: a slight increase from 20°C to 40°C, followed by the steep increase from 40°C to 60°C, and a slightly less steep increase from 60°C to 80°C. The overall shape resembles the exponential-linear range of a sigmoidal curve. The extraction data of ANX (Figure 6.2C, Figure 6.2D) had some similarities, but also showed several differences compared to AS. While the EPS protein concentrations at different temperatures followed the same exponential-linear range of a sigmoidal curve similar to what was observed in the AS samples, the carbohydrates, TC, and TN concentrations in the ANX EPS measurements appeared to follow a diauxic pattern – a full sigmoidal curve with an apparent asymptote at the higher temperatures. However, the steepest increase still occurred between 40°C to 60°C. ANA’s

extraction data (Figure 6.2E, Figure 6.2F) shows more similarities to ANX than AS. This is to be expected since the anaerobic and anoxic zones are located sequentially next to each other and the microbes experience mostly similar redox conditions in these zones due to the absence of dissolved oxygen. The extracted EPS concentrations for the parameters all followed a full sigmoidal curve. The shapes of the curves from each sample, and even the measured parameters within the same sample, can differ, suggesting that there may not be a single temperature that can be broadly applied for all samples for heat extraction procedures. The difference in curve shape between the aerobic basin's sludge from the anaerobic and anoxic sludges, which are more similar to each other, may be due to metabolic differences and sludge age, both of which can affect floc strength.

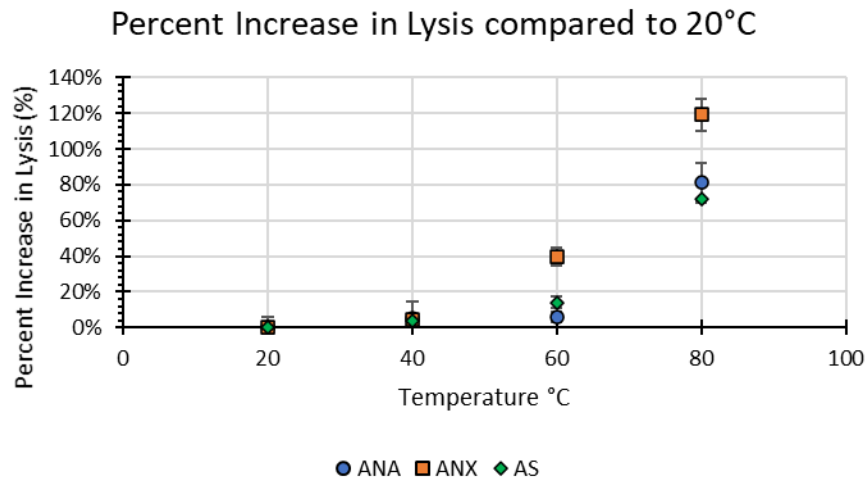


Figure 6.3 A plot of the percent increase in lysis compared to extraction at 20°C. 60°C appears to be around the threshold for excessive lysis in the activated (AS) and anaerobic sludge (ANA) but may be past the point of inflection for anoxic sludge (ANX).

Despite higher temperature extractions incurring an increased risk of potentially lysing cells and releasing intercellular materials into the bulk solution, it is not uncommon to encounter studies that heat extract samples between 80°C to 100°C, which could lead to an overestimation of SMP and EPS concentrations (Comte et al. 2007; Hong et al. 2017; Morgan et al. 1990). The

threshold for cell inactivation and thermal lysis in activated sludge has been noted in literature to occur around 60°C, which suggests that heat extraction above 60°C should be avoided if possible (Kim et al. 2013; Rocher et al. 1999). The live/dead assay corroborates the findings in literature, as 60°C appears to be an inflection point before dramatic rises in anaerobic sludge and activated sludge shown in Figure 6.3. The anoxic sludge exhibited similar behavior but saw significantly more lysis than the other samples. While more research is required to more accurately determine what temperature the aggressive onset of lysis begins, all of the samples experiencing excessive lysis at 80°C suggests that, despite its popularity as a heat extraction temperature, the results may be skewed by intracellular components (Comte et al. 2007; Hong et al. 2017; Morgan et al. 1990).

These thermal lysis problems compound with issues stemming from the overestimation of protein and carbohydrate concentrations in the SMP and EPS using colorimetric microplate assays. While the reasons for the various colorimetric analyses overestimating the SMP and EPS concentrations are not fully understood, notable interfering substances, including detergents, lipids, iron, and creatinine, which are known to be present in the wastewater matrix, could obfuscate results (Sigma-Aldrich 2011; Stuckey and McCarty 1984). Further complicating matters is the fact that, proteins have been noted to interfere with the carbohydrate measurement by reacting with sulfuric acid (Chow and Landhäuser 2004). Because colorimetric methods rely on absorbance, and thus cannot distinguish between interfering substances and the intended analyte, more advanced analytical tools such as fluorometry, are required (Felz et al. 2019; Stedmon and Bro 2008).

6.3.2 BNR Sludge Fluorometry Data

Because fluorometry is sensitive to different compounds, it can provide semi-quantitative and qualitative information about the substances in the wastewater matrix, especially with respect to proteins, which is the primary biologically associated macromolecule with strong intrinsic fluorescence characteristics (Lakowicz 2006). The EEMs of the SMP extractions for AS, ANX, and ANA can be found in Appendix C. Across all the BNR sludges, there appeared to be marginal increases in peak intensities, corroborating the extraction data's finding that SMP samples derive little benefit from additional heat extraction. These increases were slight, but likely more noticeable due to the specificity and sensitivity of fluorometric analysis compared to colorimetry. However, as the peak intensity increase was relatively negligible, the heat treatment step for general SMP analyses can usually be foregone.

In contrast to the SMP samples, the EEMs for AS and ANA EPS extractions showed significant responses with different temperatures (Figure 3); the EEMs for ANX EPS follow the same trend as ANA and can be found in Appendix C. In all three BNR samples, the most apparent fluorophores present were T1, indicative of tryptophan-like compounds, and B2, which is characteristic of tyrosine-like compounds (Henderson et al. 2009; Hudson and Reynolds 2007). While the fluorometer did not show any distinct peaks associated with humic-like (fluorophore A) or fulvic-like (fluorophore D) substances on the BNR extracts, their presence can be seen in the more diffuse profiles at 60°C and 80°C (Henderson et al. 2009; Hudson and Reynolds 2007).

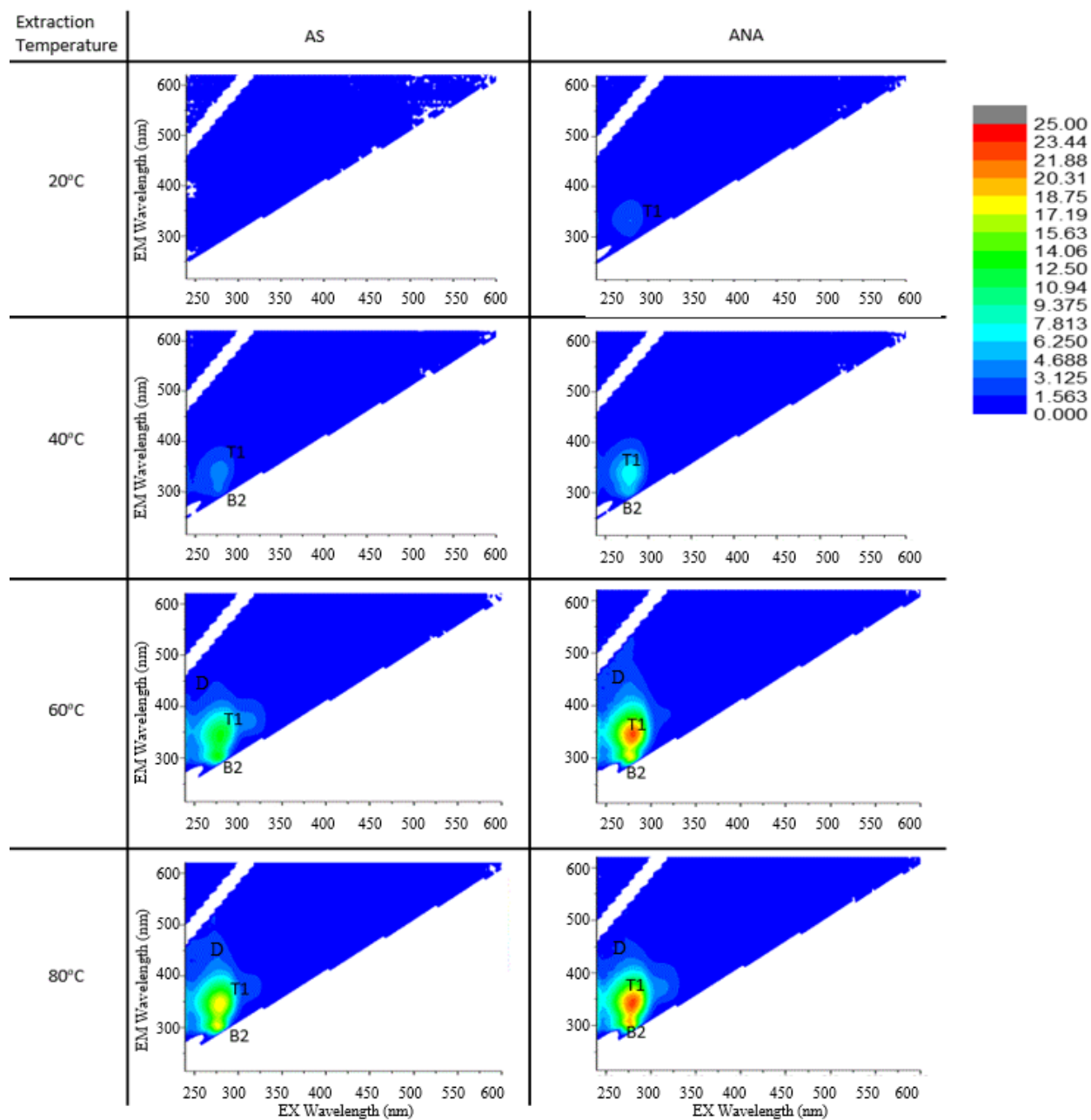


Figure 6.4 Excitation-Emission Matrices of AS1 (activated sludge) and ANA (anaerobic basin sludge) samples extracted at different temperatures. The tryptophan-like peak (fluorophore T1) was predominant, with an accompanying tyrosine-like peak (fluorophore B2), with increasing relative intensity as extraction temperatures progressively increased. A fulvic-like peak (fluorophore D) was also observed at the two higher extraction temperatures.

One important note on fluorescent spectroscopy is that the peak intensities of each fluorophore does not necessarily indicate its abundance relative to other fluorophores. For example, it may

not be appropriate to conclude that tyrosine-like compounds occur in lower concentrations than tryptophan-like compounds because of its lower peak signal because each has different spectral properties.

As with the colorimetric protein analysis data, the general trend of the EEMs shows increasing peak intensity with extraction temperature. When plotted on a scale normalized to the concentrations observed for each sample, EPS extraction at 20°C was below the visualization limit for the fluorometer for AS, and near the limit for ANX and ANA. For AS, the peak intensities of T1 and B2 increased almost linearly from 40°C to 80°C, similar to the trends in both the BCA data and TN data. In the ANX and ANA data, however, the peak intensities had a drastic increase between the 40°C to 60°C extractions, followed by negligible increases from 60°C to 80°C. This more muted response in the EEMs than would be expected, based on the BCA data, more closely resembles the diauxic peak profile of their respective TN plots for ANX and ANA samples. This likely suggests that by 60°C, the extracellular proteins have already been fully extracted in these samples. (Figure 6.2 and Figure 6.4). While further studies involving liquid chromatography and mass spectrometry are required to definitively conclude that the non-fluorescing amino acids have also been extracted, the tryptophan and tyrosine compounds are likely to have been extracted along with the other amino acids in the protein under the temperature conditions applied, as the onset of thermal decomposition of proteins into component amino acids generally occurs only after 130°C (Kasarda and Black 1968).

6.3.3 Aerobic MBR Sludge Case Study

An initial sample of aerobic MBR sludge (AeMBR0) was taken to determine its general behavior using the same procedure as with the BNR sludges (Appendix C, Figure C6). The concentrations of protein, carbohydrate, and TC-TN were higher, but the extraction behavior

with respect to temperature was similar to what was observed with activated sludge. As with BNR sludges, the EPS concentrations increased with increasing extraction temperatures above 40°C. The SMP concentrations did not change with temperature, again confirming that the soluble fraction does not benefit from heat extraction; average values and p-values demonstrating that there was no significant difference between temperatures for SMP samples are as follows: 10.6 mg/L-carbohydrate (p= 0.33), 18.7 mg/L-protein (p= 0.56), 29.18 mg/L-C (p=0.06), 2.84 mg/L-N (p=0.23).

After establishing this baseline, two samples were taken to examine the MBR sludge extraction efficiency at temperatures between 45°C and 60°C to attempt to determine if a temperature lower than 60°C would be suitable for this sample (Figure 6.5, Figure 6.6). Based on the AeMBR0 (Appendix C, Figure C6), it appears that extraction at 40°C is too ineffective to be considered a serious candidate, so 45°C was the lowest tested temperature in this setup. 60°C was chosen as the maximum temperature as it is the threshold for thermal degradation of wastewater sludges as seen both in literature and through the fluorescent microplate measurements (Figure 6.3) (Kim et al. 2013; Rocher et al. 1999). It is important to note that these two samples (AeMBR1 and AeMBR2) were taken during a period where significant amounts of bubbles and foaming was observed in the membrane bioreactor, likely caused by detergents as diagnosed through both visual inspection, odors, and personal communication with the operating staff members. Despite the foaming issue, the extraction procedures used in this study appeared to have reproducible general trends across samples while also finding the presence of surfactants, suggesting their effectiveness as diagnostic tools to also troubleshoot operational problems (Figure 6.5; Figure 6.6). The overall trends produced by the extraction data for AeMBR1 and AeMBR2 are very similar to each other, despite the difference in absolute concentrations

observed. A significant amount of protein extraction occurs by 45°C, while carbohydrate extraction was not observed until 50°C. Another significant increase occurred between 55°C and 60°C, which shows that the AeMBR sludge extractions show a diauxic response from 20°C to 60°C.

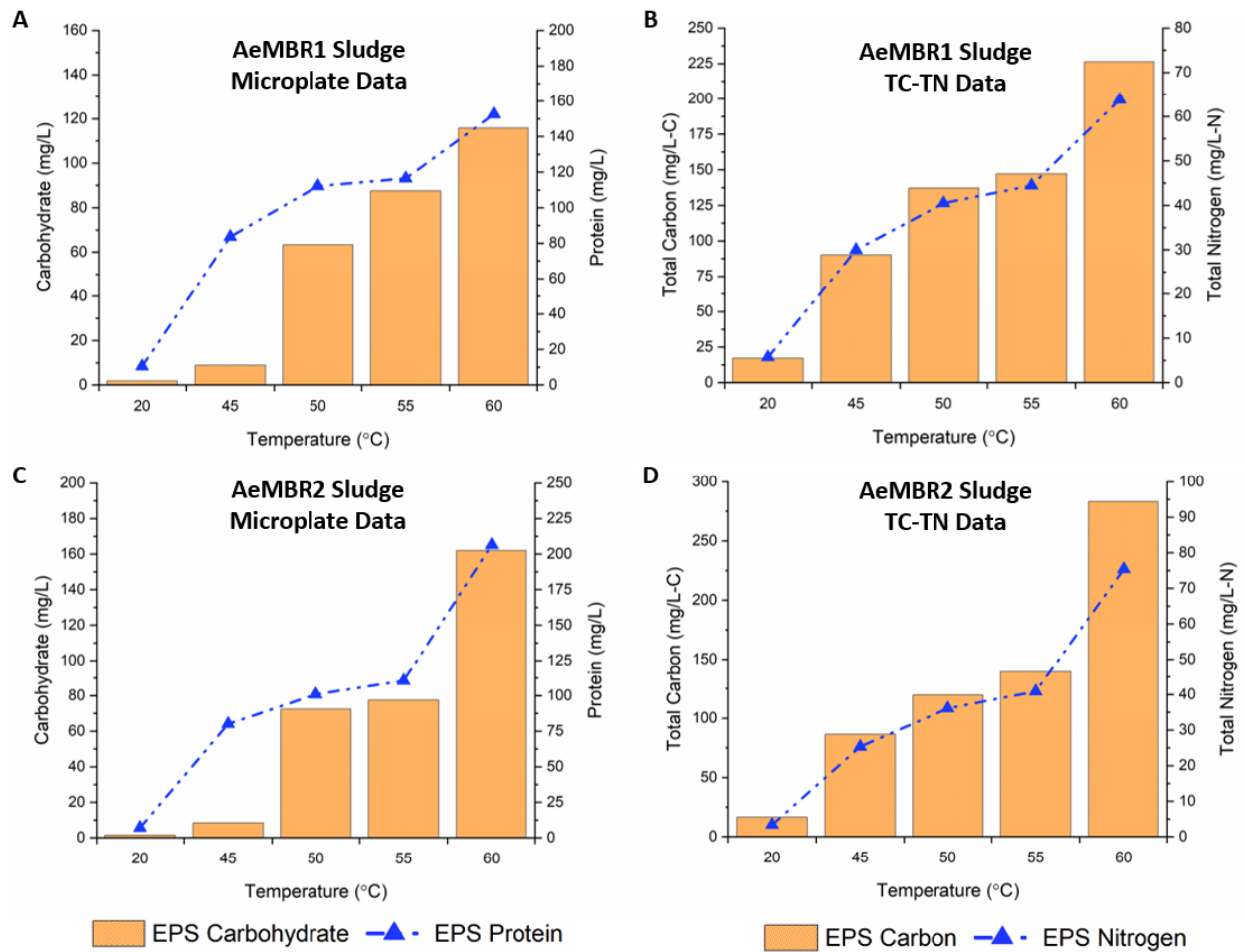


Figure 6.5 Plots of the extracted carbohydrates and proteins for aerobic membrane bioreactor sludges, AeMBR1 and AeMBR2, as measured using the phenol-sulfuric acid method and bicinchoninic acid method, respectively, as well as extracted total carbon and total nitrogen measurements versus extraction temperature. The error (n=3) was less than 10% for all datapoints.

Comparing the carbohydrate extraction with the TC extraction at 45°C reveals an apparent contradiction where carbon is being clearly measured, but carbohydrates are not, with this phenomenon occurring in both AeMBR1 and AeMBR2 samples. A noted issue with

colorimetric determination of carbohydrates is the reliance on a single pure substance standard, glucose being the most common, which is the arbitrarily chosen standard to express the results (Galib et al. 2016; Huang et al. 2010; Li and Yang 2007; Nielsen 2010; Reid et al. 2006). If a significant fraction of the carbohydrates extracted at 45°C have absorptivity significantly different from that of glucose, the calibration may be inappropriate. This potentially highlights a weakness in using colorimetric methods in complex matrices, such as wastewater, which likely contains more than one carbohydrate type and warrants further investigation (Nielsen 2010).

The TC measurement, however, does not suffer from this flaw and simply measures the carbon present in the sample with results expressed in mg/L of carbon. This downside, while major, does not render the phenol-sulfuric colorimetric method completely unusable for wastewater purposes as there appears to be good correlation with the TC data trends in both the BNR sludges and AeMBR samples (Figure 6.2, Figure 6.5, Appendix C6). While the issue of expressing results in terms of a single standard could theoretically be an issue for the BCA method in protein measurement as well, no glaring anomalies have been observed using this dataset between the protein data expressed using BSA as a standard and the TN measurements. One notable difference between the protein and carbohydrate standards is that BSA is a mixed standard, in contrast with glucose being a pure substance standard. Exploring a mixed standard developed for carbohydrates that are applicable to specific matrices may help alleviate the estimation issues but may not address the overestimation due to the lack of specificity of sulfuric acid digestion. Nevertheless, this highlights the need to pair these colorimetric methods with other analytical tools for validation, especially those that can potentially characterize the constituents comprising the sample matrix such as EEMs.

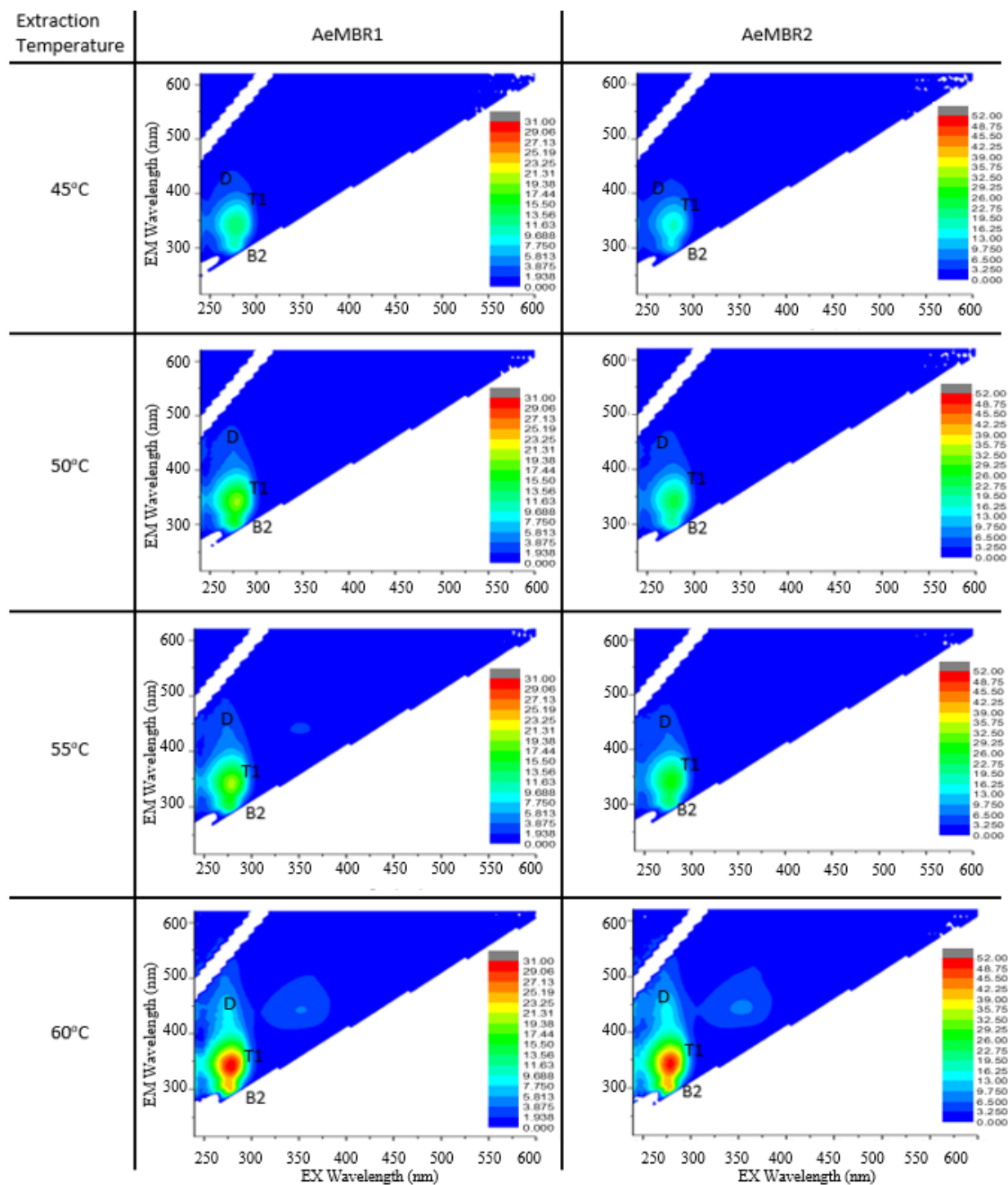


Figure 6.6 EEMs of aerobic membrane bioreactor sludges AeMRB1 and AeMRB2 extracted in the pre-determined temperature range of 45 - 60. Fluorophores T1, B2, and D correspond to tryptophan-like, tyrosine-like, and fulvic-like signatures, respectively. The unlabeled peak (EX 360, EM 450) has been observed in literature to be associated with optical brighteners.

The EPS extraction EEMs of AeMBR1 and AeMBR2 for different temperatures confirm the diauxic behavior observed in the corresponding colorimetric EPS extraction data. Similar to the BNR sludges, T1 (tryptophan-like compounds) was the most dominant fluorophore followed by B (tyrosine-like compounds) and D (fulvics). The intensities of these three constituents increased with temperature, with the peak intensities from 50°C to 55°C being rather negligible and a large increase occurring between 55°C and 60°C. There is an additional unnamed peak seen at (EX 350, EM 450) which corresponds to surfactants and optical brighteners included in washing powders observed at 55°C and 60°C on AeMBR1 and 60°C for AeMBR2, making it likely that the foaming and bubbling observed was indeed being caused by an unusually high concentration of detergents being present (Hartel et al. 2008; Henderson et al. 2009; Takahashi and Kawamura 2007). Based on the observation that extraction of the surfactants increased with increasing temperature, 60°C may not have been enough to fully extract and solubilize the detergents. However, increasing the extraction temperatures past 60°C risks lysing the cells, especially as surfactants by themselves have been known to increase the rate of cell lysis, which could invalidate SMP and EPS measurements by introducing intracellular components (Brown and Audet 2008). This demonstrates a need to incorporate techniques, such as Fourier Transform Infrared (FTIR) spectroscopy, that can directly characterize solids, and molecules that are either strongly bound to them or unable to be effectively solubilized.

6.4 Conclusion

This study concludes that the choice of heat extraction temperature has a significant impact on the extraction efficiency of EPS components. Heat extraction above 60°C appears to lead to excessive lysis. This study fixed the extraction time at 30 minutes, for practical considerations, and varying the temperature, but it may be possible to achieve higher extraction

efficiencies at lower temperatures by increasing extraction times while limiting lysis. This requires further investigation as lower temperatures may be unable to extract the more tightly bound components however, as seen with the surfactants in the AeMBR samples. In contrast to EPS, it is unlikely that the SMP in samples would benefit from heat extraction, as the constituents obtained through SMP extraction should already mostly be soluble.

The optimal general-use temperature for the heat extraction of EPS is likely to occur between 55°C and 60°C for wastewater samples, and may vary due to physical factors, such as spatio-temporal variations in the sample, sludge type, and treatment process. Because it is likely that each sample has its own specific optimal extraction temperature, the specific range should be determined through testing similar to the procedure performed in this study, focusing on a temperature range around 60°C. Additionally, some constituents may not be extractable without risking cell lysis at higher temperatures; analysis of these components may require techniques that can directly characterize the solids such as energy dispersive spectroscopy, FTIR, and microscopy.

Known issues with colorimetric analyses' lack of specificity, particularly with regard to phenol-sulfuric acid method, and their dependence on arbitrarily chosen single standards limit their stand-alone reliability, but this can be overcome by supplementing the data with validation from other analytical methods such as TC, TN, and fluorometry. In particular, fluorometry proved to be a useful, rapid method that provided qualitative and semi-quantitative information that could be used to characterize the sample matrix and corroborate or refute the observations from other analytical methods. Taken all together, the combination of colorimetry, TC-TN, and fluorometry can be applied as a rapid, non-destructive routine monitoring tool for wastewater

processes and offer more robust process control in both conventional BNR systems as well as membrane-based systems.

6.5 Summary

SMP and EPS extraction was critically evaluated and demonstrated to be effective for use with membrane systems, fulfilling [Chapter 2, objective 2.A.i]. Total Carbon (TC), Total Nitrogen (TN), and fluorometry analyses were successfully performed in tandem to supplement colorimetry data. SMP samples only marginally benefitted from heat extraction, owing to their mostly soluble nature, while EPS profiles were greatly influenced by extraction temperature. 60°C appears to be a general-purpose extraction temperature for EPS in the wastewater sludges tested, balancing lysis and extraction efficiency.

Chapter 7 - Investigation of Early Onset Membrane Fouling under Sub-Critical Flux Operation in a Novel Lab-Scale AnMBR

A lab scale gas-sparged AnMBR was designed and fabricated with the goal of characterizing membrane foulants and their attachment mechanisms [chapter 2, objective 1B]. This study aimed to isolate the impacts of fouling by feeding the AnMBR with a well-defined synthetic wastewater influent and a consistent solids concentration with the main module in continuous operation in parallel with a novel side tube module. This experimental setup thus allows for the following observations: 1) baseline system performance using a control synthetic wastewater recipe; 2) system performance when fed a synthetic wastewater recipe that has been spiked with known concentrations of humic acid and the amino acids tryptophan and tyrosine; 3) sampling of membrane fibers in the side tube to capture the effects of early onset fouling; 4) sampling of the membrane fibers in the main module at the end of operation for foulant characterization.

7.1 Materials and Methods

7.1.1 Lab Scale AnMBR Setup

A schematic of the process as well as a picture of the reactor can be seen in Figure 7.1, and a design basis table can be seen in Table 7.1. The design basis and control narrative were provided to Rocco Mazzaferro Inc. (Ontario, Canada), who fabricated the system and performed most of the SCADA programming. The membranes in the main membrane tank are set in Suez's ZeeBlok prefabricated modules, while the membranes in the side-tube were potted manually. Biogas sparging was performed with a KNF diaphragm pump (KNF UN816.1.2KT.45P IP20-T, NJ, USA) supplying biogas to the ZeeBlok module's coarse bubble sparger. The reversible

permeate pump (Micropump I-Drive IEG, WA, USA) permeated and backpulsed both the main membrane module and the side tube.

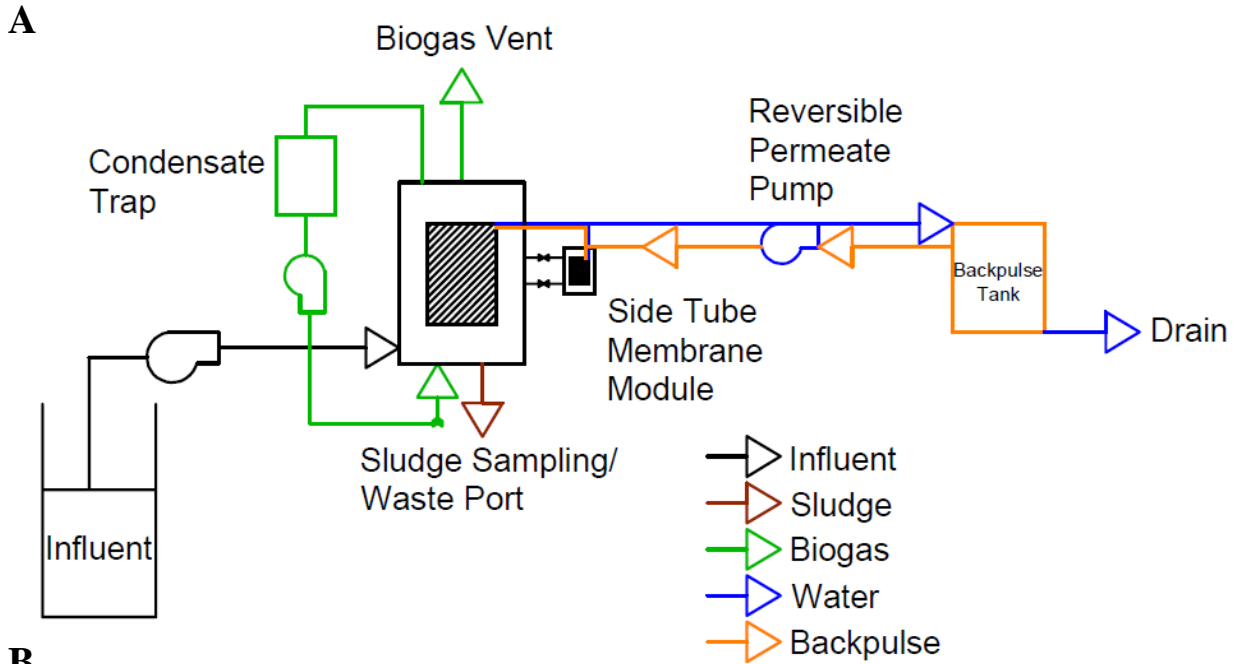


Figure 7.1 A schematic of the lab-scale gas-sparged AnMBR used in this study (A) and a picture of the system (B).

The Endress+Hauser (Reinach, Switzerland) pressure transmitters and flow meter data were recorded on a five second interval on FactoryTalk View SE (version 10, Rockwell Automation, WI, USA), which served as the lab scale reactor’s SCADA system.

Table 7.1 Design basis table and operating setpoints for the lab-scale AnMBR system

AnMBR System	Value
System Information	
Membrane make and model	Suez ZeeWeed 500d
Membrane type	PVDF on woven polyester
Pore size	0.04 μm
Membrane fiber size (OD/ID)	1.9/0.8 mm
HRT	25 h
Instantaneous flux	20 LMH
Backpulse flux	20 LMH
Gas sparging rate	20 SLPM
Production Cycle Parameters	12 min. production 2 min. backpulse 1 min. relax
Membrane Tank	
Operating reactor volume	0.11 m^3
Membrane area	0.23 m^2
Side Tube Module	
Empty bed reactor volume	500 mL
Membrane area	1212.3 mm^2

7.1.2 Reactor Startup and Operation

The reactor was inoculated with 57 L of anaerobic digester sludge obtained from the wastewater treatment plant in Salina, Kansas. Following inoculation, the system was fed with an equal volume of synthetic wastewater (SWW), recipe shown in Table 7.2, prepared using a modified SYNTHES recipe (Aiyuk and Verstraete 2004; Chen et al. 2013; Smith et al. 2013). The system was then operated in batch mode for 12 days, the time it took for the COD removal

to exceed 70%; this was to ensure that the COD removal was associated with treating the influent rather than the products of the initial digester seed sludge.

Table 7.2 Synthetic wastewater recipe used in this study. The spiked components were added to the base recipe only during the spiked testing conditions.

Base Recipe Components	Concentration (mg/L)	Spiked Components	Concentration (mg/L)
Urea	88	Tryptophan	5.8
Sodium acetate	221	Tyrosine	5.1
NH ₄ HCO ₃	219	Humic Acid	100
KH ₂ PO ₄	22		
FeSO ₄	5		
MgCl ₂	5		
Yeast extract	57		
Beef extract	65		
Peptone	57		
Starch	131		
Milk Powder	131		
ZnSO ₄	0.22		
CoCl ₂	0.12		
MnCl ₂	0.50		
CuSO ₄	0.13		
(NH ₄) ₆ Mo ₇ O ₂₄	0.10		
NiCl ₂	0.10		
Na ₂ SeO ₄	0.08		
			Average COD
			(mg/L)
		Recipe	
		Base Recipe	517±82
		Spiked Recipe	809±29

Humic acid (53680, Sigma Aldrich, USA), D-tryptophan (98% reagent grade, Sigma Aldrich, USA) and L-tyrosine (98% reagent grade, Sigma Aldrich, USA) spikes were used to supplement the complex carbonaceous and proteinaceous components, respectively, in the base recipe to mimic conditions that occurred during fouling events based on previous AnMBR studies (Lim et al. 2020; Vincent et al. 2018). The humic acid was dissolved by stirring it in DI water, adjusting the pH to 12 using NaOH, and then lowering the pH to 7 using HCl before aliquoting for spiked addition.

After the initial inoculation and acclimation, the experiment was carried out in 3 stages: Stage 1, baseline SWW; Stage 2, reseed and replicate baseline SWW; Stage 3, spiked recipe using acclimated sludge from Stage 2. Each stage began with an extended Critical Flux Test (CFT), which served to establish the baseline performance of the system and to gauge the effects of the influent SWW on fouling propensity, and then continued directly into a continuous operation stage for 3 days, after which the side tube module was extracted and replaced with a fresh membrane fiber for the subsequent test. Throughout all 3 stages, the main module remained operating and was undisturbed, except for interruptions during sampling events. Solids were monitored but were relatively stable throughout each stage and did not require wasting events, leading to the only solids wasting occurring incidentally through sampling.

7.1.3 Extended Critical Flux Test

Critical flux testing was performed using the flux step method in which a setpoint for instantaneous flux was maintained for a full production-backpulse-relaxation cycle before being adjusted for the next cycle (Cho and Fane 2002; Lutze and Engelhart 2021). Flux was increased by increments of 5 LMH until there was a cycle where one of the following conditions were met: the next TMP cycle would exceed 30 kPa, which is taken as a conservative limit to safeguard the membrane, or the change in TMP divided by the change in flux step has doubled from the previous cycle (Lutze and Engelhart 2021; Wang et al. 2008). When either of these conditions were met, a critical flux would be estimated. In this study, however, the critical flux test was extended, and the flux steps were decreased by increments of 2.5 LMH until the flux was at or below the starting flux conditions to explore the hysteresis effect. Upon conclusion of the extended critical flux test, the three-day period of continuous operation commenced using the design basis settings described in Table 7.1.

7.1.4 Sampling Procedures and Analytical Methods

One liter grab samples of SWW influent, permeate, and membrane tank mixed liquor were collected daily for analysis. pH was measured using an Accumet AB150 (MA, USA). The influent samples were directly used for COD analyses. Permeate samples were directly used for TC-TN, and spectrophotometric analyses, consisting of COD, colorimetric protein and carbohydrate measurements, and fluorometry. Mixed liquor samples were directly used for Total Suspended Solids (TSS) and Volatile Suspended Solids (VSS) analyses according to standard methods for wastewater 2540D and 2540E, respectively, but underwent heat extraction at 60°C, prior to the spectrophotometric analytical methods (Eaton et al. 2005). All heat extractions performed in this experiment were done according to the procedure described in Chapter 6 at 60°C.

COD and ssCOD measurements were conducted using Hach method 8000 on a Hach spectrophotometer (Hach DR3900, CO, USA). The ssCOD measurements were conducted on the mixed liquor filtrate through a 1.2 µm filter paper (Whatman 1822-047, Maidstone, United Kingdom). Colorimetric assays for carbohydrate and protein determination were performed on 96-well plates using the phenol-sulfuric (PS) method with glucose as the standard (Masuko et al. 2005) and the bicinchoninic acid (BCA) method (Sigma-Aldrich 2011) with bovine serum albumin (BSA) as the standard, respectively. All colorimetric analyses were performed in triplicate on a BioTek microplate reader (BioTek Epoch 2, VT, USA) with Greiner Bio-One µClear Bottom 96-well plates (Greiner Bio-One, Kremsmünster, Austria). EEMs were generated using a Horiba Aqualog fluorometer (Horiba, Kyoto, Japan) with the samples aliquoted in quartz cuvettes (Starna 3-Q-10, Ilford, UK).

To supplement the carbohydrate, protein, and EEM data, Total Carbon (TC) and Total Nitrogen (TN) analyses were performed using a Shimadzu TOC-L and TNM-L (Shimadzu, Kyoto, Japan) analyzer and ultra performance liquid chromatography (UPLC) using a Waters ACQUITY UPLC H-Class PLUS System (Waters Corp., MA, USA). Additionally, FTIR was performed on the foulant cake using a Cary 630 FTIR spectrometer (Agilent, CA, USA).

7.1.4 Membrane Foulant Sampling

Foulant sampling was performed at the end of each stage of operation. Side tube membrane fibers were extracted in stages 1, 2, and 3. The main module fibers were extracted at the end of operation, coinciding with the end of stage 3. The extraction procedure was the same for all membrane sampling events. The membrane extracts of all membrane fibers were prepared using 0.45 μ m and 0.2 μ m cartridge filters, with the filtrate from each being used for TC-TN, carbohydrate, protein, and fluorometry analyses.

First, any foulant cake retained on the membrane fiber after the tank was drained is scraped off using a stainless-steel scoopula. Eight foulant cake samples were directly dried overnight in a 105°C oven and weighed. Afterwards, four of the replicates were placed in a furnace at 550°C for 15 minutes and weighed in a loss on ignition test to determine the organic content of the sample. One sample from the 105°C dehydration and one from the 550°C ignition were each ground into a powder using a mortar and a pestle for FTIR analysis. For analyses requiring extraction, 1 g of foulant cake was suspended in 40 mL of 0.9% NaCl, heat extracted and analyzed using the same the procedures applied to the mixed liquor samples.

After the foulant was scraped off, membrane fibers were cut from the modules, trimmed to 203.2 mm segments if applicable, suspended in 40 mL of 0.9% NaCl, and subject to heat extraction at 60°C, per the optimized method developed in Chapter 6. The side tube fibers did

not require trimming and were extracted in full. The main module fibers were longer and required trimming. Additionally, the main module was comprised of many fibers, so sampling at different locations to capture possible variability due to their position along the module was considered. Three 203.2 mm segments from the main module were chosen at random, with positions determined by a random number generator: Sample M1 was taken from the front of the block and the top of the module, Sample M2 was taken from the middle of the block with the midpoint being the center height of the module, and Sample M3 was taken from the back, capturing the bottom of the module.

7.2 Results and Discussion

7.2.1 System Performance

In order to set up the fouling experiments within reasonable operating conditions that are representative of actual operation, COD removal performance and solids concentrations were tracked. COD removal, shown in Figure 7.2a, shows that a period of 7 to 10 days of batch mode operation period before the permeate was able to first achieve 70% treatment efficiency, which is comparable to other studies (Hu and Stuckey 2006; Lim et al. 2020; Smith et al. 2013), and significantly faster than the months or weeks expected of anaerobic systems (Grosser 2017; Judd 2010). The average removal efficiency across all three stages of operation was $83\pm 7\%$. This quick startup is likely due to having a consistent SWW substrate as well as an active inoculum directly obtained from an anaerobic digester. Afterwards, COD removal continued to increase with time, and efficiency increased with increased COD loading from the spiked influent. The system produced an average of 2000 ± 950 mL of biogas per day over the entire period of operation, with an average concentration of $70.4\pm 0.4\%$ v/v methane.

The sludge concentration remained relatively stable throughout the entire experiment, with an average of 12000 ± 2500 mg/L TSS and 7600 ± 1400 mg/L VSS (Figure 7.2b). Maintaining a consistent solids concentration has important implications in a fouling experiment because mixed liquor solids are often considered a controversial parameter for membrane fouling. While some studies confirm the conventional wisdom that increased solids concentrations decrease membrane performance (Judd 2010; Meng et al. 2017), other studies reported performance benefits with increase in bulk solids concentrations due to improved filterability (Chang et al. 2002; Lousada-Ferreira et al. 2015). Having a stable solids concentration limits their impact across the different stages of operation. It has been hypothesized that the composition of the mixed liquor, specifically the relative contributions of suspended solids, colloids, and dissolved organic matter, has a larger effect on membrane performance than the solids concentration itself (Bouhabila et al. 2001; Defrance et al. 2000).

ssCOD has been suggested as being one possible analysis that could help capture the contribution of colloids and DOM during long term operation (Lim et al. 2020). In this system, while the solids concentration in the bioreactor sludge was relatively stable, the ssCOD varied. ssCOD was consistently low in stage 1 but started high and decreased over time in stages 2 and 3. While ssCOD can be a useful monitoring tool for long term operation, it has shortcomings when it comes to data resolution in very short-term experiments due to its lack of ability to distinguish each component's contribution and practical limitations for generating data at high resolution during short time frames without the use of an in-line COD sensor. This indicates the need for more suitable high throughput analytical methods to obtain higher resolution to capture the effects of various foulants in real time if the ability to show distinct trends during short time intervals is desired.

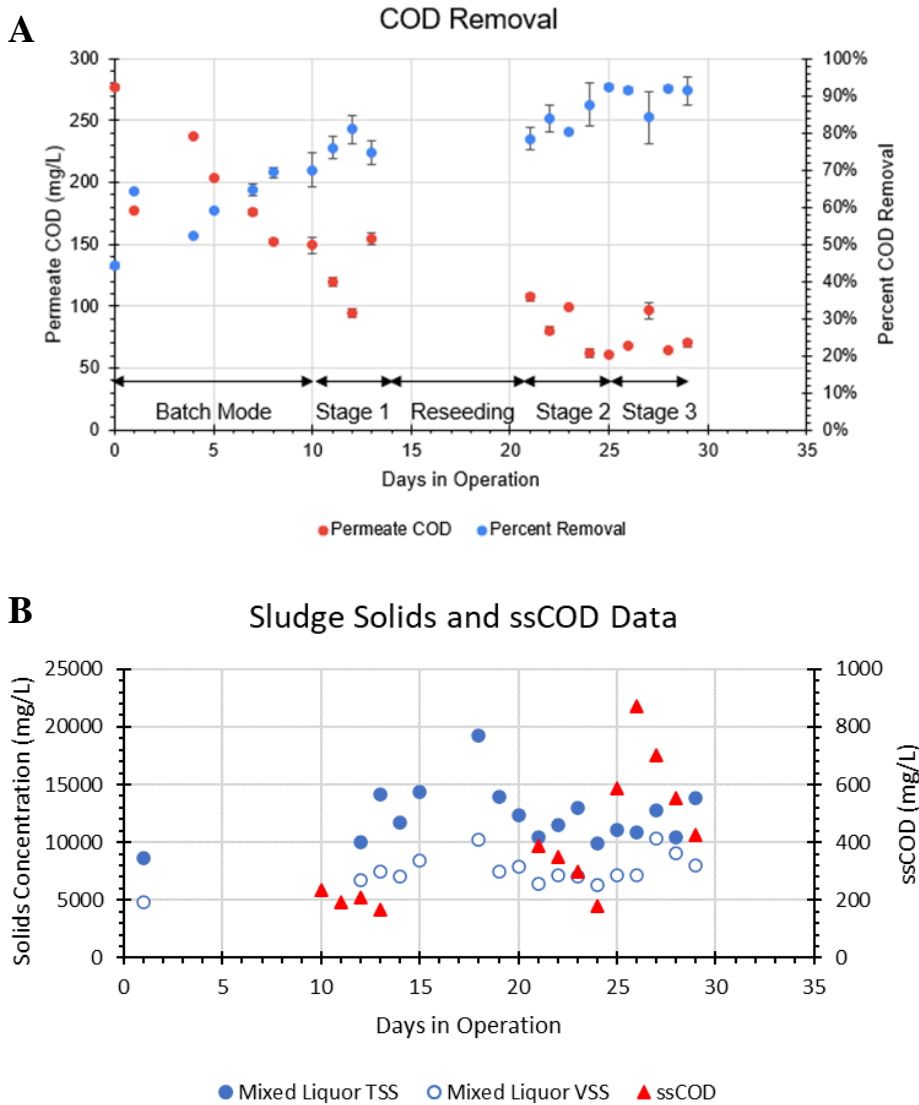


Figure 7.2 Plots of the system's COD removal performance (A) and solids concentrations juxtaposed with ssCOD (B).

7.2.2 Extended Critical Flux Tests and Continuous Operation

The first experiment performed in each stage of operation was the extended critical flux test (Figure 7.3). One of the features to notice across all three stages is the steep vertical rise in TMP at the beginning of each cycle. These spikes are due the permeate pump overshooting the flow rate to achieve the flux setpoint. After the permeate pump stabilized, the TMP tended to

increase linearly through each cycle. This dramatic TMP increase has been attributed to the physical formation of a cake layer (Chang et al. 2002; Lutze and Engelhart 2021).

When incrementally increasing the flux by 5 LMH during each production cycle, the first instance of the flux step ($\frac{\Delta TMP}{\Delta J}$) doubling was during the step to 35 LMH in stages 1 and 2, meaning the true critical flux lies somewhere between 30 and 35 LMH. In both stages, stepping the flux back down at increments of 2.5 LMH per cycle revealed a hysteresis effect, where the same flux values were achieved at higher TMP values when stepping the flux down versus stepping it up. At 20 LMH, the long-term operating condition for this study, the initial TMPs in stage 1 and stage 2 were 0.760 kPa and 1.014 kPa, respectively while the 20 LMH condition towards the end of the critical flux tests produced TMPs of 1.050 kPa and 1.447 kPa, for stage 1 and stage 2 respectively, each representing a 40% increase in TMP from the initial conditions. Stage 3's CFT with the spiked SWW deviated from the behavior of stages 1 and 2. First, the critical flux of the system was in excess of 40 LMH but was not determined, as the $\frac{\Delta TMP}{\Delta J}$ was not doubled from the previous step, and another cycle would likely experience TMPs above 35 kPa, signaling the end of the experiment to safeguard the membrane integrity. Based on this metric alone, it would appear that stage 3's performance was favorable compared to stages 1 and 2 despite being spiked with humic acid, tryptophan, and tyrosine. However, extending the CFT demonstrates that the hysteresis in Stage 3 was much more severe than in stages 1 and 2, experiencing a 241% increase in TMP at the 20 LMH flux condition from 0.99 kPa to 3.38 kPa.

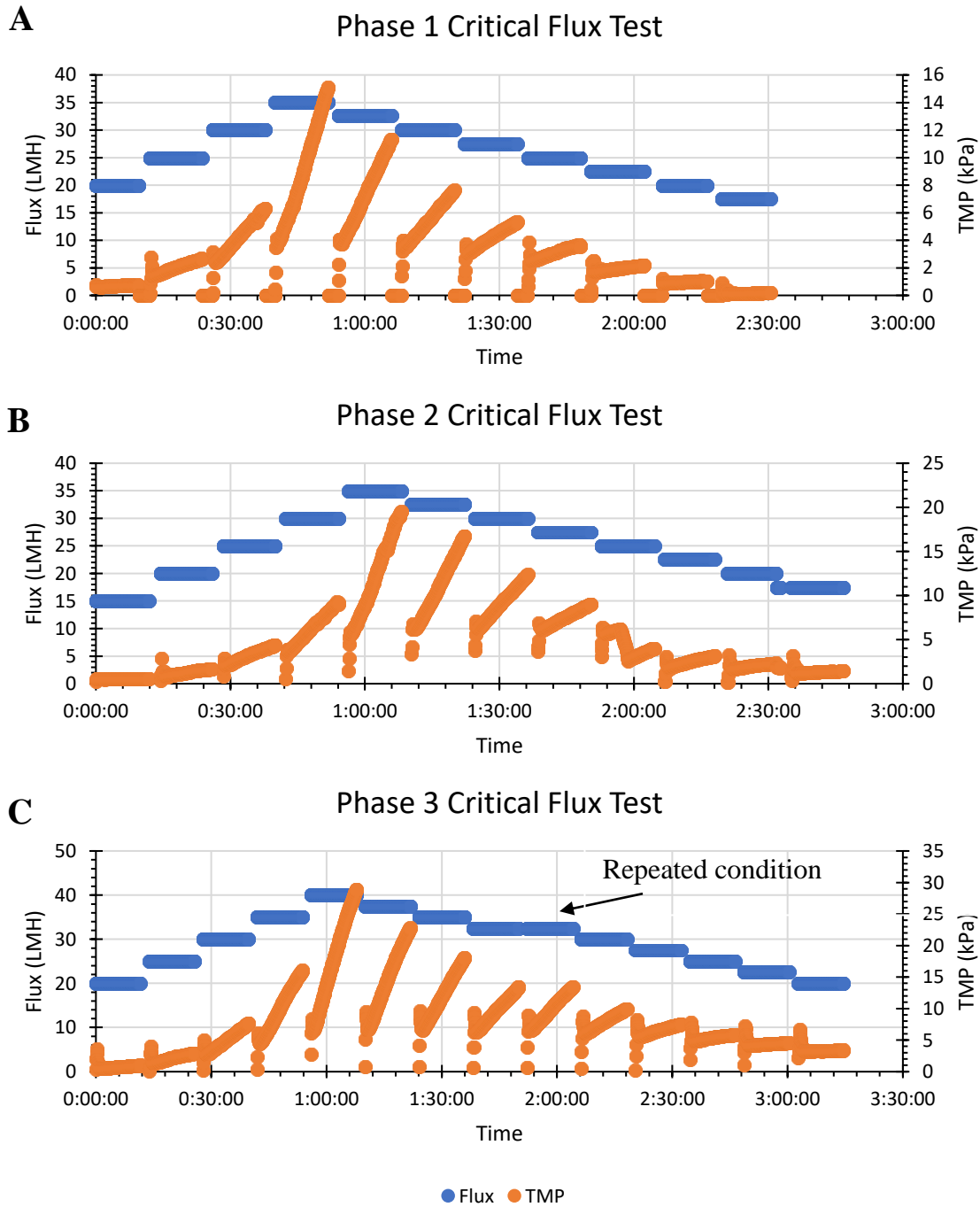


Figure 7.3 Extended critical flux testing plots from Stage 1 (A) and Stage 2 (B), both of which used the baseline synthetic wastewater recipe, and Stage 3 (C), which was spiked with tryptophan, tyrosine, and humic acid

The repeated condition at 32.5 LMH produced nearly identical responses, confirming that the combination of backpulsing and gas sparging was sufficient for removing cake layer deposition and further bolstering the hypothesis that the hysteresis in AnMBR fouling is primarily driven by pore constriction. Further evidence that pore constriction was the primary early fouling mechanism was that there was no visible evidence of cake layer formation when the tank was temporarily drained before reseeded the reactor between Stage 1 and Stage 2.

This suggests that the hysteresis is likely due to pore constriction, which is not addressed by physical maintenance methods, and directly contradicts the strong form of the critical flux hypothesis, which states that there theoretically exists a flux below which no fouling occurs (Field et al. 1995). This hysteresis effect has commonly been observed in both AnMBR and MBR literature overall, and decreases critical flux as membrane systems continue their service life (Fox and Stuckey 2015; Le-clech et al. 2006). Considering the hysteresis, it may be useful to amend the critical flux hypothesis to a more practical form as follows: there exists a flux below which the formation of a cake layer can be mitigated solely through physical management techniques; reduction in membrane performance when operating in subcritical flux conditions are primarily due to physically irremovable pore constriction.

7.2.3 Membrane Foulant Samples

Side tube membrane fiber samples were used to verify the assertion that pore constriction was the primary mechanism of early AnMBR fouling. In the side tube membrane fiber samples from all three stages, no visible cake layer at the time of sampling, and thus no foulant cake sample was able to be sampled, validating the lack of solids deposition suggested from the CFT tests. Because the membrane fibers were extracted as a whole, the foulants that accumulated on the membrane were extracted without distinguishing whether they were from inside the pores or

if they had built up on the membrane surface but could not be seen with the unaided eye. The TC, TN, protein, and carbohydrate extraction data for the side tube membrane fibers are shown in Table 7.3.

Table 7.3 Table of Total Carbon (TC), Total Nitrogen (TN), carbohydrate, and protein extractions from the side tube membrane fibers after the 3 days of operation of each stage.

Side Tube Module	Total Mass Extracted (mg)			
	TC	TN	Carbohydrate	Protein
Stage 1	0.192±0.019	0.048±0.001	0.062±0.033	0.25±0.044
Stage 2	0.190±0.004	0.071±0.001	0.081±0.019	0.192±0.025
Stage 3	0.192±0.003	0.056±0.002	0.217±0.016	0.134±0.095

The carbohydrate concentration was significantly higher in the stage 3 fiber, likely due to being spiked with humic acids, which can be partially captured as complex carbohydrates, but the protein concentration was lower despite the influent being spiked with amino acids. UPLC analyses for free amino acids on each of the side tube extracts, as well as the sludge and permeate extracts, returned results below the detection limit, which does not necessarily rule out the presence of polypeptides.

EEM data from the side tube fibers at the end of each operational stage are shown in Figure 7.4. Despite free amino acids not being detected by UPLC, the EEMs from the membrane extracts continued to show protein-like fluorescence. The tryptophan-like (fluorophore T1) and tyrosine-like (fluorophore B2) fluorescence only requires the intact aromatic rings, particularly the presence of indole groups, which would still fluoresce whether in peptide chains or as the products of amino acid degradation (Hudson and Reynolds 2007; Lakowicz 2006). This suggests some biotransformation to the tryptophan and tyrosine free amino acid spikes while in the bioreactor, which is expected to occur under anaerobic fermentative and methanogenic conditions (Li et al. 2018). With the UPLC analysis confirming

low levels of free amino acids and the extracted protein concentration decreasing in the spiked stage, it is surmised that the protein-like fluorescence from these extracts is likely from amino acid degradation products. The peaks in these EEMs that are not associated with protein-like fluorescence are all associated with humic substances. Fulvic-like peaks (fluorophore D) and marine humic-like peaks (fluorophore M) were present in all samples. The unnamed peak centered around (EX 250, EM 300) that appear in the Stage 3 is distinctly associated with the humic acid standard (Appendix C1).

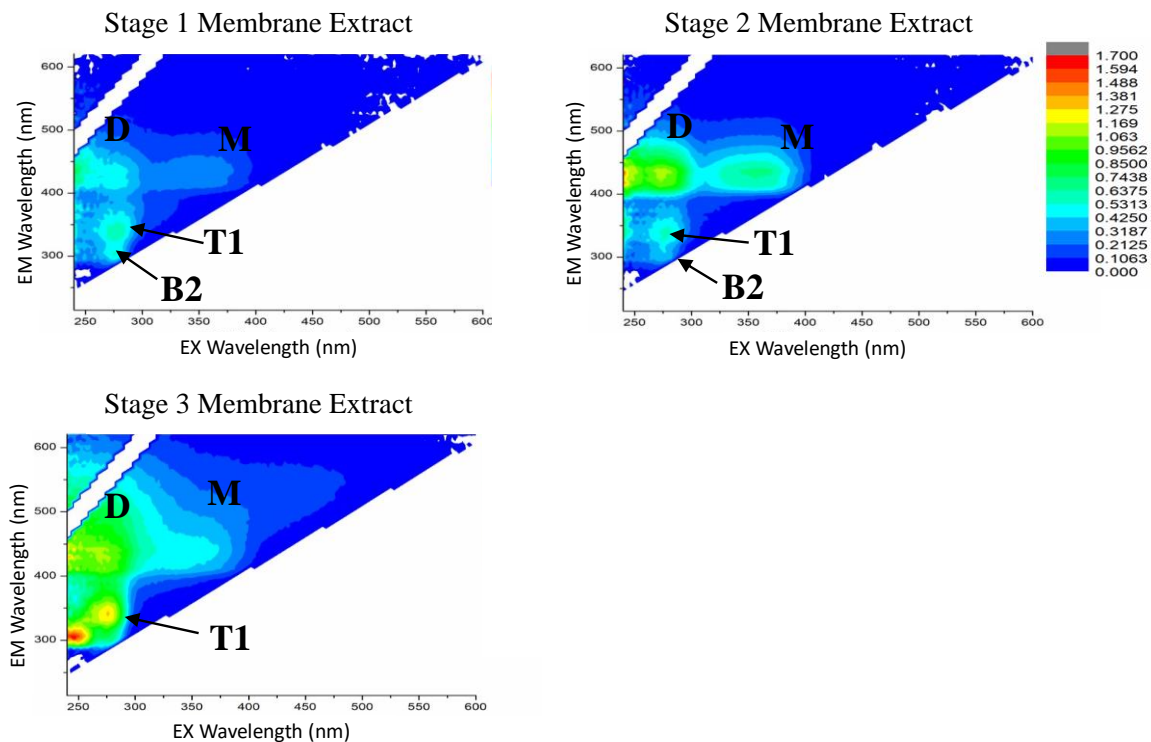


Figure 7.4 Excitation-Emission Matrices (EEMs) of the side tube membrane extracts from the end of Stages 1 and 2, using the baseline synthetic wastewater, Stage 3, using the spiked synthetic wastewater, and the main module at the end of operation.

The peaks were as follows: tryptophan-like (T1), tyrosine-like (B2), marine humic-like (M), fulvic-like (D). EEMs and extraction data associated with the main modules are shown in Figure 7.5 and Table 7.4, respectively; only one membrane fiber sample is shown, as the other two main

module samples have nearly identical EEM profiles (Appendix C3). The increased intensities for the humic substance peaks and tryptophan-like peak T1 in the main module, which was in operation for longer than the side tube modules, indicates that these were the foulants that were adsorbed in the membrane pores over time. Despite each membrane sample coming from different areas of the membrane module, both the extract concentrations and EEM characteristics were nearly identical. The foulant cake tended to be built up near the top region of the membrane module where the fibers were potted and around the plastic fittings. It is likely that these areas were benefitting less from the gas sparging, as having a physical barrier in the plastic fittings could prevent the removal of foulant solids, retain them, and form a cake layer.

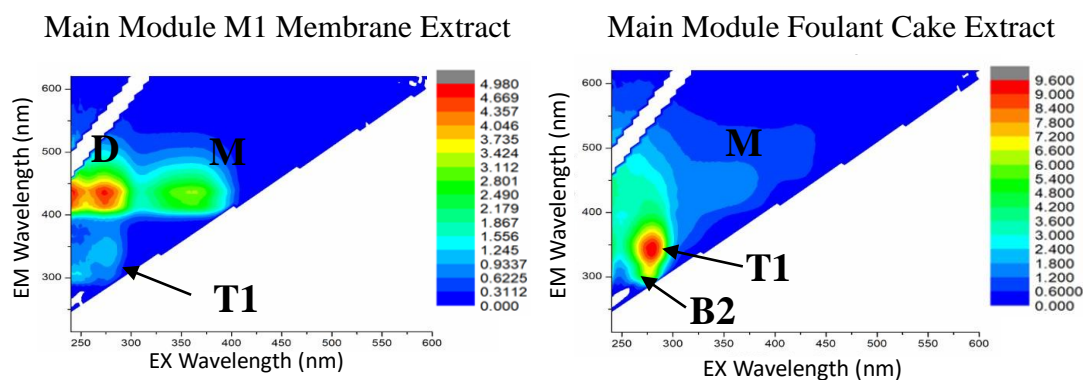


Figure 7.5 Excitation-Emission Matrices (EEMs) of the main module sample M1 and the foulant cake, both sampled at the end of the system’s operation.

Table 7.4 Table of Total Carbon (TC), Total Nitrogen (TN), carbohydrate, and protein extractions from the main module membrane fibers (M1, M2, and M3) and the foulant cake, all sampled at the end of the system’s operation.

Main Module	TC	TN	Carbohydrate	Protein
M1 (mg extracted)	4.550±0.091	1.123±0.027	0.084±0.004	0.214±0.082
M2 (mg extracted)	3.738±0.102	0.954±0.019	0.072±0.001	0.266±0.067
M3 (mg extracted)	3.157±0.088	0.749±0.046	0.077±0.004	0.363±0.087
Foulant Cake (mg extracted/g solid)	43.29±0.670	17.71±0.525	Not Reported*	50.1±9.218

*Due to measurement difficulties

In contrast to the main module extracts, the foulant cake EEM shows a much stronger signature of tryptophan-like and tyrosine-like peaks and lower levels of humic-substance peaks. The profile observed in this study and the relatively elevated protein-like peaks concentrations and present, but lower humic-like peaks is similar to previous studies (An et al. 2009; Xu et al. 2020b). The difference in the EEM profiles between the membrane fiber extract and the foulant cake illustrates a difference in the partitioning of foulant components: protein-like fouling is more prevalent in the cake layer while humic substances dominate in pore fouling.

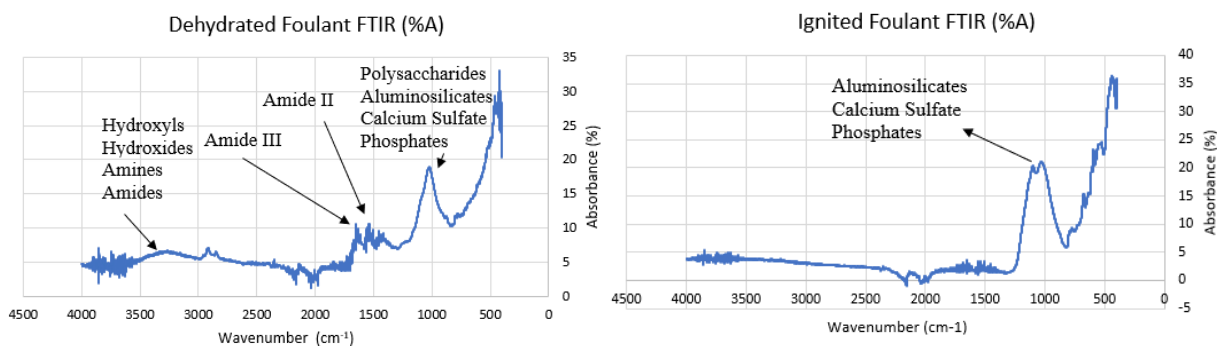


Figure 7.6 Fourier Transform Infrared spectroscopy spectra of the cake layer foulant from the main module after dehydration in a 105°C oven overnight (A) and ignition at 450°C, leaving only the inorganics (B)

Supplementing the foulant cake EEM, the FTIR profile shows Amide II and Amide III peaks at 1538 cm^{-1} and 1652 cm^{-1} , respectively, are both associated with the secondary structure of proteins, and the 3264 cm^{-1} peak that indicates the presence of primary amines and amides. The presence of regions suggesting secondary protein structure also implies that the protein-like fouling exists in peptide chains in the cake layer, which the high amount of protein extracted from the cake corroborates (Figure 7.6). This is in contrast with the pore foulants which were likely degradation products. The 1007 cm^{-1} peak has been associated with polysaccharides, aluminosilicates, calcium sulfate, and phosphates, but its predominance in the ignited foulant

sample as well as the dehydrated foulant sample suggest that it is largely inorganic in nature. These FTIR spectra signatures strongly resemble the spectra found in previous studies and corroborate the findings from Chapter 4.3 (Lim et al. 2020; Vincent et al. 2018; Yurtsever et al. 2016).

7.2.4 Continuous Operation TMP Behavior

Following each of the CFTs, the system was operated for three days with a flux setpoint of 20 LMH, well below the critical fluxes of any of the three stages in order to accumulate irremovable foulants on the membrane while operating at conditions below the critical flux. Each production cycle should ideally follow the same pattern as a critical flux test, with subcritical flux operation implying that cake layer formation will be negligible. The rate of cake layer formation, measured by $\frac{\Delta TMP \text{ (kPa)}}{\text{time (minutes)}}$ in the linear portion of each production cycle did not experience an overall increase in stages 1 and 2 and had an average slope of 0.040 ± 0.004 kPa/min (initial slope= 0.046 kPa/min; final slope=0.041 kPa/min) and 0.059 ± 0.017 kPa/min (initial slope= 0.056 kPa/min; final slope= 0.041 kPa/min), respectively.

In stage 3, however, the rate of TMP increase accelerated from an initial slope of 0.048 kPa/min to a final 0.067 kPa/min, a statistically significant increase ($p < 0.001$). This accelerating behavior over time is distinct from the simple rapid rise in TMP during each production cycle associated with cake layer formation. Combined with the lack of solids deposition visually observed in the side tube membrane sample, this suggests that this TMP increase is most likely driven by irremovable pore constriction either directly or by contributing to solids deposition by providing the initial organic matter deposits for the cake layer to begin to form on, both phenomenon which have been observed in ultrafiltration membrane studies (Costa et al. 2006).

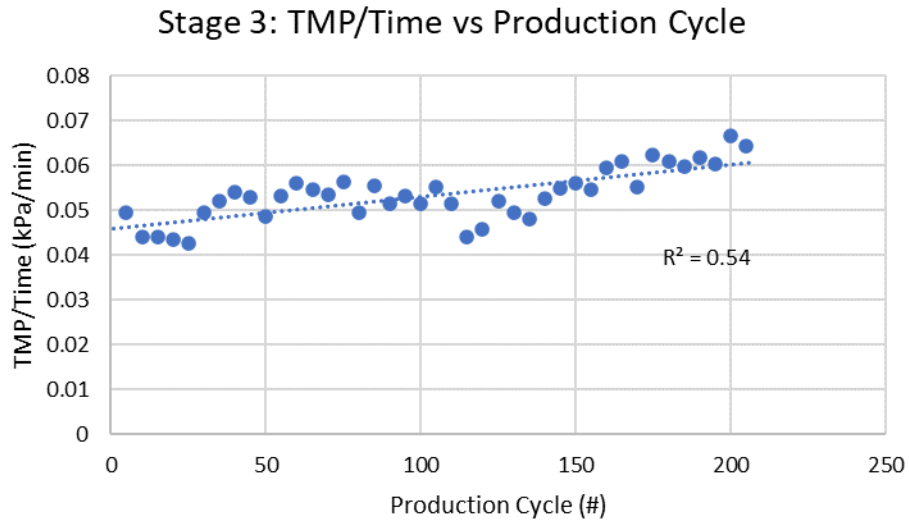


Figure 7.7 Plot of the increasing TMP/Time slope versus production cycle, demonstrating the increasing rate of cake formation

Taking the results of this study as a whole, the proposed mechanism for AnMBR fouling development in this system was that pore constriction was the primary mechanism of irremovable fouling in the early stages of AnMBR fouling under subcritical flux operations. The extended critical flux tests show that solids deposition was manageable, but the hysteresis effect was observed. As the adsorption of organic matter progresses, the rate of solids deposition onto the membrane surface increased, as shown in Figure 7.7. Many previous AnMBR studies identified cake layer formation as the dominant fouling mechanism (Charfi et al. 2012; Dereli et al. 2015) indicating that after enough adsorption of organic matter has occurred, the dominant fouling mode may transition from pore constriction to cake layer formation as the solids deposit onto previously deposited foulants (Costa et al. 2006; Xu et al. 2020b). The irremovable deposition of solids while operating under a constant flux condition would suggest that the critical flux was lowered due to pore constriction until the operating flux was above the critical flux threshold.

7.3 Summary

This study synthesized information from the end-of-life analysis on the membrane fibers and the foulant cake with data obtained from the critical flux tests and throughout regular operation [Chapter 2, Objective 3]. Both continuous operation data and foulant extract data were integral in evaluating the critical flux theory and suggest that the dominant fouling mechanism when operating below the critical flux was pore constriction driven by soluble organic matter [Chapter 2, Hypothesis 1b]. As pore constriction progressed, it appears that the rate of solids deposition increases, which implies that the critical flux is dynamically being reduced. If left unchecked, it is possible that it would continue until solids deposition can occur and become the dominant mode of fouling [Chapter 2, Hypothesis 1a]. Proteinaceous fouling was observed but was more associated with the foulant cake [Chapter 2, Hypothesis 2]. However, there were protein-like fluorescent peaks in the EEMs from the membrane fiber extracts. These peaks were likely to be caused by the degradation products from amino acids, such as indoles, rather than free amino acids or proteins.

Chapter 8 - Conclusion and Future Research

8.1 Conclusion

AnMBRs are a compelling platform for energy positive and resource recovery centric municipal wastewater treatment, which is likely the future of the entire sector. The ability of the AnMBR to treat the organics while contributing to energy neutrality through biogas generation and providing the opportunity for nutrient recovery has been demonstrated at the pilot-scale [Chapter 2, Objective 1A; Chapter 3]. The anaerobic bacteria performed well through seasonal variations, answering questions on how they would perform when confronted with ambient temperature operation. With its treatment performance established, the membrane performance of the pilot system was examined in Chapter 4, which revealed that proteinaceous foulants could be a key foulant due to its increased concentration in the permeate during fouling events [Chapter 2, hypothesis 2]. Additionally, inorganic scalants calcium phosphate and calcium sulfate were confirmed to be present in the cake layer using FTIR and electron microscopy. The analyses on the membrane foulants could only be conducted at the end of life of the AnMBR system, however, due to the practical difficulty of maintaining anaerobic conditions during membrane sampling. Additionally, the end-point analyses performed on the pilot-scale system were only conducted on the foulant cake layer, which may not provide information on the irreversible pore constriction.

To further investigate fouling, a lab scale AnMBR was designed with a side-tube module to enable the sampling of isolated membrane fibers without disrupting the performance of the main system [Chapter 7]. Proteinaceous fouling appeared to be partitioned more with the cake layer than the membrane pores, which saw elevated humic substances. The nature of the protein fouling in the cake layer likely occurs as polypeptide chains while the pore was likely from

amino acid degradation products such as indoles [Chapter 2, Hypothesis 2]. Synthesizing the continuous operation data and foulant characterization soluble organic matter was driving irremovable pore constriction as the dominant fouling mechanism in subcritical flux operation [Chapter 2, Hypothesis 1b]. As the pore constriction reduces the critical flux, it may provide the initial deposition sites for cake layer formation until it becomes the dominant mode of fouling [Chapter 2, Hypothesis 1a]. Elucidating the progression of fouling in AnMBR systems can aid in developing targeting cleaning strategies that appropriately address each stage. This could eventually pave the way for an energy positive and sustainable operation of AnMBRs paving their way for full scale adoption by society.

8.2 Future Research

While this study made several contributions towards evaluating the hypotheses set forth in Chapter 2, a few components are yet to be evaluated. First, inorganic scaling was not evaluated in the lab scale reactor and requires further research to determine their impact [Chapter 2, Hypothesis 1b]. Second, while proteinaceous materials were found in the cake layers and adsorbed in the membrane pores, whether or not these materials were colloidal in nature has not been determined [Chapter 2, Hypothesis 2]. Additionally, the study raises several potential avenues of research to pursue in future work.

8.2.1 Further Investigations on Pore Foulants

While this study largely neglected in this study was inorganic scaling in order to study the organic foulants, the impact of scaling is acknowledged and future studies should be conducted to elucidate their role in fouling development [Chapter 2, Hypothesis 1b]. The decision to neglect inorganic foulants in favor of studying organic foulants in this study was largely practical: first, few analyses can examine the foulants within the pores, and second,

extracting them would have consumed the limited number of side tube membrane modules available for this study. The latter point can be addressed by preparing more side tube modules and preparing an extraction protocol that is focused on the desorption of scalants. After extraction, analyses such as FTIR and ion chromatography could be utilized to analyze the resulting extract. The former issue, however, would require specialized advanced analyses to overcome. One such tool that has been employed, purportedly for an investigation into pore fouling, is atomic force microscopy, which has been used to characterize the adsorption of humic acid onto ultrafiltration membrane pores and investigate hardness-induced scaling in RO processes (Costa et al. 2006; Hilal et al. 2003). Atomic force microscopy is still limited to examining the surface roughness, however, which suggests that it may not be sufficient for deeper investigations into the pore. Cryo-microtomy may be one means of producing thin sections that can be imaged using various microscopy techniques in order to produce a true depth profile while preserving the foulants in-situ.

As pore foulants appear to be the primary driver of the initial stages of AnMBR fouling, increased consideration should be given to them while developing maintenance strategies. This requires additional characterization studies. Evaluating the relative impact of humics, fulvics, and protein-like foulants can lead to specific targeted backwash cleans that can desorb the prime contributors to pore constriction. Further characterization studies should also be conducted to determine whether or not the protein-like foulants are indeed the result of aromatic rings remaining from amino acid degradation; C-NMR spectroscopy or LC-MS may be appropriate analytical methods of determining this (Cook and Langford 1998; Gai et al. 2013). Performing these analytical techniques on liquid samples that have been passed through filters of various sizes can develop a particle size distribution profile and ultimately evaluate whether or not the

colloidal species are predominant as hypothesized [Chapter 2, Hypothesis 2]. Furthermore, it may be possible to evaluate the interaction between foulant particle size and the membrane pore size distribution.

8.2.2 Investigating the Partitioning of Foulants in the Bulk Sludge and Membrane Permeate

As the different foulant species appeared to be partitioned differently in either the cake layer or the pores, it may be possible to determine a relationship between the foulants, the mode of fouling, and the concentrations of the foulants in the permeate and bulk sludge. Finding correlations between the permeate and sludge characteristics and fouling would greatly improve the ability for operators to dynamically respond to pre-empt fouling events, especially as sampling the membrane fibers anaerobically remains a practical difficulty. This was demonstrated in this study when the use of ssCOD analysis and EEMs in Chapter 4 improved performance outcomes. Some preliminary work was also performed on the lab scale reactor to begin to address this point.

The TC-TN and carbohydrate and protein extraction data are shown in Figure 8.1. One note is that the sludge SMP and sludge EPS had higher concentrations of carbohydrates than in the permeate. Because these products are soluble, it is unlikely that the physical mechanism of membrane filtration was what removed the carbohydrates, which would make sludge SMP carbohydrates a potentially important parameter to track and supplement ssCOD data with. Future studies exploring size characteristics of carbohydrates and proteins in the permeate SMP, sludge SMP, and sludge EPS can also be conducted to produce a size distribution profile for each potential foulant and determine if there is a size range, such as colloids, for proteins and carbohydrates that disproportionately affects membrane fouling [Chapter 2, Hypothesis 2].

Tracking this information can also help determine whether or not certain size fractions partition in the cake layer or in the pores, which can lead to more accurate early predictions of oncoming fouling events that can be proactively managed.

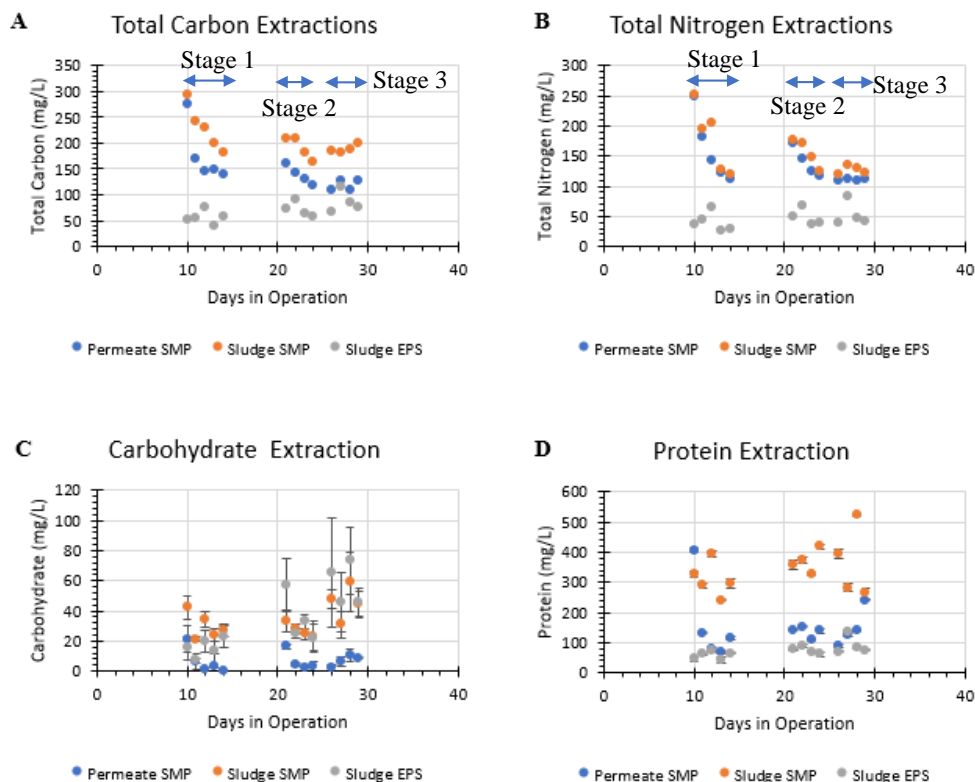


Figure 8.1 A plot of the extractions of Total Carbon (A), Total Nitrogen (B), Carbohydrates (C), and Proteins (D) for permeate SMP, sludge S MP, and sludge EPS. For Total Carbon and Total Nitrogen, all measurements were performed in triplicate and error was less than 10% on each.

8.2.3 Evaluating Chemical Cleaning Strategies

As more data is collected on the pore foulants, it may become possible to develop improved cleaning strategies. One of the first elements to examine is the choice of cleaning chemical. Sodium hypochlorite is currently the most popular membrane cleaning agent, and it has been shown that it can effectively release dissolved organic matter, including humics, from the membrane pores (Sun and Liu 2021). Cleaning with sodium hypochlorite has been associated with increases in toxic halogenated byproducts including chloroform and

trichloroethylene have been noted, however, which should be studied to determine if this poses a significant risk over the membrane system's operational life (Wang et al. 2018). The release and partitioning of organic compounds is also influenced by the presence of calcium, which can be released by anti-scalant chemical cleaning, such as citric acid backwashes, as well, which can lead to the formation of an irreversible gel layer forming (Wang et al. 2008, 2018).

These complex interactions highlight the need for further fundamental studies to determine the partitioning and nature of the foulants in order to select better chemical cleaning agents and, more broadly, develop more effective membrane maintenance strategies. These fundamental studies require methods to extract the foulants from the membrane pores, however, which implies that empirically determining what chemicals may be effective for cleaning would also determine which ones are suitable for use with pore extraction procedures, which could be a key step to advancing the fundamental understanding of foulant partitioning.

8.2.4 Overall Directions for the AnMBR Platform

While this study demonstrated an AnMBR's ability to achieve holistic wastewater treatment, the configuration used in this study was simply a first step and may not be indicative of AnMBR platform's true potential. While this study was able to demonstrate the recovery of nutrients, the chemical costs could be prohibitive with scaleup. Researching alternative chemical coagulants or even entirely different recovery platforms such as electrodialysis or microbial fuel cells can help improve the value of the nutrient products able to be obtained from AnMBR permeate and ultimately contribute to increasing the economic viability of AnMBRs (Heronemus et al. 2021; Kannan and Parameswaran 2021; Yan et al. 2018). Another avenue of research that aims to increase the economic viability of AnMBRs has been pushing the platform towards energy neutral or energy positive operation. There are several methods to reach energy positive

operation, but one strategy that has successfully demonstrated net energy production at low HRTs was the use of a staged AnMBR configuration that could recycle particulate COD from a membrane tank to anaerobic GAC fluidized bed reactors (Shin et al. 2021). The potential of AnMBRs extends beyond that of a standalone technology, however, further augmenting its opportunities for successful application. One study that highlights the flexibility of the AnMBR as an enabler of different technology platforms for nutrient and energy recovery involved a microalgal reactor, which takes advantage of the nutrient rich AnMBR permeate for algae cultivation (Vu et al. 2020). The different configurations of AnMBRs have their individual strengths and weaknesses, which necessitate further life cycle assessments (LCA) and techno-economic analysis (TEA) studies to determine their environmental, social, and economic impacts (Harclerode et al. 2020). The continued research on more effective operation of AnMBRs for energy and nutrient capture can only improve the technology's outlook.

References

- Abzac, P. D., Bordas, F., Hullebusch, E. Van, Lens, P. N. L., and Guibaud, G. (2010). "Extraction of extracellular polymeric substances (EPS) from anaerobic granular sludges : comparison of chemical and physical extraction protocols." *Applied Microbiology and Biotechnology*, 95, 1589–1599.
- Ahansazan, B., Afrashteh, H., Ahansazan, N., and Ahansazan, Z. (2014). "Activated Sludge Process Overview." *International Journal of Environmental Science and Development*, 5(1), 81–85.
- Aiyuk, S., and Verstraete, W. (2004). "Sedimentological evolution in an UASB treating SYNTHES, a new representative synthetic sewage, at low loading rates." *Bioresource Technology*, 93(3), 269–278.
- Al-halbouni, D., Traber, J., Lyko, S., Wintgens, T., Melin, T., Tacke, D., Janot, A., Dott, W., and Hollender, J. (2008). "Correlation of EPS content in activated sludge at different sludge retention times with membrane fouling phenomena." *Water Research*, 42, 1475–1488.
- Amjad, Z. (1989). "Effect of precipitation inhibitors on calcium phosphate scale formation." *Canadian Journal of Chemistry*, 850–856.
- An, Y., Wang, Z., Wu, Z., Yang, D., and Zhou, Q. (2009). "Characterization of membrane foulants in an anaerobic non-woven fabric membrane bioreactor for municipal wastewater treatment." *Chemical Engineering Journal*, 155, 709–715.
- Anjos, O., Graça, M., Contreras, P., Antunes, P., Campos, M. G., Ruiz, P. C., Antunes, P., Graça, M., Contreras, P., and Antunes, P. (2015). "Application of FTIR-ATR spectroscopy to the quantification of sugar in honey." *Food Chemistry*, 169, 218–223.
- Ashley, K., Cordell, D., and Mavinic, D. (2011). "A brief history of phosphorus: From the philosopher's stone to nutrient recovery and reuse." *Chemosphere*, Elsevier Ltd, 84(6), 737–746.
- Aslam, M., Charfi, A., Lesage, G., Heran, M., and Kim, J. (2017). "Membrane bioreactors for wastewater treatment: A review of mechanical cleaning by scouring agents to control membrane fouling." *Chemical Engineering Journal*, Elsevier B.V., 307, 897–913.
- Baek, S. H., Pagilla, K. R., and Kim, H. J. (2010). "Lab-scale study of an anaerobic membrane bioreactor (AnMBR) for dilute municipal wastewater treatment." *Biotechnology and Bioprocess Engineering*, 15(4), 704–708.
- Bandara, W. M. K. R. T. W., Satoh, H., Sasakawa, M., Nakahara, Y., Takahashi, M., and Okabe, S. (2011). "Removal of residual dissolved methane gas in an upflow anaerobic sludge blanket reactor treating low-strength wastewater at low temperature with degassing membrane." *Water Research*, Elsevier Ltd, 45(11), 3533–3540.

- Bates, J. B. (1976). "Fourier Transform Infrared Spectroscopy Published by : American Association for the Advancement of Science." *Science*, 191(4222), 31–37.
- Batstone, D. J., and Viridis, B. (2014). "The role of anaerobic digestion in the emerging energy economy." *Current Opinion in Biotechnology*, Elsevier Ltd, 27, 142–149.
- Beasley, M. M., Bartelink, E. J., Taylor, L., and Miller, R. M. (2014). "Comparison of transmission FTIR, ATR, and DRIFT spectra: Implications for assessment of bone bioapatite diagenesis." *Journal of Archaeological Science*, Elsevier Ltd, 46(1), 16–22.
- Becerik-Gerber, B., Siddiqui, M. K., Brilakis, I., El-anwar, O., El-gohary, N., Mahfouz, T., Jog, G. M., Li, S., and Kandil, A. A. (2014). "Civil Engineering Grand Challenges : Opportunities for Data Sensing , Information Analysis , and Knowledge Discovery." *Journal of Computing in Civil Engineering*, 28(4), 1–13.
- Di Bella, G., Di Trapani, D., and Judd, S. (2018). "Fouling mechanism elucidation in membrane bioreactors by bespoke physical cleaning." *Separation and Purification Technology*, Elsevier, 199(January), 124–133.
- Berkessa, Y. W., Yan, B., Li, T., Tan, M., She, Z., Jegatheesan, V., Jiang, H., and Zhang, Y. (2018). "Novel anaerobic membrane bioreactor (AnMBR) design for wastewater treatment at long HRT and high solid concentration." *Bioresource Technology*, Elsevier, 250(September 2017), 281–289.
- Bernet, N., and Buffi, P. (2002). "Methane yield as a monitoring parameter for the start-up of anaerobic fixed film reactors." *Water Research*, 36, 1385–1391.
- Bouhabila, E. H., Ben Aïm, R., and Buisson, H. (2001). "Fouling characterisation in membrane bioreactors." *Separation and Purification Technology*, 22–23, 123–132.
- Boyle-Gotla, A., Jensen, P. D., Yap, S. D., Pidou, M., Wang, Y., and Batstone, D. J. (2014). "Dynamic multidimensional modelling of submerged membrane bioreactor fouling." *Journal of Membrane Science*, Elsevier, 467, 153–161.
- Brown, R. B., and Audet, J. (2008). "Current techniques for single-cell lysis." *Journal of the Royal Society Interface*, 5(SUPPL.2).
- Cavicchioli, R. (2007). *Archaea: Molecular and Cellular Biology*. American Society Mic Series, ASM Press.
- Chang, I. I.-S. I. I.-S., Clech, P. Le, Jefferson, B., Le Clech, P., Jefferson, B., Judd, S., Clech, P. Le, Jefferson, B., Judd, S., Le Clech, P., Jefferson, B., Judd, S., Clech, P. Le, Jefferson, B., and Judd, S. (2002). "Membrane fouling in membrane bioreactors for wastewater treatment." *Journal of Environmental Engineering*, 128(11), 1018–1030.
- Charfi, A., Ben Amar, N., Harmand, J., and Amar, N. Ben. (2012). "Analysis of fouling mechanisms in anaerobic membrane bioreactors." *Water Research*, 6(8), 2637–2650.

- Chen, H., Chang, S., Guo, Q., Hong, Y., and Wu, P. (2016). “Brewery wastewater treatment using an anaerobic membrane bioreactor.” *Biochemical Engineering Journal*, Elsevier B.V., 105, 321–331.
- Chen, R., Nie, Y., Hu, Y., Miao, R., Utashiro, T., Li, Q., Xu, M., and Li, Y.-Y. (2013). “Fouling behavior of SMP and EPS in submerged AnMBR treating synthetic wastewater.”
- Cheryan, M. (1998). *Ultrafiltration and microfiltration handbook*. CRC press.
- Cho, B. D., and Fane, A. G. (2002). “Fouling transients in nominally sub-critical flux operation of a membrane bioreactor.” *Journal of Membrane Science*, 209(2), 391–403.
- Chong, S., Sen, T. K., Kayaalp, A., Ang, H. M., Kanti, T., Kayaalp, A., and Ming, H. (2012). “The performance enhancements of upflow anaerobic sludge blanket (UASB) reactors for domestic sludge treatment - A State-of-the-art review.” *Water Research*, Elsevier Ltd, 46(11), 3434–3470.
- Chow, P. S., and Landhäuser, S. M. (2004). “A method for routine measurements of total sugar and starch content in woody plant tissues.” *Tree Physiology*, 24(10), 1129–1136.
- Christian, S., Grant, S., McCarthy, P., Wilson, D., and Mills, D. (2011). “The first two years of full-scale anaerobic membrane bioreactor (AnMBR) operation treating high-strength industrial wastewater.” *Water Practice and Technology*, IWA Publishing, 6(2).
- Chuen, P., Wong, Y., Yi, J., and Wee, C. (2015). “Application of dispersed and immobilized hydrolases for membrane fouling mitigation in anaerobic membrane bioreactors.” 491, 99–109.
- Coates, J., Ed, R. A. M., and Coates, J. (2000). “Interpretation of Infrared Spectra , A Practical Approach Interpretation of Infrared Spectra , A Practical Approach.” 10815–10837.
- Comte, S., Guibaud, G., and Baudu, M. (2007). “Effect of extraction method on EPS from activated sludge: An HPSEC investigation.” *Journal of Hazardous Materials*, 140(1–2), 129–137.
- Cook, R. L., and Langford, C. H. (1998). “Structural Characterization of a Fulvic Acid and a Humic Acid Using Nuclear Magnetic Resonance.” *Environmental Science & Technology*, 32(5), 719–725.
- Costa, A. R., de Pinho, M. N., and Elimelech, M. (2006). “Mechanisms of colloidal natural organic matter fouling in ultrafiltration.” *Journal of Membrane Science*, 281(1–2), 716–725.
- Crone, B. C., Garland, J. L., Sorial, G. A., and Vane, L. M. (2016). “Significance of dissolved methane in effluents of anaerobically treated low strength wastewater and potential for recovery as an energy product : A review.” *Water Research*, Elsevier Ltd, 104, 520–531.
- Dagnew, M., Parker, W., and Seto, P. (2012). “Anaerobic membrane bioreactors for treating waste activated sludge : Short term membrane fouling characterization and control tests.”

Journal of Membrane Science, Elsevier, 421–422, 103–110.

- Dagnew, M., Parker, W., Seto, P., Waldner, K., Hong, Y., Bayly, R., and Cumin, J. (2011). “Pilot testing of an AnMBR for municipal wastewater treatment.” *Proceedings of the Water Environment Federation*, Water Environment Federation, 2011(11), 4931–4941.
- Dai, Y. F., Xiao, Y., Zhang, E. H., Liu, L. D., Qiu, L., You, L. X., Mahadevan, G. D., Chen, B. L., and Zhao, F. (2016). “Effective methods for extracting extracellular polymeric substances from *Shewanella oneidensis* MR-1.” *Water Science and Technology*, 74(12), 2987–2996.
- De-Bashan, L. E., and Bashan, Y. (2004). “Recent advances in removing phosphorus from wastewater and its future use as fertilizer (1997-2003).” *Water Research*, 38(19), 4222–4246.
- Defrance, L., Jaffrin, M. Y., Gupta, B., Paullier, P., and Geaugey, V. (2000). “Contribution of various constituents of activated sludge to membrane bioreactor fouling.” *Bioresource Technology*, 73(2), 105–112.
- Dereli, R. K., Heffernan, B., Grelot, A., Zee, F. P. Van Der, Lier, J. B. Van, Van Der Zee, F. P., Van Lier, J. B., Zee, F. P. Van Der, and Lier, J. B. Van. (2015). “Influence of high lipid containing wastewater on filtration performance and fouling in AnMBRs operated at different solids retention times.” *Separation and Purification Technology*, Elsevier B.V., 139, 43–52.
- Ding, Y., Tian, Y., Li, Z., Zuo, W., and Zhang, J. (2015). “A comprehensive study into fouling properties of extracellular polymeric substance (EPS) extracted from bulk sludge and cake sludge in a mesophilic anaerobic membrane bioreactor.” *Bioresource Technology*, Elsevier Ltd, 192, 105–114.
- Dong, Q. (2015). “Characterization of Anaerobic Membrane Bioreactors (AnMBR) Treating Municipal Wastewater.” UWSpace, 133.
- Du, Q., Liu, S., Cao, Z., and Wang, Y. (2005). “Ammonia removal from aqueous solution using natural Chinese clinoptilolite.” *Separation and Purification Technology*, 44(3), 229–234.
- Eaton, A. D., Clesceri, L. S., Franson, M. A. H., Association, A. W. W. P. H., Greenberg, A. E., Rice, E. W., Association, A. W. W. P. H., and Federation, W. E. (2005). *Standard Methods for the Examination of Water & Wastewater*. Standard Methods for the Examination of Water and Wastewater, American Public Health Association.
- El-mashad, H. M., and Zhang, R. (2010). “Biogas production from co-digestion of dairy manure and food waste.” *Bioresource Technology*, Elsevier Ltd, 101(11), 4021–4028.
- El-Shafai, S. A., El-Gohary, F. A., Nasr, F. A., Peter van der Steen, N., and Gijzen, H. J. (2007). “Nutrient recovery from domestic wastewater using a UASB-duckweed ponds system.” *Bioresource Technology*, 98(4), 798–807.

- Evans, P. J., Doody, A., Harclerode, M., Vila, P., Parameswaran, P., Lim, K., Bae, J., Shin, C., Lee, P.-H., Tan, A., McCarty, P., Parker, W., Guy, K., Page, M., and Maga, S. (2018). *Anaerobic Membrane Bioreactor (AnMBR) for Sustainable Wastewater Treatment. Project ER-201434. Department of Defense Environmental Security Technology Program Final Report.*
- Evans, P. J., Parameswaran, P., Lim, K., Bae, J., Shin, C., Ho, J., and McCarty, P. L. (2019). “A Comparative Pilot-Scale Evaluation of Gas-Sparged and Granular Activated Carbon-Fluidized Anaerobic Membrane Bioreactors for Domestic Wastewater Treatment.” *Bioresource Technology*, Elsevier Ltd.
- Felz, S., Vermeulen, P., van Loosdrecht, M. C. M., and Lin, Y. M. (2019). “Chemical characterization methods for the analysis of structural extracellular polymeric substances (EPS).” *Water Research*, Elsevier Ltd, 157, 201–208.
- Ferry, J. G. (2012). *Methanogenesis: ecology, physiology, biochemistry & genetics*. Springer Science & Business Media.
- Field, R. W., Wu, D., Howell, J. A., and Gupta, B. B. (1995). “Critical flux concept for microfiltration fouling.” *Journal of Membrane Science*, 100(3), 259–272.
- Fox, R. A., and Stuckey, D. C. (2015). “The effect of sparging rate on transmembrane pressure and critical flux in an AnMBR.” *Journal of Environmental Management*, Elsevier Ltd, 151, 280–285.
- Friedler, E. (2001). “Water reuse—an integral part of water resources management:: Israel as a case study.” *Water policy*, Elsevier, 3(1), 29–39.
- Gai, Y., Chen, H., Wu, C., Feng, F., Wang, Y., Liu, W., and Wang, S. (2013). “Analysis of the traditional medicine YiGan San by the fragmentation patterns of cadambine indole alkaloids using HPLC coupled with high-resolution MS.” 3723–3732.
- Galib, M. A. (2014). “Investigation of Performance of a Submerged Anaerobic Membrane Bioreactor (AnMBR) Treating Meat Processing Wastewater.”
- Galib, M., Elbeshbishy, E., Reid, R., Hussain, A., and Lee, H. S. (2016). “Energy-positive food wastewater treatment using an anaerobic membrane bioreactor (AnMBR).” *Journal of Environmental Management*, Elsevier Ltd, 182, 477–485.
- Ganesh Saratale, R., Kumar, G., Banu, R., Xia, A., Periyasamy, S., Dattatraya Saratale, G., Ganesh, R., Kumar, G., Banu, R., and Xia, A. (2018). “A critical review on anaerobic digestion of microalgae and macroalgae and co-digestion of biomass for enhanced methane generation.” *Bioresource Technology*, Elsevier, 262(March), 319–332.
- Gao, D. W., Zhang, T., Tang, C. Y. Y., Wu, W. M., Wong, C. Y., Lee, Y. H., Yeh, D. H., and Criddle, C. S. (2010). “Membrane fouling in an anaerobic membrane bioreactor: Differences in relative abundance of bacterial species in the membrane foulant layer and in suspension.” *Journal of Membrane Science*, Elsevier B.V., 364(1–2), 331–338.

- Gao, W. J., Leung, K. T., Qin, W. S., and Liao, B. Q. (2011). "Effects of temperature and temperature shock on the performance and microbial community structure of a submerged anaerobic membrane bioreactor." *Bioresource Technology*, Elsevier Ltd, 102(19), 8733–8740.
- Gerardo, M. L., Zacharof, M. P., and Lovitt, R. W. (2013). "Strategies for the recovery of nutrients and metals from anaerobically digested dairy farm sludge using cross-flow microfiltration." *Water Research*, Elsevier Ltd, 47(14), 4833–4842.
- Giménez, J. B., Robles, A., Carretero, L., Durán, F., Ruano, M. V., Gatti, M. N., Ribes, J., Ferrer, J., and Seco, A. (2011). "Experimental study of the anaerobic urban wastewater treatment in a submerged hollow-fibre membrane bioreactor at pilot scale." *Bioresource Technology*, 102(19), 8799–8806.
- Gouveia, J., Plaza, F., Garralon, G., Fdz-polanco, F., and Peña, M. (2015). "Long-term operation of a pilot scale anaerobic membrane bioreactor (AnMBR) for the treatment of municipal wastewater under psychrophilic conditions." *Bioresource Technology*, Elsevier Ltd, 185, 225–233.
- Green, D. ., and Perry, R. . (2008). "Perry's Chemical Engineers' Handbook, 8th Edition."
- Greenberg, G., Hasson, D., and Semiat, R. (2005). "Limits of RO recovery imposed by calcium phosphate precipitation." 183(May), 273–288.
- Grosser, A. (2017). "The influence of decreased hydraulic retention time on the performance and stability of co-digestion of sewage sludge with grease trap sludge and organic fraction of municipal waste." *Journal of Environmental Management*, Elsevier Ltd, 203, 1143–1157.
- Guest, J. S., Skerlos, S. J., Barnard, J. L., Beck, M. B., Daigger, G. T., Hilger, H., Jackson, S. J., Karvazy, K., Kelly, L., Macpherson, L., Mihelcic, J. R., Pramanik, A., Raskin, L., Van Loosdrecht, M. C. M., Yeh, D., and Love, N. G. (2009). "A new planning and design paradigm to achieve sustainable resource recovery from wastewater." *Environmental Science and Technology*, 43(16), 6126–6130.
- Guo, X., Larry, L., Li, X., and Park, H. (2008). "Ammonium and potassium removal for anaerobically digested wastewater using natural clinoptilolite followed by membrane pretreatment." *Journal of Hazardous Materials*, 151, 125–133.
- Hagos, K., Zong, J., Li, D., Liu, C., and Lu, X. (2017). "Anaerobic co-digestion process for biogas production : Progress , challenges and perspectives." *Renewable and Sustainable Energy Reviews*, Elsevier Ltd, 76(November 2016), 1485–1496.
- Hara, H., Kimura, K., Hara, H., and Watanabe, Y. (2005). "Removal of pharmaceutical compounds by submerged membrane bioreactors (MBRs)." *Desalination*, 178(1-3 SPEC. ISS.), 135–140.
- Harclerode, M., Doody, A., Brower, A., Vila, P., Ho, J., and Evans, P. J. (2020). "Life cycle assessment and economic analysis of anaerobic membrane bioreactor whole-plant

- configurations for resource recovery from domestic wastewater.” *Journal of Environmental Management*, Elsevier Ltd, 269(August 2019), 110720.
- Hartel, P. G., Rodgers, K., Moody, G. L., Hemmings, S. N. J., Fisher, J. A., and McDonald, J. L. (2008). “Combining targeted sampling and fluorometry to identify human fecal contamination in a freshwater creek.” *Journal of water and health*, England, 6(1), 105–116.
- He, Y., Xu, P., Li, C., and Zhang, B. (2005). “High-concentration food wastewater treatment by an anaerobic membrane bioreactor.” *Water Research*, 39(17), 4110–4118.
- Henderson, R. K., Baker, A., Murphy, K. R., Hambly, A., Stuetz, R. M., and Khan, S. J. (2009). “Fluorescence as a potential monitoring tool for recycled water systems: A review.” *Water Research*, Elsevier Ltd, 43(4), 863–881.
- Her, N., Amy, G., McKnight, D., Sohn, J., and Yoon, Y. (2003). “Characterization of DOM as a function of MW by fluorescence EEM and HPLC-SEC using UVA, DOC, and fluorescence detection.” *Water Research*, 37(17), 4295–4303.
- Heronemus, E., Gamage, K. H. H., Hettiarachchi, G. M., and Parameswaran, P. (2021). “Efficient recovery of phosphorus and sulfur from Anaerobic Membrane Bioreactor (AnMBR) permeate using chemical addition of iron and evaluation of its nutrient availability for plant uptake.” *Science of the Total Environment*, Elsevier B.V., 783, 146850.
- Hilal, N., Mohammad, A. W., Atkin, B., and Darwish, N. A. (2003). “Using atomic force microscopy towards improvement in nanofiltration membranes properties for desalination pre-treatment : a review.” *Desalination*, 157, 137–144.
- Ho, J., and Sung, S. (2010). “Methanogenic activities in anaerobic membrane bioreactors (AnMBR) treating synthetic municipal wastewater.” *Bioresource Technology*, Elsevier Ltd, 101(7), 2191–2196.
- Hoang, T. A., Ang, D. H. M., and B, A. L. R. (2009). “Effects of Organic Additives on Calcium Sulfate Scaling in Pipes.” 927–933.
- Hoinkis, J., Deowan, S. A., Panten, V., Figoli, A., Huang, R. R., and Drioli, E. (2012). “Membrane bioreactor (MBR) technology - A promising approach for industrial water reuse.” *Procedia Engineering*, 33(2009), 234–241.
- Hong, P. N., Honda, R., Noguchi, M., and Ito, T. (2017). “Optimum selection of extraction methods of extracellular polymeric substances in activated sludge for effective extraction of the target components.” *Biochemical Engineering Journal*, Elsevier B.V., 127, 136–146.
- Hu, A. Y., and Stuckey, D. C. (2006). “Treatment of Dilute Wastewaters Using a Novel Submerged Anaerobic Membrane Bioreactor.” *Journal of Environmental Engineering*, 132(2), 190–198.
- Hu, Y. Q., Wei, W., Gao, M., Zhou, Y., Wang, G. X., and Zhang, Y. (2019). “Effect of pure

- oxygen aeration on extracellular polymeric substances (EPS) of activated sludge treating saline wastewater.” *Process Safety and Environmental Protection*, 123, 344–350.
- Huang, Z., Ong, S. L., and Ng, H. Y. (2010). “Submerged anaerobic membrane bioreactor for low-strength wastewater treatment : Effect of HRT and SRT on treatment performance and membrane fouling.” *Water Research*, Elsevier Ltd, 45(2), 705–713.
- Hudson, N., and Reynolds, D. (2007). “FLUORESCENCE ANALYSIS OF DISSOLVED ORGANIC MATTER IN NATURAL , WASTE AND POLLUTED WATERS — A REVIEW.” *River Research and Applications*, 23, 631–649.
- Ishiguro, K., Imai, K., and Sawada, S. (1994). “Effects of biological treatment conditions on permeate flux of UF membrane in a membrane/activated-sludge wastewater treatment system.” *Desalination*, Elsevier, 98(1–3), 119–126.
- J. Madejová. (2003). “FTIR techniques in clay mineral studies.” *Vibrational Spectroscopy*, 31(1), 1–10.
- Jang, N., Ren, X., Choi, K., and Kim, I. S. (2006). “Comparison of membrane biofouling in nitrification and denitrification for the membrane bioreactor (MBR).” *Water Science and Technology*, 53(6), 43–49.
- Jennett, J. C., Dennis, N. D., Jennett, J. C., and Dennis, N. D. (2018). “Anaerobic filter treatment of pharmaceutical waste.” *Journal - Water Pollution Control Federation*, 47(1), 104–121.
- Jensen, P. S., Bak, J., Andersen, P. E., Anderssonengesb, S., and Andersson-Engels, S. (2003). “Fourier transform infrared spectroscopy of aqueous solutions using optical subtraction.” *Optical Diagnostics and Sensing of Biological Fluids and Glucose and Cholesterol Monitoring II*, 4624, 150–159.
- Jeppsson, U., Pons, M.-N., Nopens, I., Alex, J., Copp, J. B., Gernaey, K. V, Rosén, C., Steyer, J.-P., and Vanrolleghem, P. A. (2007). “Benchmark simulation model no 2: general protocol and exploratory case studies.” *Water Science and Technology*, IWA Publishing, 56(8), 67–78.
- Jiang, T., Kennedy, M. D., van der Meer, W. G. J., Vanrolleghem, P. A., and Schippers, J. C. (2003). “The role of blocking and cake filtration in MBR fouling.” *Desalination*, 157(1–3), 335–343.
- Jin, L., Ong, S. L., and Yong, H. (2013). “Fouling control mechanism by suspended biofilm carriers addition in submerged ceramic membrane bioreactors.” *Journal of Membrane Science*, Elsevier, 427, 250–258.
- Judd, S. (2008). “The status of membrane bioreactor technology.” *Trends in Biotechnology*, 26(2), 109–116.
- Judd, S. (2010). *The MBR Book: Principles and Applications of Membrane Bioreactors for Water and Wastewater Treatment*. Elsevier Science.

- Jun, D., Kim, Y., Hafeznezami, S., Yoo, K., Hoek, E. M. V, and Kim, J. (2017). “Biologically induced mineralization in anaerobic membrane bioreactors : Assessment of membrane scaling mechanisms in a long-term pilot study.” *Journal of Membrane Science*, Elsevier B.V., 543(August), 342–350.
- Kampbell, D. H., Wilson, J. T., and Vandegrift, S. A. (1989). “Dissolved Oxygen and Methane in Water by a GC Headspace Equilibration Technique.” *International Journal of Environmental Analytical Chemistry*, Taylor & Francis, 36(4), 249–257.
- Kang, I. J., Yoon, S. H., and Lee, C. H. (2002). “Comparison of the filtration characteristics of organic and inorganic membranes in a membrane-coupled anaerobic bioreactor.” *Water Research*, 36(7), 1803–1813.
- Kannan, A., and Parameswaran, P. (2021). “Ammonia adsorption and recovery from swine wastewater permeate using naturally occurring clinoptilolite.” *Journal of Water Process Engineering*, Elsevier Ltd, 43(August), 102234.
- Kasarda, D. D., and Black, D. R. (1968). “Thermal degradation of proteins studied by mass spectrometry.” *Biopolymers: Original Research on Biomolecules*, Wiley Online Library, 6(7), 1001–1004.
- Kim, J., Kim, K., Ye, H., Lee, E., Shin, C., McCarty, P. L., and Bae, J. (2010). “Anaerobic Fluidized Bed Membrane Bioreactor for Wastewater Treatment.” *Environmental science & technology*, 45(2), null--null.
- Kim, J., Yu, Y., and Lee, C. (2013). “Thermo-alkaline pretreatment of waste activated sludge at low-temperatures: Effects on sludge disintegration, methane production, and methanogen community structure.” *Bioresource Technology*, Elsevier Ltd, 144, 194–201.
- Kimura, K., Ogyu, R., Miyoshi, T., and Watanabe, Y. (2015). “Transition of major components in irreversible fouling of MBRs treating municipal wastewater.” *SEPARATION AND PURIFICATION TECHNOLOGY*, Elsevier B.V., 142, 326–331.
- Kocadagistan, E., and Topcu, N. (2007). “Treatment investigation of the Erzurum City municipal wastewaters with anaerobic membrane bioreactors.” *Desalination*, 216(1–3), 367–376.
- Kolarik, L. O., Kolarik, L. O., and Priestly, A. J. (1996). *Modern Techniques in Water and Wastewater Treatment*. Knovel Library, CSIRO Publishing.
- Kunacheva, C., and Stuckey, D. C. (2014). “Analytical methods for soluble microbial products (SMP) and extracellular polymers (ECP) in wastewater treatment systems: A review.” *Water Research*, Elsevier Ltd, 61, 1–18.
- Lakowicz, J. R. (Ed.). (2006). “Protein Fluorescence.” *Principles of Fluorescence Spectroscopy*, Springer US, Boston, MA, 529–575.
- Laspidou, C. S., and Rittmann, B. E. (2002). “A unified theory for extracellular polymeric substances, soluble microbial products, and active and inert biomass.” *Water Research*, 36,

2711–2720.

- Le-clech, P., Chen, V., and Fane, T. A. G. G. (2006). “Fouling in membrane bioreactors used in wastewater treatment.” *Journal of Membrane Science*, 284(1–2), 17–53.
- Le, C., Kunacheva, C., and Stuckey, D. C. (2016). “‘protein’ Measurement in Biological Wastewater Treatment Systems: A Critical Evaluation.” *Environmental Science and Technology*, 50(6), 3074–3081.
- Lee, S. M., Jung, J. Y., and Chung, Y. C. (2001). “Novel method for enhancing permeate flux of submerged membrane system in two-phase anaerobic reactor.” *Water Research*, Elsevier, 35(2), 471–477.
- Lei, Z., Yang, S., Li, Y. you, Wen, W., Wang, X. C., and Chen, R. (2018). “Application of anaerobic membrane bioreactors to municipal wastewater treatment at ambient temperature: A review of achievements, challenges, and perspectives.” *Bioresource Technology*, Elsevier, 267(July), 756–768.
- Leyva, A., Quintana, A., Sánchez, M., Rodríguez, E. N., Cremata, J., and Sánchez, J. C. (2008). “Rapid and sensitive anthrone-sulfuric acid assay in microplate format to quantify carbohydrate in biopharmaceutical products: Method development and validation.” *Biologicals*, 36(2), 134–141.
- Li, X., Dai, X., Takahashi, J., Li, N., Jin, J., Dai, L., and Dong, B. (2014). “New insight into chemical changes of dissolved organic matter during anaerobic digestion of dewatered sewage sludge using EEM-PARAFAC and two-dimensional FTIR correlation spectroscopy.” *Bioresource Technology*, Elsevier Ltd, 159, 412–420.
- Li, X., Guo, J., Dong, R., and Zhang, W. (2018). “Indolic Derivatives Metabolism in the Anaerobic Reactor Treating Animal Manure: Pathways and Regulation.” *ACS Sustainable Chemistry and Engineering*, 6(9), 11511–11518.
- Li, X. Y., and Yang, S. F. (2007). “Influence of loosely bound extracellular polymeric substances (EPS) on the flocculation, sedimentation and dewaterability of activated sludge.” *Water Research*, 41(5), 1022–1030.
- Liao, B. Q., Kraemer, J. T., and Bagley, D. M. (2006). “Anaerobic membrane bioreactors: Applications and research directions.” *Critical Reviews in Environmental Science and Technology*, 36(6), 489–530.
- Liew Abdullah, A. G., Idris, A., Ahmadun, F. R., Baharin, B. S., Emby, F., Megat Mohd Noor, M. J., and Nour, A. H. (2005). “A kinetic study of a membrane anaerobic reactor (MAR) for treatment of sewage sludge.” *Desalination*, 183(1–3), 439–445.
- Lim, K., Evans, P. J., and Parameswaran, P. (2019). “Long-Term Performance of a Pilot-Scale Gas-Sparged Anaerobic Membrane Bioreactor under Ambient Temperatures for Holistic Wastewater Treatment.” *Environmental Science & Technology*, research-article, American Chemical Society, 53(13), 7347–7354.

- Lim, K., Evans, P. J., Utter, J., Malki, M., and Parameswaran, P. (2020). “Dynamic monitoring and proactive fouling management in a pilot scale gas-sparged anaerobic membrane bioreactor.” *Environmental Science: Water Research and Technology*, Royal Society of Chemistry, 6(10), 2914–2925.
- Lin, H., Chen, J., Wang, F., Ding, L., and Hong, H. (2011). “Feasibility evaluation of submerged anaerobic membrane bioreactor for municipal secondary wastewater treatment.” *DES*, Elsevier B.V., 280(1–3), 120–126.
- Lin, H. J., Xie, K., Mahendran, B., Bagley, D. M., Leung, K. T., Liss, S. N., and Liao, B. Q. (2009). “Sludge properties and their effects on membrane fouling in submerged anaerobic membrane bioreactors (SAnMBRs).” *Water Research*, Elsevier Ltd, 43(15), 3827–3837.
- Lin, H., Peng, W., Zhang, M., Chen, J., Hong, H., and Zhang, Y. (2013). “A review on anaerobic membrane bioreactors: Applications, membrane fouling and future perspectives.” *Desalination*, Elsevier B.V., 314, 169–188.
- Liu, Z. H., Yin, H., Dang, Z., and Liu, Y. (2014). “Dissolved methane: A hurdle for anaerobic treatment of municipal wastewater.” *Environmental Science and Technology*, 48(2), 889–890.
- Liu, Z., Zhu, X., Liang, P., Zhang, X., Kimura, K., and Huang, X. (2019a). “Distinction between polymeric and ceramic membrane in AnMBR treating municipal wastewater: In terms of irremovable fouling.” *Journal of Membrane Science*, Elsevier B.V., 588(May), 117229.
- Liu, Z., Zhu, X., Liang, P., Zhang, X., Kimura, K., and Huang, X. (2019b). “Distinction between polymeric and ceramic membrane in AnMBR treating municipal wastewater: In terms of irremovable fouling.” *Journal of Membrane Science*, Elsevier B.V., 588(July), 117229.
- Lousada-Ferreira, M., van Lier, J. B., and van der Graaf, J. H. J. M. (2015). “Impact of suspended solids concentration on sludge filterability in full-scale membrane bioreactors.” *Journal of Membrane Science*, Elsevier, 476, 68–75.
- Lu, Y., Nakicenovic, N., Visbeck, M., and Stevance, A.-S. (2015). “Five priorities for the UN Sustainable Development Goals.” 7–8.
- Lundin, M., Bengtsson, M., and Molander, S. (2000). “Life cycle assessment of wastewater systems: Influence of system boundaries and scale on calculated environmental loads.” *Environmental Science and Technology*, 34(1), 180–186.
- Luo, K., Yang, Q., Li, X., Chen, H., Liu, X., Yang, G., and Zeng, G. (2013). “Novel insights into enzymatic-enhanced anaerobic digestion of waste activated sludge by three-dimensional excitation and emission matrix fluorescence spectroscopy.” *Chemosphere*, 91(5), 579–585.
- Lutze, R., and Engelhart, M. (2021). “Effects of Sludge Characteristics on the Critical Flux of an AnMBR for Sludge Treatment.” *Chemie-Ingenieur-Technik*, 93(9), 1375–1382.
- Lv, J., Zhao, F., Feng, J., Liu, Q., Nan, F., and Xie, S. (2019). “Extraction of extracellular

- polymeric substances (EPS) from a newly isolated self-flocculating microalga *Neocystis mucosa* SX with different methods.” *Algal Research*, Elsevier, 40.
- Maaz, M., Yasin, M., Aslam, M., Kumar, G., Atabani, A. E., Idrees, M., Anjum, F., Jamil, F., Ahmad, R., Khan, A. L., Lesage, G., Heran, M., and Kim, J. (2019). “Anaerobic membrane bioreactors for wastewater treatment: Novel configurations, fouling control and energy considerations.” *Bioresource Technology*, 283, 358–372.
- Malik, O. A., Hsu, A., Johnson, L. A., and Sherbinin, A. De. (2015). “A global indicator of wastewater treatment to inform the Sustainable Development Goals (SDGs).” *Environmental Science and Policy*, Elsevier Ltd, 48, 172–185.
- Marlow, D. R., Moglia, M., Cook, S., Beale, D. J., Land, C., and Road, G. (2013). “ScienceDirect Towards sustainable urban water management : A critical reassessment.” *Water Research*, Elsevier Ltd, 47(20), 7150–7161.
- Martinez-Sosa, D., Helmreich, B., Netter, T., Paris, S., Bischof, F., and Horn, H. (2011). “Anaerobic submerged membrane bioreactor (AnSMBR) for municipal wastewater treatment under mesophilic and psychrophilic temperature conditions.” *Bioresource Technology*, Elsevier Ltd, 102(22), 10377–10385.
- Maruyama, T., Katoh, S., Nakajima, M., Nabetani, H., Abbott, T. P., Shono, A., and Satoh, K. (2001). “FT-IR analysis of BSA fouled on ultrafiltration and microfiltration membranes.” *Journal of Membrane Science*, Elsevier, 192(1–2), 201–207.
- Massart, N., Doyle, J., Jenkins, J., Rowan, J., Wallis-lage, C., and City, K. (2008). “Anaerobic digestion-improving energy efficiency with mixing.” *Proceedings of the Water Environment Federation*, 554–568.
- Masuko, T., Minami, A., Iwasaki, N., and Majima, T. (2005). “Carbohydrate analysis by a phenol – sulfuric acid method in microplate format.” *Analytical Biochemistry*, 339, 69–72.
- McCarty, P. L., Bae, J., and Kim, J. (2011). “Domestic wastewater treatment as a net energy producer - can this be achieved?” *Environmental science & technology*, 45(17), 7100–6.
- Meng, F., Chae, S., Drews, A., Kraume, M., and Shin, H. (2009a). “Recent advances in membrane bioreactors (MBRs): Membrane fouling and membrane material.” *Water Research*, Elsevier Ltd, 43(6), 1489–1512.
- Meng, F., Chae, S. R., Drews, A., Kraume, M., Shin, H. S., and Yang, F. (2009b). “Recent advances in membrane bioreactors (MBRs): Membrane fouling and membrane material.” *Water Research*, Elsevier Ltd, 43(6), 1489–1512.
- Meng, Y., Wang, M., Guo, B., Zhu, F., Wang, Y., Lu, J., Ma, D., Sun, Y., and Gao, B. (2017). “Characterization and C-, N-disinfection byproduct formation of dissolved organic matter in MBR and anaerobic-anoxic-oxic (AAO) processes.” *Chemical Engineering Journal*, 315, 243–250.

- Merlic, C., and Strouse, J. (1997). "Table of IR Absorptions." *WebSpectra Problems in NMR and IR Spectroscopy*, <<https://webspectra.chem.ucla.edu/irtable.html>>.
- Meroney, R. N., and Sheker, R. E. (2014). "CFD Simulation of Vertical Linear Motion Mixing in Anaerobic Digester Tanks." *Water Environment Research*, 86(9).
- Metcalf, L., Eddy, H. P., and Tchobanoglous, G. (2004). *Wastewater engineering: treatment, disposal, and reuse*. McGraw-Hill New York.
- Mo, W., and Zhang, Q. (2013). "Energy-nutrients-water nexus: Integrated resource recovery in municipal wastewater treatment plants." *Journal of Environmental Management*, Elsevier Ltd, 127, 255–267.
- Molina-moreno, V., Carlos, J., Llorens-montes, F. J., and Joaquin, F. (2017). "Design of Indicators of Circular Economy as Instruments for the Evaluation of Sustainability and Efficiency in Wastewater from Pig Farming Industry." *Water*, 9(653).
- Morgan, J. W., Forster, C. F., and Evison, L. (1990). "A comparative study of the nature of biopolymers extracted from anaerobic and activated sludges." *Water Research*, Pergamon, 24(6), 743–750.
- NAE. (2017). "NAE Grand Challenges for Engineering." *National Academy of Engineering*, 56.
- Namkung, E., and Rittmann, B. E. (1986). "Soluble microbial products (SMP) formation kinetics by biofilms." *Water Research*, Elsevier, 20(6), 795–806.
- Nghiem, L. D., Koch, K., Bolzonella, D., and Drewes, J. E. (2017). "Full scale co-digestion of wastewater sludge and food waste : Bottlenecks and possibilities." *Renewable and Sustainable Energy Reviews*, Elsevier Ltd, 72, 354–362.
- Nielsen, P. H. (2017). "Microbial biotechnology and circular economy in wastewater treatment." 10, 1102–1105.
- Nielsen, P. H., Jahn, A., and Palmgren, R. (1997). "Conceptual model for production and composition of exopolymers in biofilms." *Water Science and Technology*, Elsevier, 36(1), 11–19.
- Nielsen, S. S. (2010). "Phenol-Sulfuric Acid Method for Total Carbohydrates BT - Food Analysis Laboratory Manual." S. S. Nielsen, ed., Springer US, Boston, MA, 47–53.
- Ognier, S., Wisniewski, C., and Grasmick, A. (2004). "Membrane bioreactor fouling in sub-critical filtration conditions: A local critical flux concept." *Journal of Membrane Science*, 229(1–2), 171–177.
- Park, C., and Novak, J. T. (2007). "Characterization of activated sludge exocellular polymers using several cation-associated extraction methods." *Water Research*, 41(8), 1679–1688.
- Polat, E., Karaca, M., Demir, H., and Onus, a N. (2004). "Use of natural zeolite (clinoptilolite)

- in agriculture.” *Journal of Fruit and Ornamental Plant Reserarch*, 12(April), 183–189.
- Porcelli, N., and Judd, S. (2010). “Chemical cleaning of potable water membranes: A review.” *Separation and Purification Technology*, 71(2), 137–143.
- Pretel, R., Shoener, B. D., Ferrer, J., and Guest, J. S. (2015). “Navigating environmental, economic, and technological trade-offs in the design and operation of submerged anaerobic membrane bioreactors (AnMBRs).” *Water Research*, Elsevier Ltd, 87, 531–541.
- Prieto, A. L., Futselaar, H., Lens, P. N. L., Bair, R., and Yeh, D. H. (2013). “Development and start up of a gas-lift anaerobic membrane bioreactor (Gl-AnMBR) for conversion of sewage to energy, water and nutrients.” *Journal of Membrane Science*, Elsevier, 441, 158–167.
- Qin, J. J., Wai, M. N., Oo, M. H., Kekre, K. A., and Seah, H. (2009). “Impact of anti-scalant on fouling of reverse osmosis membranes in reclamation of secondary effluent.” *Water Science and Technology*, 60(11), 2767–2774.
- Rabuni, M. F., Nik Sulaiman, N. M., Aroua, M. K., Yern Chee, C., and Awanis Hashim, N. (2015). “Impact of in situ physical and chemical cleaning on PVDF membrane properties and performances.” *Chemical Engineering Science*, Elsevier, 122, 426–435.
- Ramesh, A., Lee, D. J., and Hong, S. G. (2006). “Soluble microbial products (SMP) and soluble extracellular polymeric substances (EPS) from wastewater sludge.” *Applied Microbiology and Biotechnology*, 73(1), 219–225.
- Redmile-Gordon, M. A., Brookes, P. C., Evershed, R. P., Goulding, K. W. T., and Hirsch, P. R. (2014). “Measuring the soil-microbial interface : Extraction of extracellular polymeric substances (EPS) from soil biofilms.” *Soil Biology and Biochemistry*, Elsevier Ltd, 72, 163–171.
- Reid, E., Liu, X., and Judd, S. J. (2006). “Effect of high salinity on activated sludge characteristics and membrane permeability in an immersed membrane bioreactor.” *Journal of Membrane Science*, 283(1–2), 164–171.
- Rittmann, B. E., Mayer, B., Westerhoff, P., and Edwards, M. (2011). “Capturing the lost phosphorus.” *Chemosphere*, Elsevier Ltd, 84(6), 846–853.
- Rittmann, B. E., and McCarty, P. L. (2001). *Environmental Biotechnology: Principles and Applications*. McGraw-Hill international editions : Biological sciences series, McGraw-Hill.
- Robles, Á., Durán, F., Giménez, J. B., Jiménez, E., Ribes, J., Serralta, J., Seco, A., Ferrer, J., and Rogalla, F. (2020). “Anaerobic membrane bioreactors (AnMBR) treating urban wastewater in mild climates.” *Bioresource Technology*, Elsevier, 314, 123763.
- Rocher, M., Goma, G., Pilas Begue, A., Louvel, L., and Rols, J. L. (1999). “Towards a reduction in excess sludge production in activated sludge processes: Biomass physicochemical treatment and biodegradation.” *Applied Microbiology and Biotechnology*, 51(6), 883–890.

- Rogalla, F., and Bourbigot, M. M. (1990). "New developments in complete nitrogen removal with biological aerated filters." *Water Science and Technology*, 22(1–2), 273–280.
- Saddoud, A., Ellouze, M., Dhouib, A., and Sayadi, S. (2007). "Anaerobic membrane bioreactor treatment of domestic wastewater in Tunisia." *Desalination*, 207(1–3), 205–215.
- Sahinkaya, E., Yurtsever, A., Isler, E., Coban, I., and Akta, Ö. (2018). "Sulfate reduction and filtration performances of an anaerobic membrane bioreactor (AnMBR)." *Chemical Engineering Journal*, 349, 47–55.
- Seco, A., Mateo, O., Zamorano-lópez, N., Sanchis-perucho, P., Serralta, J., Martí, N., Borrás, L., and Ferrer, J. (2018). "Exploring the limits of anaerobic biodegradability of urban wastewater by AnMBR technology." *Environmental Science: Water Research and Technology*, Royal Society of Chemistry, 4(11), 1877–1887.
- Sheng, G. P., Yu, H. Q., and Li, X. Y. (2010). "Extracellular polymeric substances (EPS) of microbial aggregates in biological wastewater treatment systems: A review." *Biotechnology Advances*, Elsevier Inc., 28(6), 882–894.
- Shin, C., and Bae, J. (2018). "Current status of the pilot-scale anaerobic membrane bioreactor treatments of domestic wastewaters: A critical review." *Bioresource Technology*, Elsevier, 247(June 2017), 1038–1046.
- Shin, C., Mccarty, P. L., Kim, J., and Bae, J. (2014). "Pilot-scale temperate-climate treatment of domestic wastewater with a staged anaerobic fluidized membrane bioreactor (SAF-MBR)." *Bioresource Technology*, Elsevier Ltd, 159, 95–103.
- Shin, C., Tilmans, S. H., Chen, F., McCarty, P. L., and Criddle, C. S. (2021). "Temperate climate energy-positive anaerobic secondary treatment of domestic wastewater at pilot-scale." *Water Research*, Elsevier Ltd, 204.
- Shizas, I., Bagley, D. M., and Asce, M. (2004). "Experimental Determination of Energy Content of Unknown Organics in Municipal Wastewater Streams." *Journal of Energy Engineering*, 130(2), 45–53.
- Sigma-Aldrich. (2011). "BCA assay Technical bulletin." 1–6.
- Silvestre, G., Fernández, B., and Bonmatí, A. (2015). "Significance of anaerobic digestion as a source of clean energy in wastewater treatment plants." *Energy Conversion and Management*, Elsevier Ltd, 101, 255–262.
- Skouteris, G., Hermosilla, D., López, P., Negro, C., and Blanco, Á. (2012). "Anaerobic membrane bioreactors for wastewater treatment: A review." *Chemical Engineering Journal*, Elsevier B.V., 198–199, 138–148.
- Smith, A. L., Skerlos, S. J., and Raskin, L. (2013). "Psychrophilic anaerobic membrane bioreactor treatment of domestic wastewater." *Water Research*, Elsevier Ltd, 47(4), 1655–1665.

- Smith, A. L., Skerlos, S. J., and Raskin, L. (2015). “Anaerobic membrane bioreactor treatment of domestic wastewater at psychrophilic temperatures ranging from 15 °c to 3 °c.” *Environmental Science: Water Research and Technology*, Royal Society of Chemistry, 1(1), 56–64.
- Smith, A. L., Stadler, L. B., Cao, L., Love, N. G., Raskin, L., and Skerlos, S. J. (2014). “Navigating wastewater energy recovery strategies: A life cycle comparison of anaerobic membrane bioreactor and conventional treatment systems with anaerobic digestion.” *Environmental Science and Technology*, 48(10), 5972–5981.
- Smith, B. C. (2011). *Fundamentals of Fourier transform infrared spectroscopy*. CRC press.
- Stedmon, C. A., and Bro, R. (2008). “Characterizing dissolved organic matter fluorescence with parallel factor analysis: a tutorial.” *Limnology and Oceanography*, 6, 572–579.
- Stedmon, C. A., Markager, S., Colin A. Stedmon, author, and Stiig Markager, author. (2005). “Tracing the Production and Degradation of Autochthonous Fractions of Dissolved Organic Matter by Fluorescence Analysis.” *Limnology and Oceanography*, 50(5), 1415.
- Stuckey, D. C., and McCarty, P. L. (1984). “The effect of thermal pretreatment on the anaerobic biodegradability and toxicity of waste activated sludge.” *Water Research*, 18(11), 1343–1353.
- Sun, H., and Liu, Y. (2021). “Chemical Cleaning-Triggered Release of Dissolved Organic Matter from a Sludge Suspension in a Ceramic Membrane Bioreactor : A Potential Membrane Foulant.” *ACS ES&T Water*.
- Sweetapple, C., Fu, G., and Butler, D. (2013). “Identifying key sources of uncertainty in the modelling of greenhouse gas emissions from wastewater treatment.” *Water Research*, Elsevier Ltd, 47(13), 4652–4665.
- Takahashi, M., and Kawamura, K. (2007). “Simple measurement of 4,4'-bis(2-sulfostyryl)-biphenyl in river water by fluorescence analysis and its application as an indicator of domestic wastewater contamination.” *Water, Air, and Soil Pollution*, 180(1–4), 39–49.
- Tang, C. Y., Kwon, Y. N., and Leckie, J. O. (2007). “Probing the nano- and micro-scales of reverse osmosis membranes-A comprehensive characterization of physiochemical properties of uncoated and coated membranes by XPS, TEM, ATR-FTIR, and streaming potential measurements.” *Journal of Membrane Science*, 287(1), 146–156.
- Tchobanoglous, G., Franklin, B., and Stensel, D. (2003). *Wastewater engineering: Treatment and reuse*. McGraw-Hill, Boston.
- Teng, J., Zhang, M., Leung, K. T., Chen, J., Hong, H., Lin, H., and Liao, B. Q. (2019). “A unified thermodynamic mechanism underlying fouling behaviors of soluble microbial products (SMPs) in a membrane bioreactor.” *Water Research*, Elsevier Ltd, 149, 477–487.
- Titiz-Sargut, S., Sayan, P., and Avcı, B. (2007). “Influence of citric acid on calcium sulfate

- dihydrate crystallization in aqueous media.” *Crystal Research and Technology: Journal of Experimental and Industrial Crystallography*, 126(2), 119–126.
- Tram, P., Hao, H., Guo, W., Zhou, J. L., Dan, P., Listowski, A., and Wang, X. C. (2014). “A mini-review on the impacts of climate change on wastewater reclamation and reuse.” *Science of the Total Environment*, Elsevier B.V., 494–495, 9–17.
- Ueno, Y., and Fujii, M. (2001). “Three years experience of operating and selling recovered struvite from full-scale plant.” *Environmental Technology*, Taylor & Francis, 22(11), 1373–1381.
- Vargas, G., Alarco, N., and Vergara-ferna, A. (2008). “Evaluation of marine algae as a source of biogas in a two-stage anaerobic reactor system.” *Biomass and Bioenergy*, 32, 338–344.
- Vincent, N. M., Tong, J., Yu, D., Zhang, J., and Wei, Y. (2018). “Membrane fouling characteristics of a side-stream tubular anaerobic membrane bioreactor (AnMBR) treating domestic wastewater.” *Processes*, 6(5), 1–17.
- Vu, M. T., Vu, H. P., Nguyen, L. N., Semblante, G. U., Johir, M. A. H., and Nghiem, L. D. (2020). “A hybrid anaerobic and microalgal membrane reactor for energy and microalgal biomass production from wastewater.” *Environmental Technology and Innovation*, Elsevier B.V., 19, 100834.
- Walker, J. M. (2009). “The Bicinchoninic Acid (BCA) Assay for Protein Quantitation BT - The Protein Protocols Handbook.” J. M. Walker, ed., Humana Press, Totowa, NJ, 11–15.
- Wang, F., and Tarabara, V. V. (2008). “Pore blocking mechanisms during early stages of membrane fouling by colloids.” *Journal of Colloid and Interface Science*, Elsevier Inc., 328(2), 464–469.
- Wang, J., and Chu, L. (2016). “Biological nitrate removal from water and wastewater by solid-phase denitri fi cation process.” *Biotechnology Advances*, Elsevier Inc., 34(6), 1103–1112.
- Wang, Z., Ding, J., Xie, P., Chen, Y., Wan, Y., and Wang, S. (2018). “Formation of halogenated by-products during chemical cleaning of humic acid-fouled UF membrane by sodium hypochlorite solution.” *Chemical Engineering Journal*, Elsevier, 332, 76–84.
- Wang, Z., Wu, Z., Yin, X., and Tian, L. (2008). “Membrane fouling in a submerged membrane bioreactor (MBR) under sub-critical flux operation: Membrane foulant and gel layer characterization.” *Journal of Membrane Science*, 325(1), 238–244.
- Wen, C., Huang, X., and Qian, Y. (1999). “Domestic wastewater treatment using an anaerobic bioreactor coupled with membrane filtration.” *Process Biochemistry*, 35(3–4), 335–340.
- Xie, K., Lin, H. J., Mahendran, B., Bagley, D. M., Leung, K. T., Liss, S. N., and Liao, B. Q. (2010). “Performance and fouling characteristics of a submerged anaerobic membrane bioreactor for kraft evaporator condensate treatment.” *Environmental Technology*, 31(5), 511–521.

- Xiong, Y., Harb, M., and Hong, P. Y. (2015). "Characterization of biofoulants illustrates different membrane fouling mechanisms for aerobic and anaerobic membrane bioreactors." *Separation and Purification Technology*, Elsevier B.V., 157, 192–202.
- Xu, B., Albert Ng, T. C., Huang, S., Shi, X., and Ng, H. Y. (2020a). "Feasibility of isolated novel facultative quorum quenching consortiums for fouling control in an AnMBR." *Water Research*, Elsevier Ltd, 169, 115251.
- Xu, B., Ng, T. C. A., Huang, S., and Ng, H. Y. (2020b). "Effect of quorum quenching on EPS and size-fractionated particles and organics in anaerobic membrane bioreactor for domestic wastewater treatment." *Water research*, Elsevier Ltd, 179, 115850.
- Yan, T., Ye, Y., Ma, H., Zhang, Y., Guo, W., Du, B., Wei, Q., Wei, D., and Ngo, H. H. (2018). "A critical review on membrane hybrid system for nutrient recovery from wastewater." *Chemical Engineering Journal*, Elsevier, 348, 143–156.
- Yeo, H., An, J., Reid, R., Rittmann, B. E., and Lee, H. S. (2015). "Contribution of Liquid/Gas Mass-Transfer Limitations to Dissolved Methane Oversaturation in Anaerobic Treatment of Dilute Wastewater." *Environmental Science and Technology*, 49(17), 10366–10372.
- Yurtsever, A., Özer, Ç., and Sahinkaya, E. (2016). "Treatment of textile wastewater using sequential sulfate-reducing anaerobic and sulfide-oxidizing aerobic membrane bioreactors." *Journal of Membrane Science*, 511, 228–237.
- Zhang, J., Padmasiri, S. I., Fitch, M., Norddahl, B., Raskin, L., and Morgenroth, E. (2007). "Influence of cleaning frequency and membrane history on fouling in an anaerobic membrane bioreactor." *Desalination*, 207, 153–166.
- Zheng, X., Khan, M. T., and Croué, J. P. (2014). "Contribution of effluent organic matter (EfOM) to ultrafiltration (UF) membrane fouling: Isolation, characterization, and fouling effect of EfOM fractions." *Water Research*, 65, 414–424.

Appendix A - Accompanying Chapter 3

Coagulation dosage determination through jar testing

A standard Phipps and Bird jar tester was used. For each test, 1 L of permeate was collected. Chemical additions were made during rapid mixing at 120 min⁻¹ for 2 minutes, which was followed by slow mixing at 30 min⁻¹ for 20 minutes. After mixing, the beaker contents were poured into 1-L graduated cylinders and allowed to settle for 30 minutes prior to sampling and analysis. A representative testing matrix and the results are shown in Table A1.

Table A1 The results and coagulant dosing conditions used to determine the approximate rates of chemical addition for the pilot plant's nutrient recovery system

FeCl3 (mg/L-Fe)	ACH (mg/L)	Polymer Dose (mg/L)	Results (description)	pH	ORP	Turbidity (NTU)	Influent Sulfide (mg/L)	Sludge Volume (ml)	Residual Sulfide (mg/L)
61	26	1.3	Failure. Black color throughout, no settling	6.8	-156	113	1.50	0	1.50
61	52	1.3	Floc formation, some settling, lots of flocs suspended still.	6.8	-158	59	1.00	25	1.00
61	77	1.3	Cloudy	6.8	-153	23	0.75	45	0.75
61	103	1.3	Larger flocs, better settling many suspended particles	6.9	-144	25	1.00	55	1.00
121	26	1.3	Not as many suspended flocs. Large floc size. Good settling	6.7	-154	97	0.85	0.1	0.85
121	52	1.3	Failure. Black color throughout; small discrete flocs	6.7	-131	42	0.90	20	0.90
121	77	1.3	Small or medium size flocs, suspended solids, decent settleability.	6.7	-132	44	1.25	25	1.25
121	103	1.3	Medium size flocs, good settability, some suspended solids, mostly clear water	6.7	-127	36	0.95	35	0.95
182	26	1.3	Clear water, medium size flocs, lower concentration of suspended solids than previous condition	6.5	-85	18	0.12	35	0.12
182	52	1.3	Ashy gray, very good settleability, low turbidity	6.6	-98	15	0.13	45	0.13
182	77	1.3	Black-green flocs, few suspended flocs	6.6	-94	9	0.13	40	0.13
182	103	1.3	Black-green flocs, very clear water, denser settling flocs	6.7	-93	15	0.11	85	0.11
243	26	1.3	Black-green flocs, very clear water, some white wispy clouds.	6.4	-69	7	0.10	40	0.10
243	52	1.3	Golden flocs, great settling, very low turbidity	6.4	-67	5	0.10	50	0.10
243	77	1.3	Golden flocs, great settling, very low turbidity	6.4	-67	5	0.10	60	0.10
243	103	1.3	Golden flocs, great settling, very low turbidity	6.4	-68	4	0.09	85	0.09

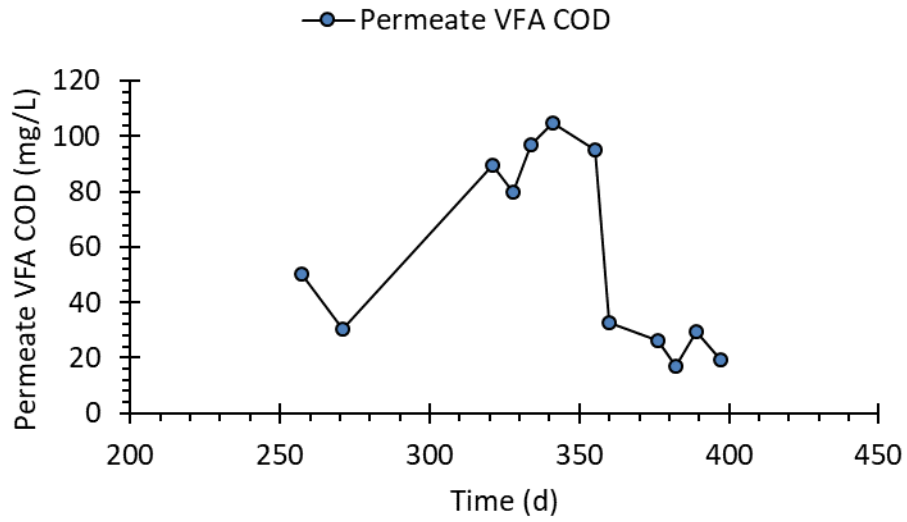


Figure A1 The COD associated with Volatile Fatty Acids (VFA) measured in the permeate between days 250 and 400. The upset conditions from day 300 to day 355 is associated with elevated VFA concentration

Appendix B - Accompanying Chapter 4

Table B1 Table of LSI and pH values over the first 96 days of operation. The LSI values were consistently negative after the startup period, indicating that calcium carbonate scaling was not likely to occur.

Days	LSI	pH
17	-0.07	7.05
20	0.19	7.34
24	0.24	7.44
27	-0.39	6.76
31	-0.26	6.95
34	0.01	7.10
38	-0.22	7.01
40	-0.46	6.77
47	-0.24	6.92
54	-0.29	6.88
59	-0.30	6.97
61	-0.78	6.67
66	-0.56	6.63
68	-0.51	6.68
83	-0.19	7.06
87	-0.20	7.07
96	-0.05	7.10

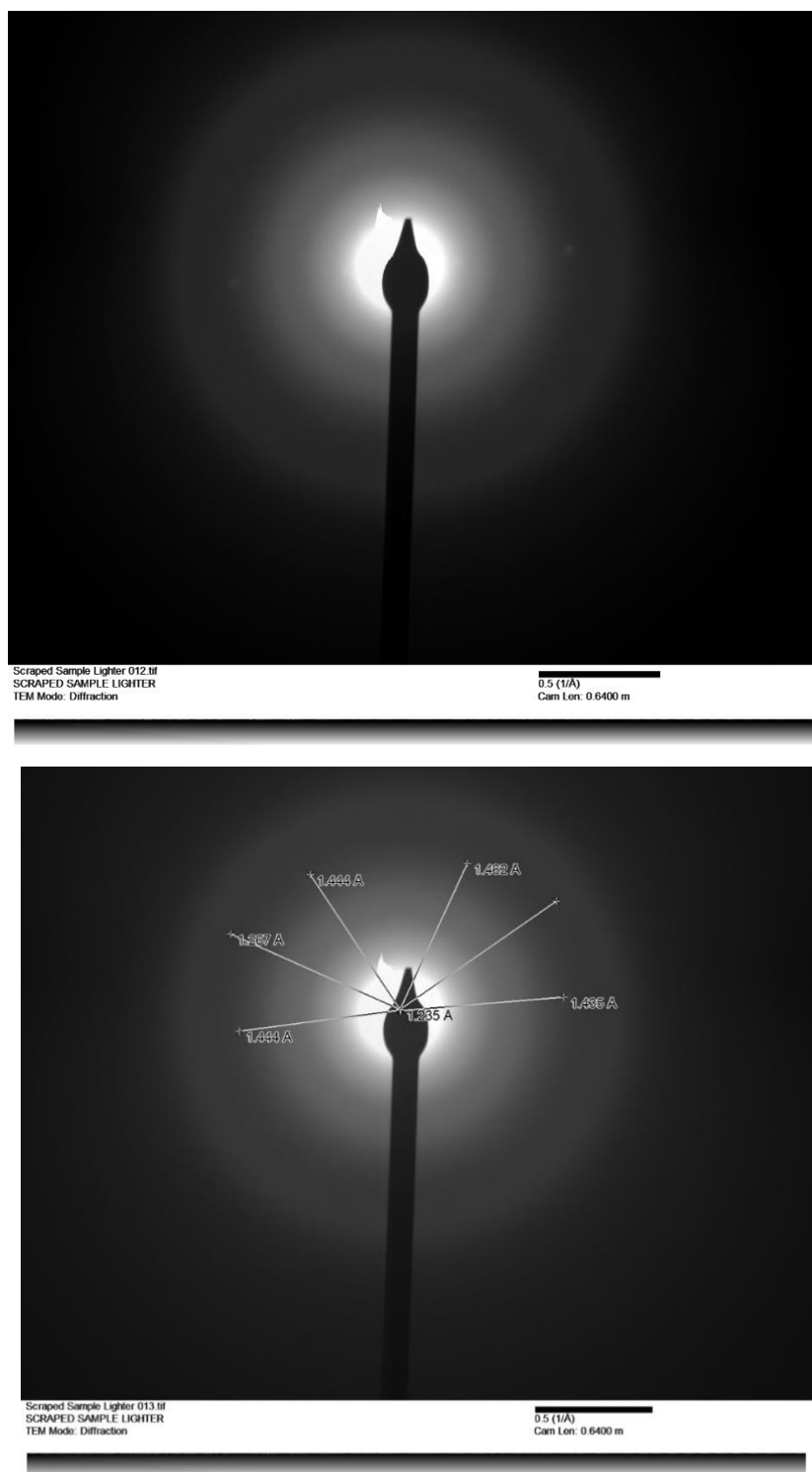


Figure B1 Transmission electron microscope crystal diffraction images. The diffraction patterns are diffused due to the high organic content present throughout the wastewater matrix, but diffraction spots can be seen in (A). Measurements to determine d-spacing are shown in (B), which identified the crystalline material as calcium sulfate.

Appendix C - Accompanying Chapter 6

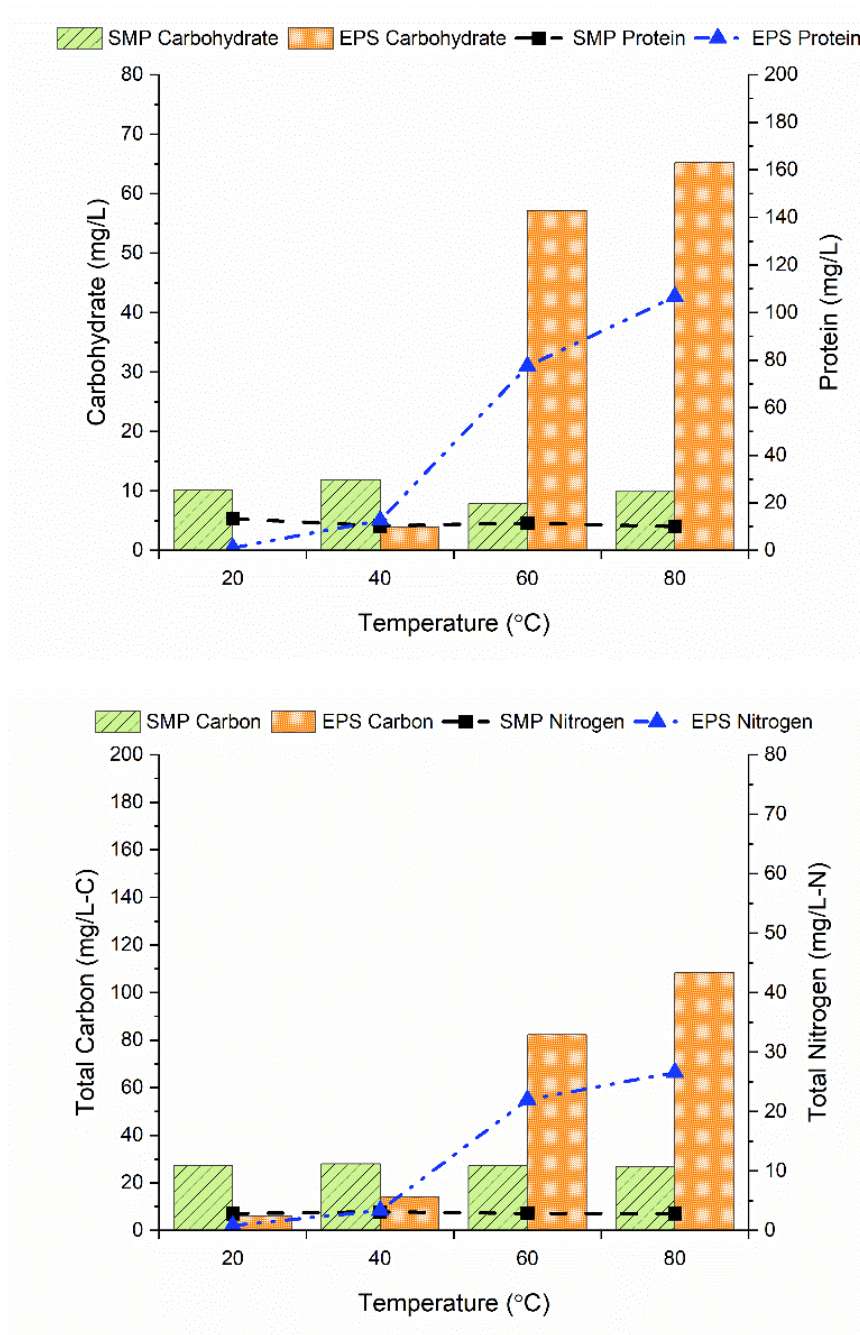


Figure C1 Extraction data for activated sludge sample AS0, taken from the Manhattan, Kansas wastewater treatment plant. The solids concentrations were 2640 mg/L TSS and 2320 mg/L VSS. Despite the differences in sludge concentration, the general trends were consistent with those observed in the AS sample discussed in the main manuscript.

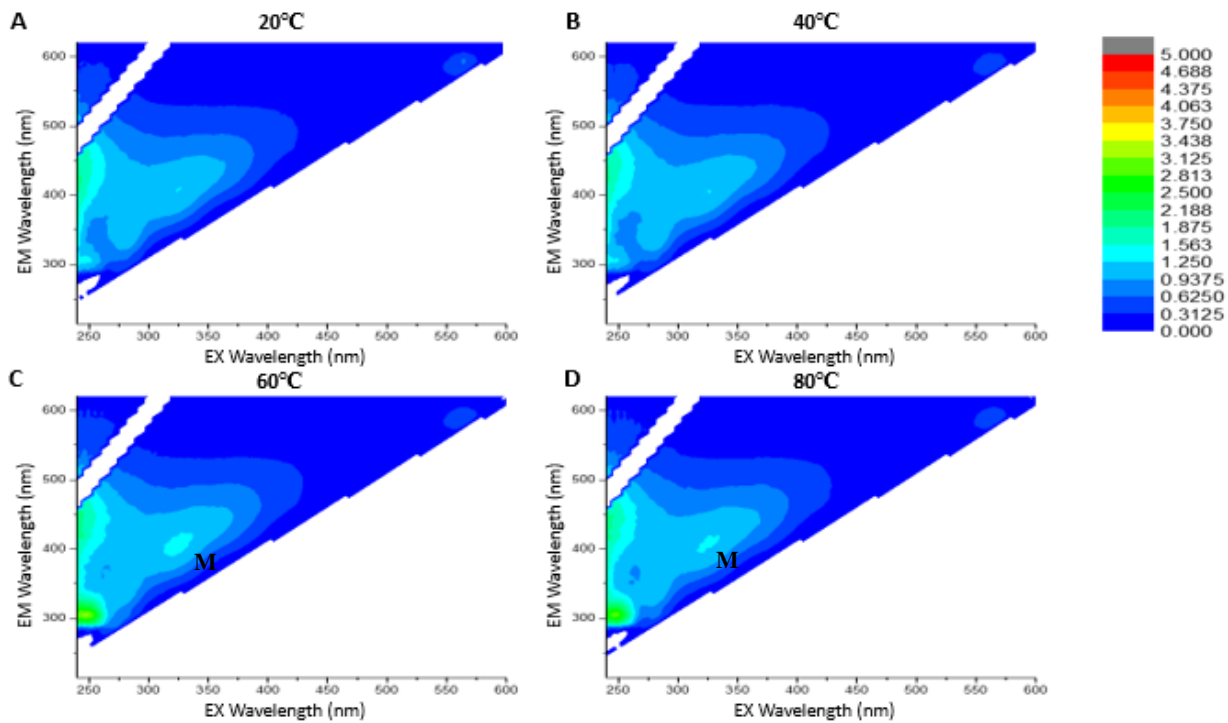


Figure C2 Excitation-Emission Matrices of AS1 (activated sludge) SMP extracted at different temperatures. Increasing temperatures beyond 60°C revealed extracted fluorophores characteristic of marine humic-like (fluorophore M) substances, but the peak intensities are low and relatively comparable among all extraction temperatures tested.

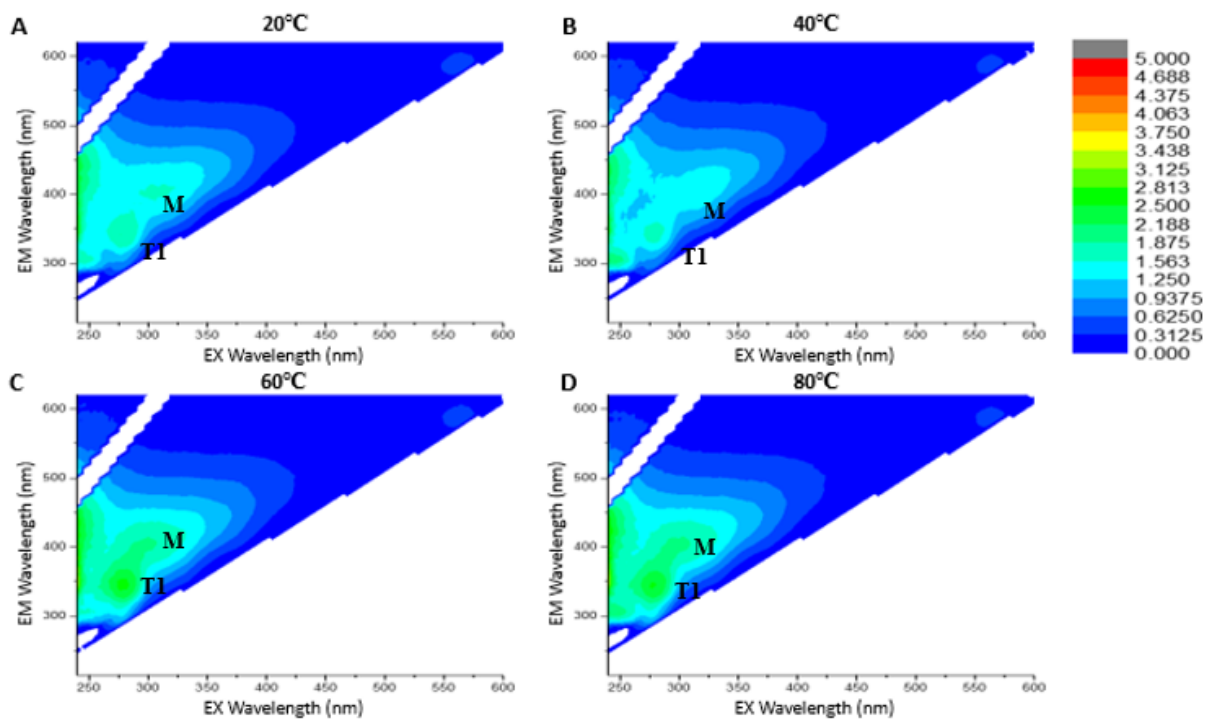


Figure C3 Excitation-Emission Matrices of ANX (anoxic sludge) SMP extracted at different temperatures. The tryptophan-like peak (fluorophore T1) and marine humic-like peak (fluorophore M) appear slightly more intense with increasing temperature, but the peak intensities are low and relatively comparable among all extraction temperatures tested.

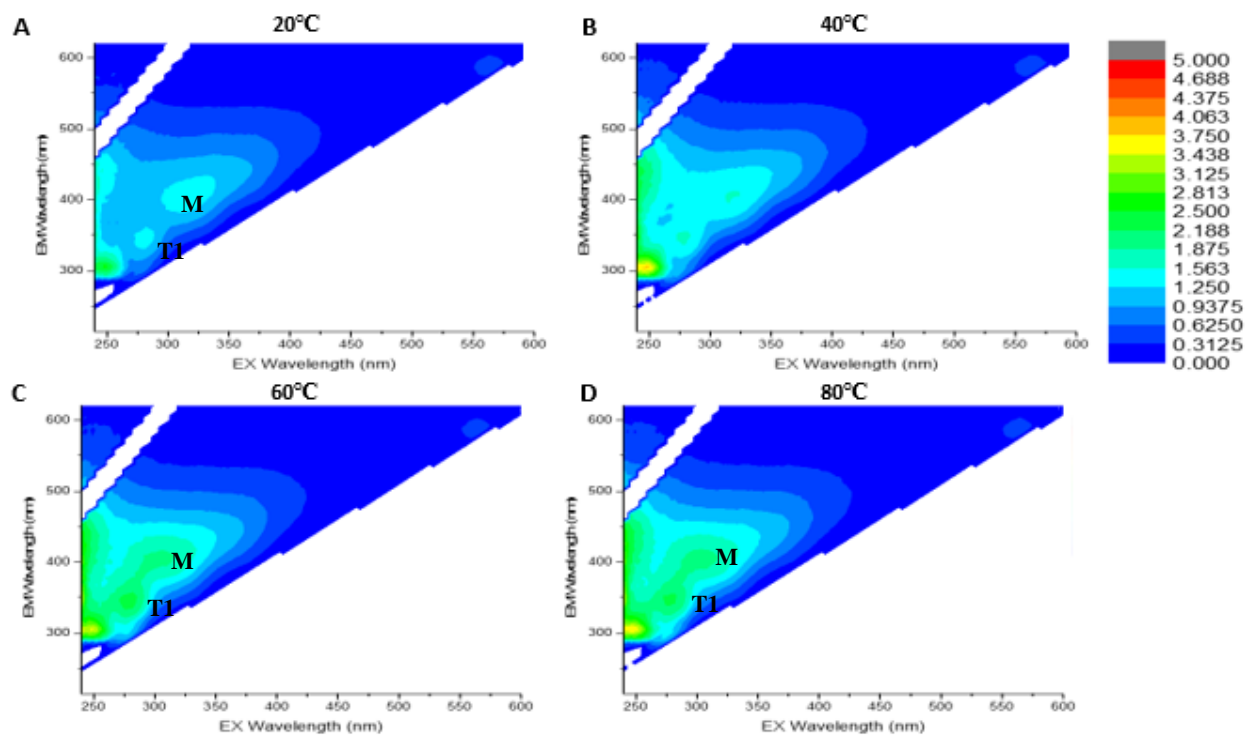


Figure C4 Excitation-Emission Matrices of ANA (anaerobic sludge) SMP extracted at different temperatures. The tryptophan-like peak (fluorophore T1) and marine humic-like peak (fluorophore M) appear slightly more intense with increasing temperature, but the peak intensities are low and relatively comparable among all extraction temperatures tested.

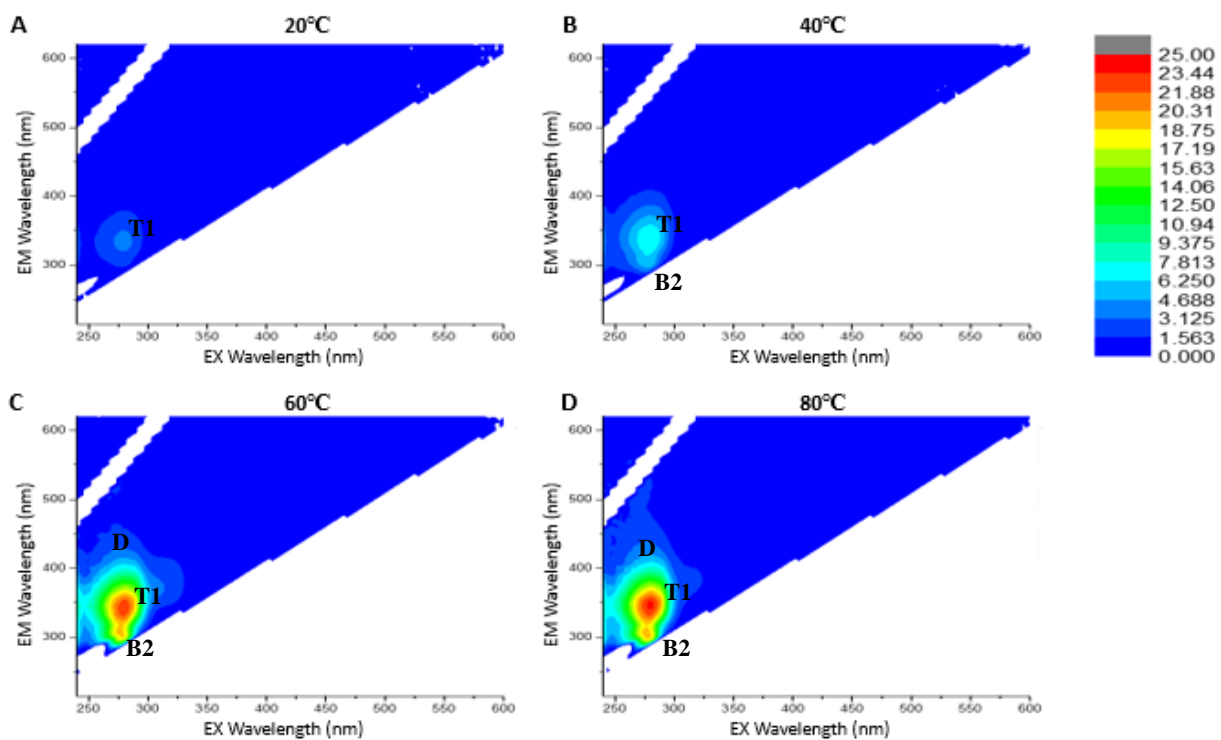


Figure C5 Excitation-Emission Matrices of ANX (anoxic sludge) EPS extracted at different temperatures. The tryptophan-like peak (fluorophore T1) was predominant, with an accompanying tyrosine-like peak (fluorophore B2), with increasing relative intensity as extraction temperatures progressively increased. A fulvic-like peak (fluorophore D) was also observed at the two higher extraction temperatures.

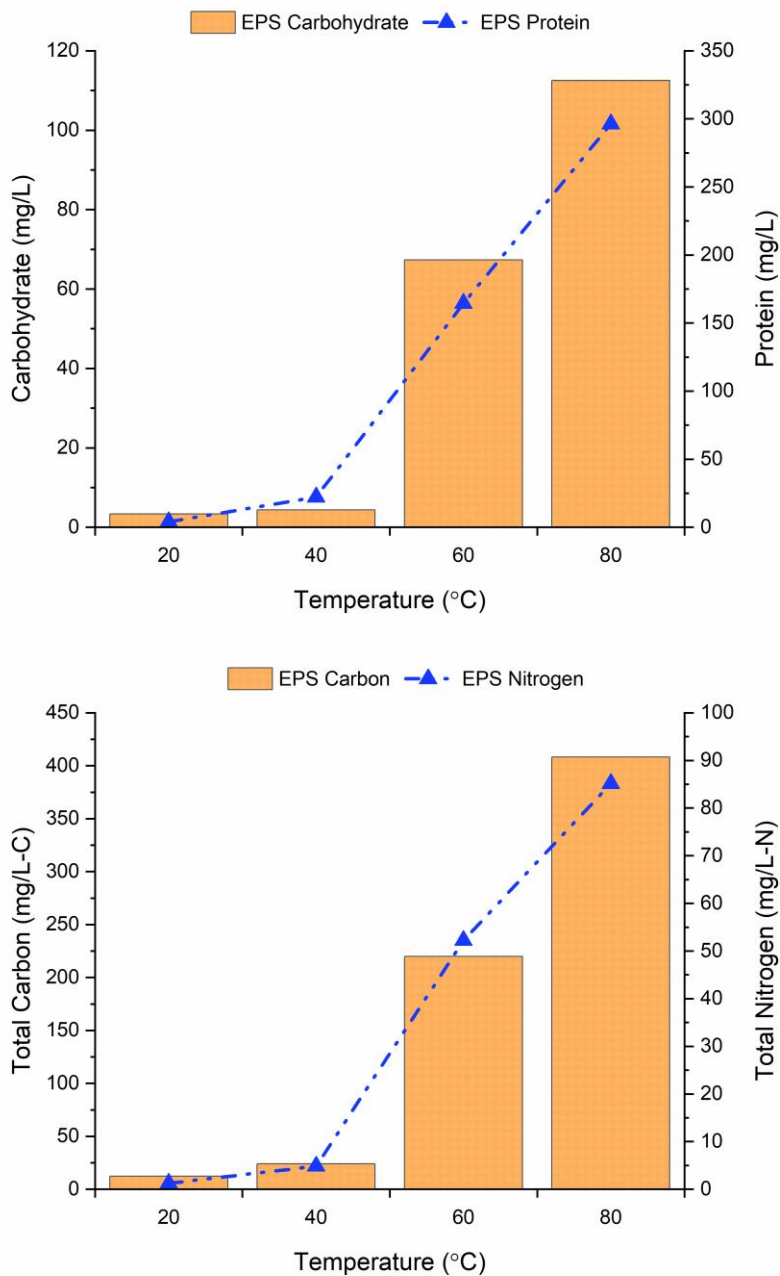


Figure C6 Extraction data for aerobic membrane bioreactor sludge sample AeMBR0 as measured using the phenol-sulfuric acid method and bicinchoninic acid method, respectively, as well as extracted total carbon and total nitrogen measurements versus extraction temperature. The error (n=3) was less than 10% for all datapoints. The trends were similar to those observed in activated sludge extractions.

Appendix D - Accompanying Chapter 7

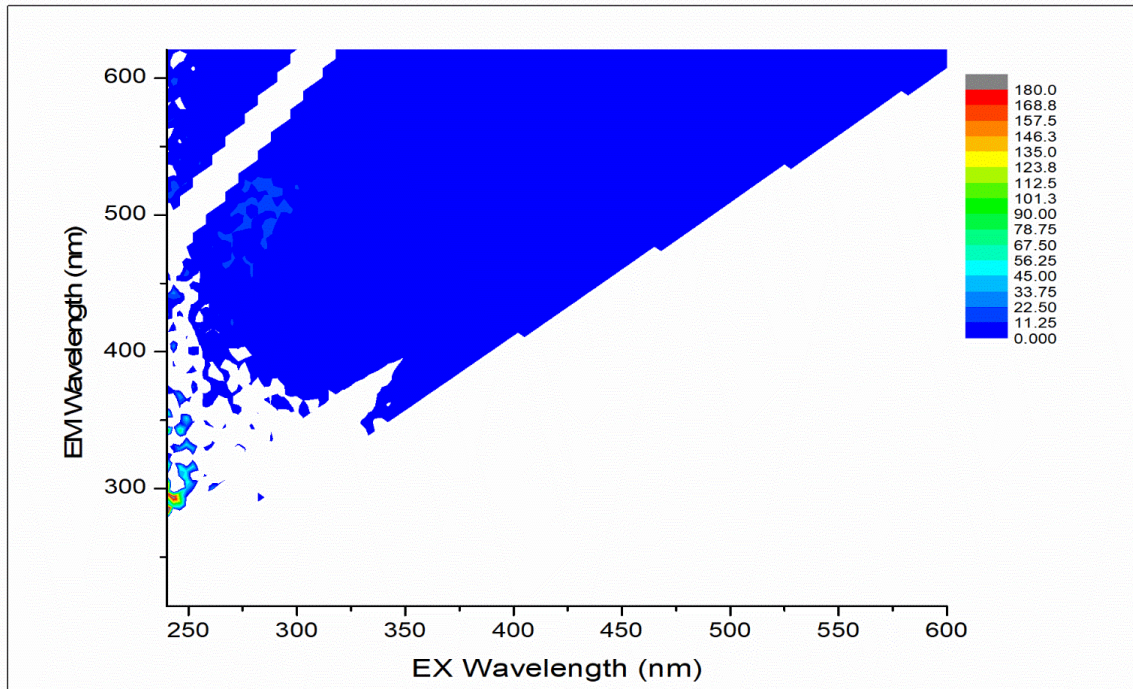


Figure D1 Excitation-Emission Matrices of humic acid used in the spiked synthetic wastewater recipe.

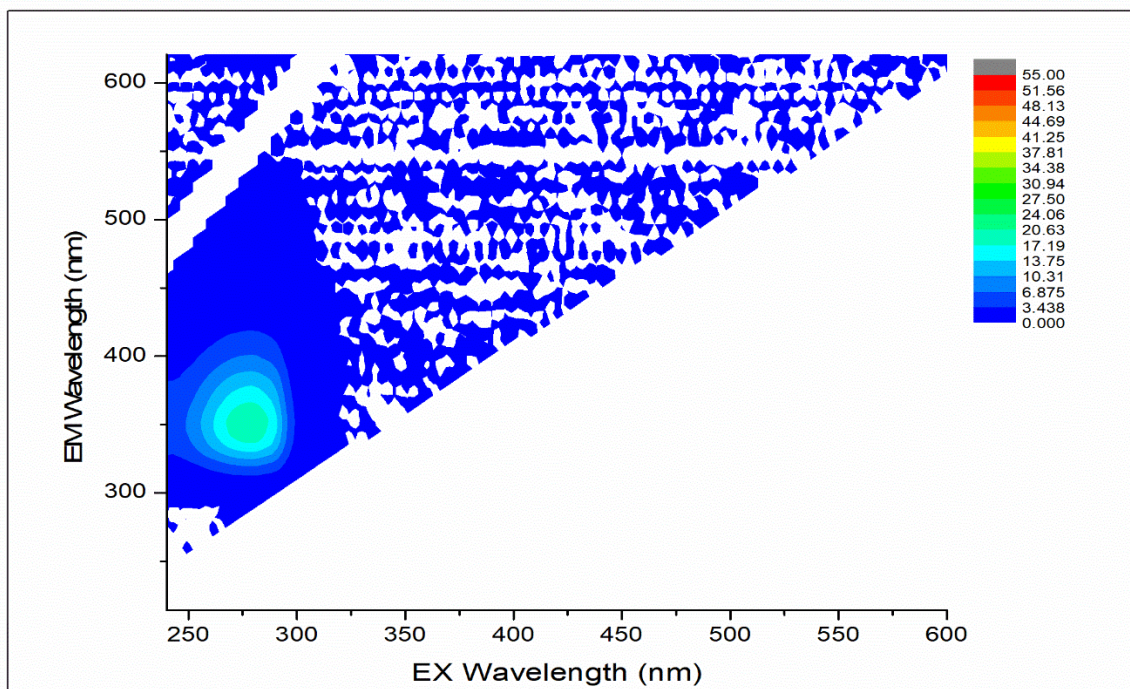
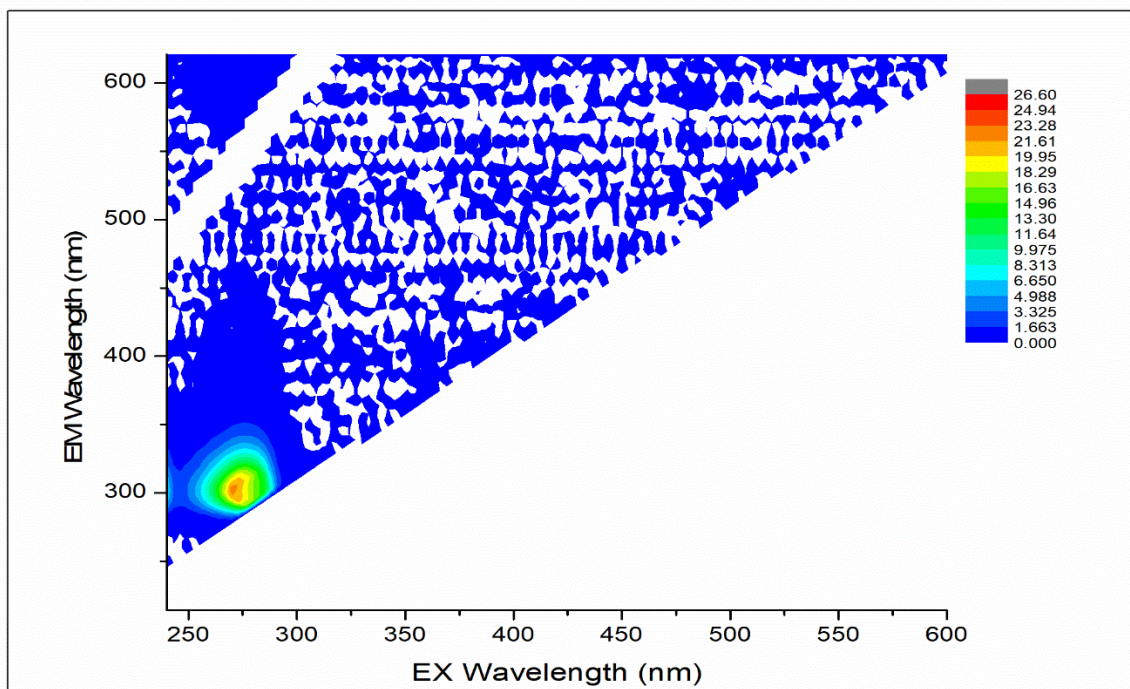
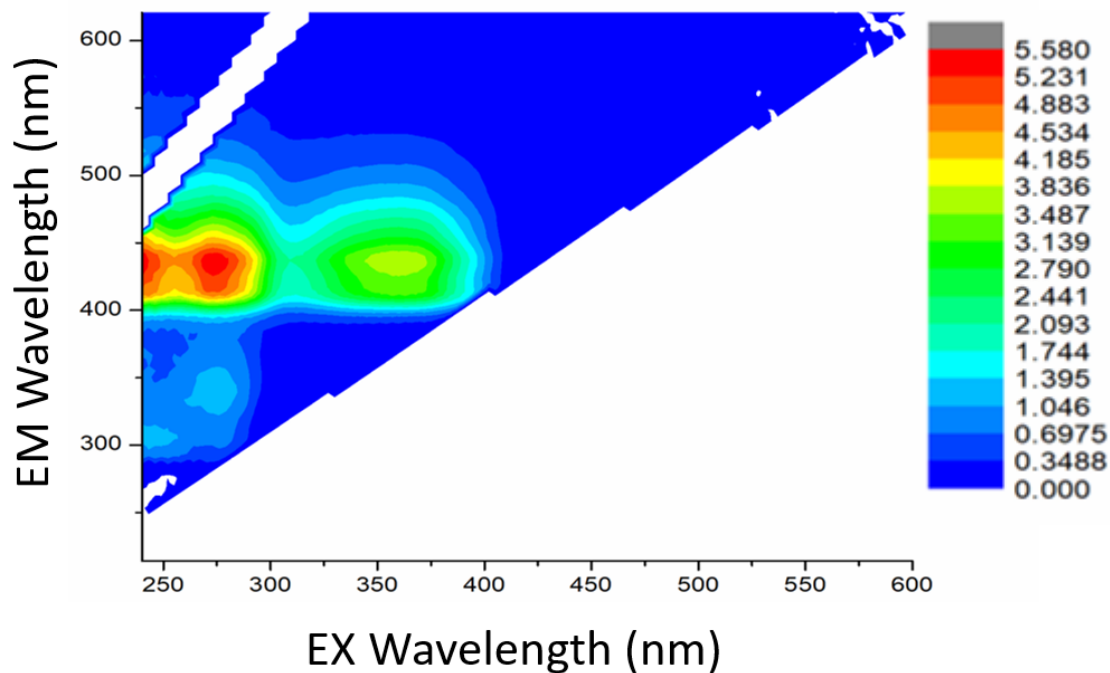
A**B**

Figure D2 Excitation-Emission Matrices (EEMs) of the amino acids, tryptophan (A) and tyrosine (B) used in the spiked synthetic wastewater recipe

Main Module M2 Membrane Extract



Main Module M3 Membrane Extract

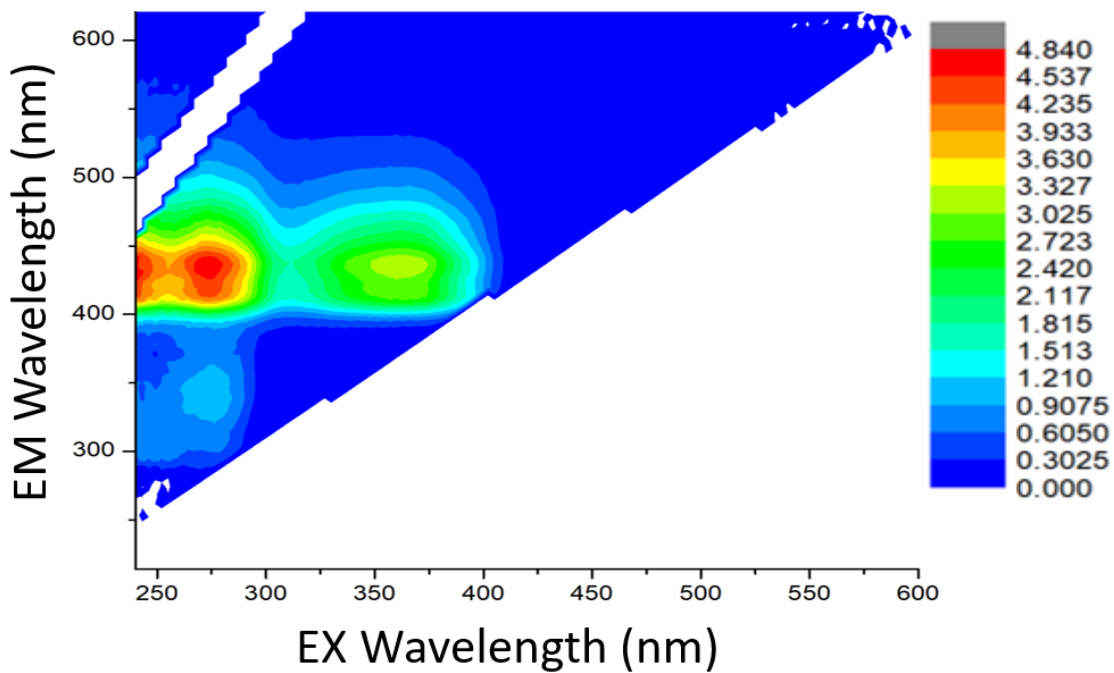


Figure D3 Excitation-Emission Matrices (EEMs) of main module membrane fiber samples M2 and M3, which have almost identical profiles to sample M1